

**Pathway Analysis of Phenol Degradation by UV/TiO₂ Photocatalysis
Using the Carbon-13 Isotopic Labelling Technique**

by

Lindelwa Jay

Submitted in partial fulfilment of the requirements for the degree

Master of Science (Applied Science) (Water Utilisation)

in the

Department of Chemical Engineering

Faculty of Engineering, Built Environment and Information Technology

UNIVERSITY OF PRETORIA

2018

ABSTRACT

PATHWAY ANALYSIS OF PHENOL DEGRADATION BY UV/ TiO₂ PHOTOCATALYSIS USING THE CARBON-13 ISOTOPIC LABELING TECHNIQUE

by

Lindelwa Jay

Supervisor: Professor Evans Chirwa
Department: Chemical Engineering
University: University of Pretoria
Degree: Master of Science (Applied Science) (Water Utilisation)
Keywords: Photocatalysis, Degradation intermediates, Carbon-13, Titanium dioxide

The United States Environmental Protection Agency (USEPA) has enlisted phenolic compounds as pollutants of priority concern, as they tend to persist in the environment over a long period, accumulate and exert toxic effects on humans and animals. The entrance of phenolic compounds into the aquatic environment results from natural, industrial, domestic and agricultural activities. Their presence may be due to the degradation or decomposition of natural organic matter present in the water, through the disposal of industrial and domestic wastes into water bodies and through runoffs from agricultural land.

Several specific new technologies, called Advanced Oxidation Processes (AOP), have been developed to eliminate dangerous organic chemicals such as phenol from polluted waters. The photocatalytic process, based on UV irradiated semiconductor (TiO₂), represents one of AOP that provide an interesting route to the destruction of many organic substances to CO₂, H₂O and corresponding mineral acids.

TiO₂ is usually used as a photocatalyst in two crystal structures: Rutile and Anatase. The photoreactivity of P-25 Degussa, consisting of anatase and rutile (4/1 w/w), exceeds that of pure anatase and rutile in several reaction systems. This study characterised the three TiO₂ powder

forms by BET, XRD, XRF and SEM analyses to contribute to a better understanding of their physical properties. Anatase was revealed to have 98.4% purity x-ray fluorescence analysis, Degussa at 96.7% and rutile at 75.7% was reported to have the most impurities (~25%).

This study investigated the UV/TiO₂ photocatalytic degradation of phenol, with emphasis on the effects of; solution pH, catalyst load, initial phenol concentration, dissolved oxygen and UV radiation intensity. Degradation studies were conducted in a batch reactor with photons for catalyst (TiO₂) activation supplied by a medium pressure 400 W UV lamp immersed in the pollutant solution housed in a double jacket quartz sleeve, which served as the cooling system for the lamp. Temperature control in the reactor was achieved by circulating cold water through the outer cavity of the quartz sleeve. The reactor contents in all batches were aerated at a flow rate of 10 mL/min. Thorough mixing of the contents of the reactor was achieved by continuous agitation with a magnetic stirrer. The experimental reaction time was set at 60-100minutes. Samples were monitored by GC-MS analysis. Results showed that UV/TiO₂ photocatalysis is an effective method for the removal of phenol from wastewaters. The efficiency of the process depends strongly on the experimental conditions.

Degradation of organic compounds in water is often accompanied by the formation of several intermediate compounds, some of which may be more toxic than the original pollutant. The carbon-13 isotopic labelling technique was employed to track the degradation mechanism of phenol to better understand the degradation pathway. Carbon-13 tracking results revealed that hydroquinone, catechol, benzoquinone, resorcinol and maleic acid were the main intermediates containing the C-13 isotope. A reaction pathway was postulated based on these findings.

Kinetic isotope effect (KIE) experiments were conducted and a primary isotope effect was observed. This confirmed that the C-13 isotope position on the labelled phenol was the site of bond breaking in the rate-limiting step.

DECLARATION

I, **Lindelwa Jay**, hereby declare that all the work provided in this dissertation is to the best of my knowledge original (except where cited) and that neither the whole work nor any part of it has been, or is to be submitted for another degree at this or any other University or tertiary education institution or examining body.

SIGNATURE:

DATE:

DEDICATION

To my parents

Nothemba Jay and Thamsanqa Mfeketo,

For their love and support throughout my life, and for being my first teachers

My late grandmother

Kerry Jay

A strong and gentle soul who taught me to trust in God, believe in hardwork and that so much
could be done with little

and

To my siblings

Busisiwe Jay and Vuyo Jay

My cheerleaders

This humble work is a sign of my love to you!

ACKNOWLEDGMENTS

I would like to express my sincere gratitude to the study leader, Professor Evans Chirwa, for his support and his patience. I am grateful for his excellent guidance and technical expertise that set high standards for my MSc work. I also thank him for securing funding for my research, such as the NRF Grantholder linked bursary in 2017 and 2018, funds for conference presentations in 2017 and 2018, and funds from the NRF Grant-holder bursary linked to the NRF Competitive Support for Unrated Researchers Grant No. CSUR160506164236 awarded to Prof Evans Chirwa of the Water Utilisation Division at the University of Pretoria.

The author expresses gratitude for funds from the City of Cape Town bursary. The author is sincerely thankful to Dr. Rembu Magoba for his mentorship and for always going the extra mile.

I would like to express my heart-felt gratitude to colleagues from the Water Utilisation and Environmental Division research group, of the Department of Chemical Engineering, University of Pretoria for their concern and words of encouragement. I thank Mrs Alette Devega and Mrs Elmerie Otto, for always attending to the needs around the lab beyond the call of duty.

I also wish to thank Dr. Sherperd M. Tichapondwa for his contribution towards the characterisation of titanium dioxide, Dr Zakhele Khuzwayo for his contribution towards a method development for carbon-13 isotope tracking by GC-MS analysis.

Finally yet importantly, I thank my family and friends especially Malesela Tloana for always believing in me, I appreciate the love and support they give me in everything I do.

TABLE OF CONTENTS

	Page
TABLE OF CONTENTS.....	v
LIST OF FIGURES.....	ix
LIST OF TABLES.....	xii
LIST OF NOMENCLATURE.....	xiv
RESEARCH OUTPUTS.....	xix
CHAPTER 1: INTRODUCTION:	1
1.1 BACKGROUND.....	1
1.2 PROBLEM STATEMENT.....	2
1.3 CHARACTERISATION OF PHENOL.....	2
1.3.1 Phenol Toxicity.....	3
1.4 RESEARCH GAP	4
1.5 STUDY MOTIVATION.....	4
1.6 AIM.....	5
1.6.1 Study Objectives.....	5
1.7 THESIS SCOPE.....	6
1.8 CONVENTIONAL WATER TREATMENT PROCESSES.....	8
CHAPTER 2: LITERATURE REVIEW.....	10
2.1 COMPARISON OF WATER TREATMENT TECHNOLOGIES.....	11
2.2 PHOTOCATALYSIS.....	14
2.3 MECHANISM OF TITANIUM DIOXIDE PHOTOCATALYSIS.....	17
2.4 SEMICONDUCTORS	18
2.5 TITANIUM DIOXIDE (TiO ₂) PHOTOCATALYSIS.....	20
2.6 APPLICATIONS OF UV/TiO ₂ PHOTOCATALYSIS	22
2.7 PATHWAY ANALYSIS.....	23
2.8 TiO ₂ PHOTOCATALYTIC HYDROXYLATION OF AROMATICS.....	26
2.9 PHOTOCATALYTIC CLEAVAGE OF AN ARYL-RING ON TiO ₂ SURFACE.....	30
2.10 PHOTOCATALYTIC DECARBOXYLATION OF CARBOXYLIC ACIDS..	33
2.10.1 Schmitt Reaction (Kolbe Process)	33

2.10.2	Russell Mechanism	34
2.11	ISOTOPIC LABELLING FOR STUDYING REACTION MECHANISM	35
2.12	FACTORS AFFECTING THE OPERATION OF A PHOTOCATALYTIC REACTOR.....	36
2.12.1	Catalyst Loading.....	36
2.12.2	Reaction pH.....	36
2.12.3	Temperature.....	37
2.12.4	Dissolved Oxygen.....	38
2.12.5	Contaminants and Their Loading.....	39
2.12.6	Light Intensity.....	39
2.12.7	Turbidity.....	40
2.13	REACTOR DESIGN CHALLENGES.....	43
	CHAPTER 3: METHODS AND MATERIALS.....	45
3.1	BATCH EXPERIMENTS.....	43
3.1.1	Chemical Reagents.....	43
3.1.2	Experimental Methods.....	43
3.1.3	Analytical Methods.....	44
3.1.4	Degradation Studies.....	45
3.1.5	Total Organic Carbon (TOC) Analysis.....	45
3.1.6	Titanium Dioxide Characterisation.....	46
3.1.7	Pathway Analysis.....	48
	CHAPTER 4: CHARACTERISATION OF TITANIUM DIOXIDE.....	49
4.1	INTRODUCTION.....	49
4.2	X-RAY DEFFRACTION (XRD).....	48
4.3	X-RAY FLUORESCENCE (XRF).....	49
4.4	PARTICLE SIZE DISTRIBUTION (PSD).....	50
4.5	SCANNING ELECTRON MICROSCOPY (SEM).....	
4.6	A Comparison Between the Three TiO ₂ Powder Forms and Their Effect on the Photocatalytic Activity.....	52
4.6.1	DISCUSSION.....	55
4.6.2	CONCLUSION.....	57

CHAPTER 5: PHENOL DEGRADATION STUDIES.....	58
5.1 EFFECT OF INITIAL PHENOL CONCENTRATION.....	58
5.2 TOC ANALYSIS.....	59
5.3 EFFECT OF TiO ₂ CONCENTRATION.....	60
5.4 EFFECT OF DISSOLVED OXYGEN.....	61
5.5 EFFECT OF pH.....	62
5.6 EFFECT OF CONTACT TIME AND INITIAL PHENOL CONCENTRATION	63
.....	
5.7 EFFECT OF UV LIGHT INTENSITY.....	65
5.8 CONCLUSION.....	67
CHAPTER 6: PATHWAY ANALYSIS.....	68
6.1 INTRODUCTION.....	68
6.1.1 ANALYTICAL TECHNIQUES FOR ISOTOPE	
STUDIES.....	68
6.1.2 CARBON AND ITS ISOTOPES.....	71
6.2 METHODOLOGY.....	
6.2.1 Experimental Setup.....	72
6.2.2 Chemicals.....	73
6.2.3 Batch Studies.....	74
6.2.4 Analytical Methods.....	76
6.3 RESULTS AND DISCUSSION.....	77
6.4 CARBON-13 ISOTOPE TRACKING.....	90
6.4.1 Method Development.....	90
6.4.2 Carbon-13 Tracking Results of Results of Phenol Degradation by	90
UV/TiO ₂ Photocatalysis.....	
6.4.3 Carbon-13 Tracking Results of Results of Phenol Degradation by	
UV/TiO ₂ Photocatalysis under Anaerobic Conditions.....	100
6.4.4 Reaction Pathway Under Anaerobic Conditions (Absence	100
of Electron scavenger).....	
6.5.5 Effect of Catalyst on Reaction	101
6.4.6 Effect of UV light on Reaction	103

6.4.7	Effects of Solvent in Reaction	103
6.5	KINETICS AND MODELLING.....	104
6.5.1	The Kinetic Isotope Effect.....	105
6.5.2	Kinetic Isotope Effect Experiments.....	106
6.5.3	A Comparison between Kinetic Studies of Phenol- ¹² C and Phenol- ¹³ C	109
6.5.4	Evaluation of Kinetic Isotope Effects in Multi-Step Reaction.....	112
6.6	KINETICS	113
6.6.1	Langmuir-Hinshelwood (L-H) Kinetic Model.....	113
6.6.2	Adsorption Isotherms.....	114
6.7	MODELLING AND SIMULATION.....	117
6.8	CONCLUSION.....	118
	CHAPTER 7: CONCLUSIONS AND RECOMMENDATIONS.....	121
	REFERENCES	122
	APPENDICE A: AQUASIM file programme listing	126
	APPENDICE B: HPLC Chromatogram.....	138
	APPENDICE C: GC-MS Chromatograms.....	146

LIST OF FIGURES

	Page
Figure 1.1 A schematic of the conventional water treatment process (oregon.gov, 2017).....	8
Figure 1.2 A depiction of the different classes of treatment methods with specificity to the Advanced Oxidation umbrella (Gökhan Eğilmez, Gürsel A. Süer,Özgüner, 2012).....	9
Figure 2.1 A schematic representation of the basic processes of photocatalytic water splitting on a semiconductor surface (Fujishima, Zhang and Tryk, 2008).....	15
Figure 2.2 The position of different semiconductor band gap (Ola and Maroto-Valer., 2015).....	19
Figure 2.3 Excitation, charge recombination and reaction paths occurring on semiconductor surface (G. Cacciato et al, 2016).....	20
Figure 2.4 A representation of the three main processes of TiO ₂ photocatalytic oxidation of aromatic compounds (Pang et al., 2014b).....	24
Figure 2.5 A schematic of the proposed pathways involved in the TiO ₂ photocatalytic degradation of benzene.(Bui et al., 2011).....	25
Figure 2.6 The postulated reaction pathway of phenol by the •OH radical (Gaya and Abdullah, 2008).....	26
Figure 2.7 A representation of the different regio-isomers of electrophilic (E ⁺) substitution of aromatic compounds (Palmisano et al., 2006).....	27
Figure 2.8 The main hydroxylated products obtained during the photocatalytic oxidation of aromatic compounds containing either an EDG or EWG (Palmisano et al., 2006).....	28
Figure 2.9 Representation of the postulated reaction pathways for oxidation of phenol in the TiO ₂ photocatalytic system. (Ng et al., 2012).....	30
Figure 2.10 The proposed mechanism for TiO ₂ photocatalytic cleavage of aryl-ring via a dioxetane intermediate (Pang et al., 2014b).....	31

Figure 2.11	A representation of the structures of the main intermediate products of photocatalytic cleavage of 3,5-di-tert-butylcatechol (DTBC) by TiO ₂ , with the main products divided into three groups(a,b and c) and the values in brackets indicating the highest (Pang et al., 2014b).....	32
Figure 2.12	The carboxylation of phenol to salicylic acid for the industrial synthesis of aspirin (Hermann Kolbe, 1860; R.Schmitt,1885).....	33
Figure 2.13	A schematic diagram of the Russell Mechanism (Miyamoto et al., 2014).....	34
Figure 3.1	Experimental set-up of photocatalytic batch reactor. (Wang C. et al, 2004).....	44
Figure 4.1	An X-ray diffraction pattern for TiO ₂ in the Anatase, Rutile and Degussa form.....	48
Figure 4.2	SEM images of Anatase (a&b), Degussa (c&d) and Rutile (e&f)....	51
Figure 4.3	Effect of initial phenol concentration on the photocatalytic performance of the three powder forms of TiO ₂ is depicted in the graph at a constant catalyst concentration of 20mg/L	52
Figure 4.4	The ideal initial phenol concentration for each TiO ₂ powder as observed in Figure 4.3 was kept at constant and the TiO ₂ concentration was varied from 2 – 10mg/L, and results are depicted in the graph	53
Figure 4.5	The degradation profile for the three powder forms of TiO ₂ at their ideal initial phenol and catalyst concentrations.....	54
Figure 5.1	The effect of initial phenol concentration on the degradation efficiency expressed as percentage.....	54
Figure 5.2	The phenol degradation profile for different initial phenol concentrations at a constant TiO ₂ concentration of 20mg/L....	56
Figure 5.3	The % phenol degradation for TiO ₂ (2mg/L – 10mg/L)	57
Figure 5.4	The % phenol degradation under aerobic and anaerobic conditions.....	59
Figure 5.5	The % phenol degradation with change in pH.....	60

Figure 5.6	The effect of contact time and initial phenol concentration on the % phenol degradation are shown by the graph	61
Figure 5.7	The graph shows the effect of UV light and its intensity on the photocatalytic degradation profile.....	62
Figure 5.8	The graph shows the degradation profile for the different control conditions.....	64
Figure 6.1	The three main isotopes of carbon (Kuensting S., 2004).....	72
Figure 6.2	Chemical structure of the Phenol-1- ¹³ C.....	75
Figure 6.3	The degradation profile of phenol- ¹² C and phenol- ¹³ C over 100 minutes is depicted in the graph.....	76
Figure 6.4	Overall reaction for oxidation of ethanol by NAD'. Numbers indicate positions of labelling in the reactants and products that will generate isotope effects as indicated in the text (Adopted from; Cook, 1998)	77
Figure 6.5	Dependence of primary kinetic isotope effects on reactant coordinate position. The deuterium isotope effect reaches a maximum value of 6-8 for a symmetric transition state. The ¹³ C isotope effect for breaking a bond to carbon increases monotonically to the maximum theoretical value of 1.07 until the bond is almost broken, and the isotope effect then decreases sharply to near one (1) (Adopted from Cook, 1998)...	78
Figure 6.6	Phenol degradation mechanism (Devi and Rajashekhar 2011).....	81
Figure 6.7	A scheme of phenol degradation with reaction pathways (Nagaveni et al., 2004).....	82
Figure 6.8	Intermediate products of EC phenol degradation on anodes (A) Ti/SnO ₂ -Sb, (B) Ti/RuO ₂ , and (C) Pt (Adopted from Xiao-yan et al., 2005).....	83
Figure 6.9	Reaction pathway of electrochemical phenol degradation (Adopted from Xiao-yan et al., 2005).....	85

Figure 6.10	The evolution of phenol and hydroxylated phenolic intermediates derived from UV-vis spectra using TiO ₂ P-25 Degussa. [B], [C], [H] and [P] indicate the benzoquinone, catechol, hydroquinone and phenol concentration curves, respectively (Adopted from Su et al, 2012) ...	90
Figure 6.11	The postulated reaction pathway for the UV/TiO ₂ photocatalytic degradation of phenol.....	92
Figure 6.12	The UV/TiO ₂ photocatalytic degradation profile of phenol-12C and phenol- ¹³ C labeled experiments with and without aeration.....	95
Figure 6.13	The proposed degradation pathway of Phenol.....	99
Figure 6.14	Conversion between hydroquinone and benzoquinone (Adopted from Shanmugam et al., 2007).....	99
Figure 6.15	The proportion of particles that have enough energy to react is increased in the presence of a catalyst (Adopted from Behr, 2002)....	101
Figure 6.16	The effect of a catalyst on the activation energy of an endothermic reaction. The catalyst would act in the same way for an exothermic reaction (Adopted from Behr, 2002).....	101
Figure 6.17	Experiment A; KIE determined from absolute rates of two parallel reactions as depicted (Simmons and Hartwig, 2012).....	105
Figure 6.18	Experiment B; KIE determined from an intermolecular competition as depicted (Simmons and Hartwig, 2012).....	106
Figure 6.19	Experiment C; KIE determined from an intramolecular competition as depicted (Simmons and Hartwig, 2012).....	107
Figure 6.20	The photo degradation profile of phenol C-13 over TiO ₂	108
Figure 6.21	A linear plot of the Langmuir-Hinshelwood equation to determine rate constant, k, for phenol-13C experiments.....	109
Figure 6.22	The photo degradation profile of phenol-12C over TiO ₂ .	110
Figure 6.23	A linear plot of the Langmuir-Hinshelwood equation to determine rate constant, k, for phenol- ¹² C experiments.....	110
Figure 6.24	Langmuir adsorption isotherm plots of phenol.....	114

Figure 6.25	A depiction of the fit of the Langmuir model against measured data for different initial phenol concentrations (mg/L).....	114
Figure 9A-1	A chromatogram from HPLC analysis for the degradation of phenol- ¹² C over TiO ₂	143
Figure 9A-2	A chromatogram from HPLC analysis for the degradation of phenol- ¹³ C over TiO ₂	144
Figure 9B-1	A chromatogram of resorcinol from the photodegradation of phenol- ¹² C.....	147
Figure 9B-2	A chromatogram of resorcinol from the photodegradation of phenol- ¹³ C.....	148
Figure 9B-3	A chromatogram of maleic acid from the photodegradation of phenol- ¹³ C.....	149
Figure 9B-4	A chromatogram of maleic acid from the photodegradation of phenol- ¹² C.....	150
Figure 9B-5	A chromatogram of hydroquinone from the photodegradation of phenol- ¹² C.....	151
Figure 9B-6	A chromatogram of hydroquinone from the photodegradation of phenol- ¹³ C.....	152
Figure 9B-7	A chromatogram of the hydroquinone peak.....	153

LIST OF TABLES

	Page
Table 2.1 Common oxidants and their oxidation potentials.....	16
Table 2.2 The structural properties of the TiO ₂ crystalline forms (Ola, O. and Maroto-Valer, M. M., 2015).....	21
Table 2.3 The classes of organics that have been successfully photomineralised.	22
Table 2.4 The yields obtained for each aromatic compound and the ortho:meta:para ratios under irradiation (Palmisano et al., 2006)...	29
Table 4.1 The chemical composition of the three powders of TiO ₂	49
Table 4.2 The Brunauer-Emmett-Teller (BET) surface area and the specific area for each of the three powder forms of TiO ₂	50
Table 4.3 The average phenol degradation rates for each TiO ₂ powders over a 100 minutes reaction time.....	55
Table 6.1 The NPOC results (mg/L) with change in initial phenol concentration (mg/L).....	58
Table 6.2 The table shows the physical properties of the carbon-12/carbon-13 isotopes (Man-Sung and Francois, 2006).....	73
Table 6.3 The physical properties of the C-13 isotope labeled phenol.....	74
Table 6.4 The intermediates detected by GC-MS analysis during the course of UV/TiO ₂ photocatalytic degradation of phenol.....	85
Table 6.5 The evolution of intermediates detected during the course of phenol C-12 and phenol-C-13 degradation by UV/TiO ₂ Photocatalysis.....	87
Table 6.6 The table reports the intermediates detected from C-13 tracking results by UV/TiO ₂	89

Table 6.7	The phenol photo degradation intermediates detected by GC-MS analysis for phenol C-12 and phenol C-13 under anaerobic conditions (absence of electron scavenger)	94
Table 6.8	The intermediates detected during the course of phenol-C-13 degradation by UV/TiO ₂ Photocatalysis under anaerobic conditions (absence of electron scavenger)	95
Table 6.9	Average values of rate constants (k) for phenol C-13 are reported in the table and their regression coefficients (R ²)	107
Table 6.10	Average values of rate constants (k) for phenol C-12 are reported in the table and their regression coefficients (R ²)	109
Table 6.11	The table reports the average and standard deviation of the data collected in 5 experiments as shown in Figure 6.24.....	107
Table 6.12	The parameters of Langmuir isotherms for the adsorption of phenol onto TiO ₂	109
Table 6.13	The average and standard deviation of the data collected in 5 experiments as shown in Figure 6.24	113
Table 6.14	The parameters of Langmuir isotherms for the adsorption of phenol onto TiO ₂	113
Table 6.15	The simulated values for Langmuir adsorption constant (K _a), rate constant (k _r) and their Chi ² values for different initial phenol concentrations.....	114
Table 9A-1	The peak results during the photocatalytic degradation of phenol C-12	141
Table 9A-2	The peak results during the photocatalytic degradation of C-13 labeled phenol	142

LIST OF NOMENCLATURE

AOP	Advanced Oxidation Process
WWTP	Waste Water Treatment Plant
WHO	World Health Organisation
EPA	Environmental Protection Agency
USEPA	United States Environmental Protection Agency
USA	United States of America
COD	Chemical Oxygen Demand
BOD	Biochemical Oxygen Demand
UV	Ultra-Violet
TOC	Total Organic Carbon
UVC	Ultra-Violet C spectrum
EDG	Electron Donater Group
EWG	Electron Withdrawer Group
PZC	Point Of Zero Charge
DO	Dissolved Oxygen
ROS	Reactive Oxygen Species
TiO ₂	Titanium dioxide
rpm	Revolutions per minute
HPLC	High Performance Liquid Chromatograph
GC-MS	Gas Chromatograph- Mass Spectrometer
UNICEF	United Nations International Children's Emergency Fund.

WDR	Water Desalination Report
NPOC	Nonpurgable Organic Carbon
XRD	X-ray defraction
XRF	X- ray fluorescence
PSD	Particle Size Diameter
BET	Brunauer-Emmett-Teller
SEM	Scanning Electron Microscopy
C-13	Carbon-13 isotope
ppm	Parts per million
nm	nano-metres
μm	micro-metres
m^2	square metre
m^{-1}	per minute
m^2/g	square metre per gram
mg	milli-gram
L	litre
mg/L	milli-gram per litre
eV	electron volt

RESEARCH OUTPUTS

Journal Articles

1. Jay L., Chirwa E.M.N., 2018, An investigation of UV/TiO₂ photocatalytic degradation mechanism of phenol, utilising the c-13 isotopic labelling technique, Water Science and Technology (Under review)
2. Jay L., Chirwa E.M.N., 2018, Pathway analysis of phenol degradation by uv/tio₂ photocatalysis utilising the c-13 isotopic labelling technique , Chemical Engineering Transactions, 70, 181-186 DOI:10.3303/CET1870031
3. Chirwa E.M.N., Molokwane P.E., Tikilili P.V., Makgato S.S., Bamuza-Pemu E.E., Jay L., 2018, Biological remediation and removal of radioactive metals and complex aromatic compounds from nuclear and radioactive waste , Chemical Engineering Transactions, 70, 85-90 DOI:10.3303/CET1870015

Conference Presentations

4. Jay L., Chirwa E.M.N., 2017. Phenol Degradation Pathway Analysis By Advanced Oxidation Process: TiO₂ Photocatalysis Using Radioisotopic Labelling. The 14th IWA Leading Edge Conference. 29 May - 02 June 2017 Oceania Convention Centre Florianapolis, Santa Catarina, Brazil. (Poster)
5. Jay L., Chirwa E.M.N., 2018. Pathway Analysis for the Degradation of Phenol by UV/TiO₂ Photocatalysis using the C-13 Isotopic Labeling Technique. WISA Biennial Conference & Exhibition. 24-27 June 2018 CTICC Cape Town (Oral)
6. Jay L., Chirwa E.M.N., 2018. Pathway Analysis for the Degradation of Phenol by UV/TiO₂ Photocatalysis using the C-13 Isotopic Labelling Technique. Chemical Engineering Transactions. Proceedings of the 21st Conference Process Integration, Modeling and Optimisation for Energy Saving and Pollution Reduction. 25–29 August 2018 Clarion Congress Hotel Prague in Prague, Czech Republic (Oral)

CHAPTER 1 INTRODUCTION

1.1 BACKGROUND

In recent years, the discharge of large amounts of synthetic chemicals such as solvents, plasticisers, insecticides, herbicides and fungicides into the environment through industrial, agricultural, medical and domestic activities has produced significant ecotoxicological problems with serious consequences for all living organisms. These substances include phenols which have been classified as priority pollutants by the United States Environmental Protection Agency (USEPA) (Michałowicz & Duda 2007).

Increasing demand and shortage of clean water sources due to the rapid development of industrialisation, population growth and long-term droughts have become an issue worldwide. It is estimated that around 4 billion people worldwide experience what it's like to have little or no access to clean and sanitised water supply, and millions of people die of severe waterborne diseases annually. These statistical figures are expected to grow in the short future, as a result of increasing water contamination due to overwhelming discharge of micro pollutants and contaminants into the natural water cycle. In view to suppress the worsening of clean water shortage, development of advanced with low-cost and high efficiency water treatment technologies to treat the wastewater is desirable.

With this growing demand, various practical strategies and solutions have been adopted to yield more viable water resources. The storage of rainwater for daily activities and increasing the catchment capacity for stormwater are just a few examples that could resolve the problems in short-term.

One of a few attractive options is the possible reuse of onsite rural wastewater or the treated municipal wastewater from treatment plants for agricultural and industrial activities. Since these wastewaters constitute one of the largest possible water resources, its reuse is anticipated to offset more clean water resource.

Recycling wastewater is usually associated with the presence of suspended solids, health-threat coliforms and soluble refractory organic compounds that are both tedious and expensive to treat. Currently available water treatment technologies such as adsorption or coagulation merely

concentrate the pollutants present by transferring them to other phases, but still remain and not being completely “eliminated” or “destroyed”.

These have led to the rapid research and development in the field of “Advanced Oxidation Processes (AOPs)” as the innovative water treatment technologies. The rationale of these AOPs is based on the insitu generation of highly reactive transitory species for mineralization of refractory organic compounds, water pathogens and disinfection by-products.

1.2 PROBLEM STATEMENT

The widespread occurrence of phenols and its derivatives in the environment has raised serious concerns and has become a threat to our water supply network. Phenols occur in surface waters, groundwater, and wastewater and sludge products. Phenols also enter the environment through accidental spills, hazardous waste disposals sites, storage tanks or municipal landfills. They are also contained in insecticides, herbicides, wood preservatives and also occur as intermediates in the production of dyes and pharmaceuticals. These compounds are not metabolized and are discharged into sewers and wastewater treatment plants (WWTPs). The existing conventional water treatment plants were not designed for these contaminants and are not effective in elimination of the different classes of emerging contaminants as they have not been monitored due to the absence of stringent regulation specific to the contaminants. These undesirable compounds are being released, knowingly or unknowingly, into the aquatic environment that affect the whole living organism. These pose challenges to the designers of future treatment plants and related methodology for their eradication.

1.3 CHARACTERISATION OF PHENOL

Phenolic waste imparts a carbolic odour to river water and is toxic to fish and human beings. Total phenol concentration in the wastewater of a typical Indian refinery processing 5.0 million tons of crude per year is around 135 mg/L and the discharge rate of wastewaters varies from 125 to 250 m³/h with pH being in the range of 8.8–9.4. The concentration of phenolic compounds in the wastewater from resin plants is typically in the range of 12–300 mg/L. The wastewater with the highest concentration of phenol (>1000 mg/L) is typically generated from coke processing. Phenolic compounds also emanate from resin plants with a concentration range of 12–300 mg/L.

Environmental Protection Agency (EPA) has set a limit of 0.1 mg/L of phenol in wastewater. The World Health Organisation (WHO) is stricter on phenol regulation. It sets a 0.001 mg/L as the limit of phenol concentration in potable water (Michałowicz and Duda, 2007).

Toxic influence of organic compounds depends on many factors. Penetration of phenol to organisms is related with diffusion of the compound across a cell's membrane. The factor that strongly affects diffusion is hydrophobicity of the individual compound. The increase of hydrophobicity affects the more effective penetration of a cells membrane by phenol and thus enhances the toxicity of xenobiotics.

Most phenolic compounds including phenol, chlorophenols, nitrophenols and aminophenols are characterized by toxic activity.

1.3.1 Phenol Toxicity

Phenol irritates skin and causes its necrosis, it damages kidneys, liver, muscle and eyes. Damage to skin is caused by its coagulation related to reaction to phenol with amino acids contained in keratin of epidermis and collagen in inner skin. A dose of 1 g phenol may be lethal for an adult man, but individual tolerance for this compound can be high. Some reports reveal that a man can survive even after administration of 30 g of this compound (60 ml of 50% solution). With regards to fast absorption by skin (from 60%-90%) even contact of hand or forehead with phenol solution may cause death (Michałowicz and Duda, 2007).

Phenols are recalcitrant to biodegradation and consequently persistent in the environment. A variety of phenol derivatives compounds are highly toxic, mutagenic and carcinogenic for all living organisms. At present, the importance of phenol is proved by its ever-increasing production that reached 1900 million kg in 1995 in the USA alone (Fortuny et al., 1998). Industrial wastewaters that may contain many phenolic compounds are highly toxic to most aquatic life. Therefore, the removal of phenol from wastewater is of environmental interest.

1.4 RESEARCH GAP

Effective use of reactive species generated in-situ by photonic excitation of solid catalyst particles for the degradation of organic pollutants in water has been shown to be an effective technology for the treatment of a variety of organic pollutants in water. Degradation of organic compounds in water is often accompanied by the formation of several intermediate compounds, some of which are feared to be more toxic than the original pollutant being treated. Effective treatment is expected to mineralise the parent pollutant and degradation intermediates formed during the treatment process, or reduce the pollutant/intermediates to environmentally insignificant concentrations. Profiling the intermediates produced in the course of the degradation of pollutants in water would provide valuable information on the degradative pathways and the degradability of the intermediates formed (Laoufi et al, 2008; Bamuza-Pemu and Chirwa, 2013).

Very few of studies have reported results on the degradation pathway analysis of phemol and occurrence of potentially harmful intermediates formed during the photocatalytic degradation process.

This study presents results on the degradation profile of intermediates which indicate the mode of fragmentation of the cyclic compounds in water. This will contribute to a better understanding of the degradation mechanism of the studied compound and other similar organic pollutants.

1.5 STUDY MOTIVATION

It has been frequently observed that pollutants not amenable to biological treatment may also be characterised by high chemical stability and/or by strong difficulty to be completely mineralized. In these cases, it is necessary to adopt reactive systems much more effective than those adopted in conventional purification processes.

This has led to the advancement of new methods and adoption of improved methods for the removal of pollutants from water. Numerous studies have been carried out to find a suitable technology for wastewater treatment. Advanced oxidation processes (AOP) have led the way in the treatment of aqueous waste. AOP is fast becoming the leading wastewater treatment technology due to its many applications such as organic pollutant destruction by reducing toxicity,

biodegradability improvement BOD/COD removal as well as odour and colour removal (Mandal *et al.*, 2010).

The term advanced oxidation processes (AOP) collectively refers to processes in which oxidation of organic contaminants occurs primarily through reactions with hydroxyl radicals. In water treatment applications, AOPs usually refer to a specific subset of processes that involve O₃, H₂O₂, and/or UV light.

Photocatalysis is a reaction which uses light to activate a substance which modifies the rate of a chemical reaction without being involved itself. Semiconductor heterogeneous photocatalysis is a versatile, low-cost and environmentally benign treatment technology for a host of pollutants. These may be of biological, organic and inorganic in origin within water and air. The efficient and successful application of photocatalysis demands that the pollutant, the catalyst and source of illumination are in close proximity or contact with each other (Ibhadon and Fitzpatrick, 2013).

The ability of advanced oxidation technology to remove low levels of persistent organic pollutants as well as microorganisms in water has been widely demonstrated and, progressively, the technology is now being commercialized in many areas of the world including developing nations.

1.6 AIM

The main aim of this study is to investigate the reaction pathway for the degradation of phenol by TiO₂ photocatalysis using the Carbon-13 isotopic labeling technique.

1.6.1 Study Objectives

- Evaluate the performance of a laboratory scale treatment unit employing a chemical free photocatalytic system for the degradation of environmentally significant levels of phenol.
- Identify and investigate the intermediates formed during the photocatalytic degradation.
- Investigate the degradative pathway for the model compound phenol.
- Design a reactor system to optimize photocatalysis.
- Model and simulate the photocatalytic process using intrinsic kinetic parameters.

1.7 THESIS SCOPE

Chapter1: Background/Introduction

This chapter introduces the context of the study, outlines the problem of water scarcity, pollution of water resources with recalcitrant compounds and the challenges associated with the eradication of these pollutants. The study compound (phenol) is characterised, the research gap is identified and the study motivation was described. Lastly, this chapter describes the aims and objectives of the study.

Chapter2: Literature Review

This chapter looks into the theory of UV/TiO₂ photocatalysis as a treatment technology for organic contaminants, factors affecting its performance, its challenges and limitations. Lastly, it studies the degradation mechanism of aromatic compounds, including phenol. The use of the isotopic labeling technique as a method for studying reaction mechanism was also studied.

Chapter3: Methods and Materials

This chapter provides information on the materials used during this study. It also gives a detailed description of the experimental methodologies used, as well as the analytical techniques employed.

Chapter4: Characterisation of Titanium Dioxide

This chapter characterizes the performance of titanium dioxide with regards to the three powder forms, anatase, rutile and Degussa.

Chapter5: Phenol Degradation Studies

This chapter studies the factors affecting the performance of UV/TiO₂ photocatalysis, assesses how each of these factors impact on the degree of degradation of the study compound, phenol.

Chapter6: Pathway Analysis

This chapter gives an in-depth study of the degradation mechanism followed by phenol during UV/TiO₂ photocatalysis. A phenol compound labeled with a carbon-13 isotope was used to track the break-down of the study pollutant. Intermediates were studied to contribute to the

understanding of the reaction pathway. Experiments with the unlabeled phenol and the C-13 labeled phenol were conducted in parallel for comparison.

Chapter7: Conclusions and Recommendations

This chapter summarises research findings. It addresses the challenges and limitations encountered in the study. Lastly, recommends on ways to improve the study methodology.

1.8 CONVENTIONAL WATER TREATMENT PROCESSES

Conventional water treatment processes as depicted by (Fig 1.1) involves coagulation (chemical mixing), flocculation, sedimentation, filtration and disinfection. Some recent treatment trains have incorporated ion exchange and adsorption. The conventional water treatment system is not very efficient in removing volatile and semi-volatile organic compounds.

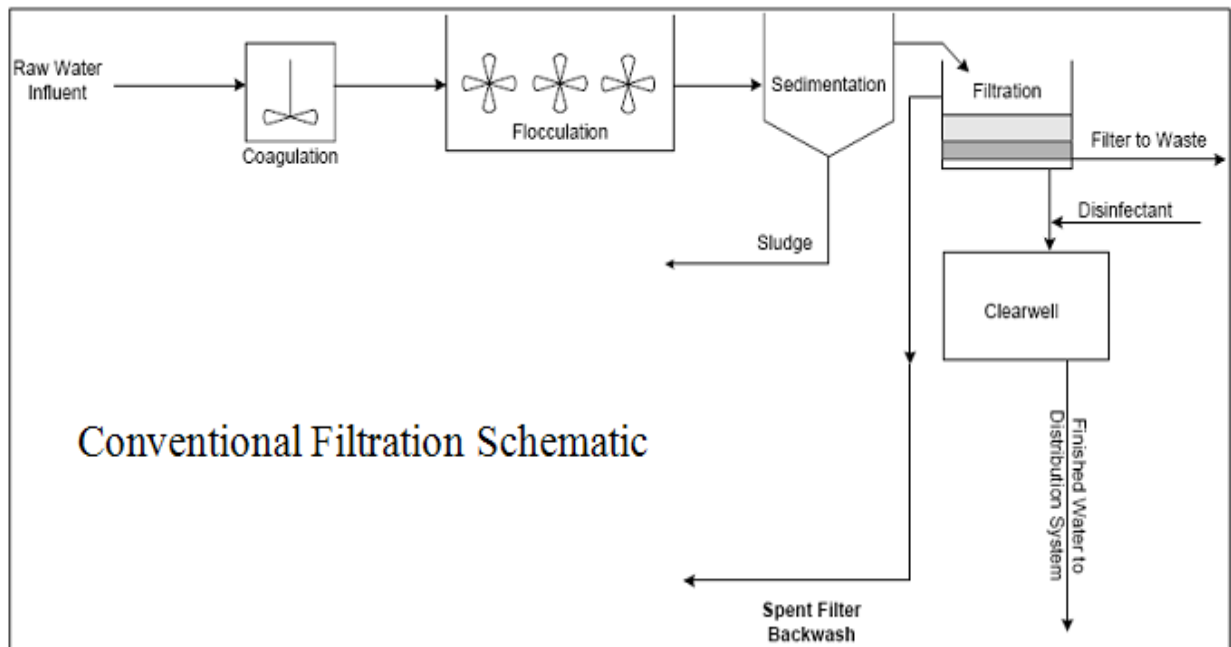


Figure 1.1: A schematic of the conventional water treatment process (oregon.gov, 2017).

Biological transformation using microorganisms is one of the prevalent options for the remediation of pollution caused by these toxic compounds. However, the use of biosurfactants for pollution remediation caused by toxic compounds has proven to be inefficient due to lag, which is a phenomenon inherent to microbial kinetics. Lag can be described as a delayed response of the microbial population to a sudden change in the environment. A lag phase can occur in both growth and inactivation processes. In case of growth conditions, the lag phase is an adjustment period during which bacterial cells modify themselves in order to take advantage of a new environment and also to initiate exponential growth. (Mandal *et al.*, 2010)

AOPs are a group of technologies (figure 1.2) that lead to hydroxyl radical ($\text{OH}\cdot$) generation. Hydroxyl radicals are extremely unstable and reactive. They are characterised by a high oxidation

potential and attack organic molecules and form oxidised intermediates with lower molecular weight until they are completely mineralized to CO₂ and H₂O. AOPs are powerful and efficient treatment methods for degrading recalcitrant materials or mineralizing stable, inhibitory or toxic contaminants. As a result, AOPs are gaining increasing popularity due to their potential of converting harmful organic pollutants into innocuous compounds such as CO₂ and H₂O.

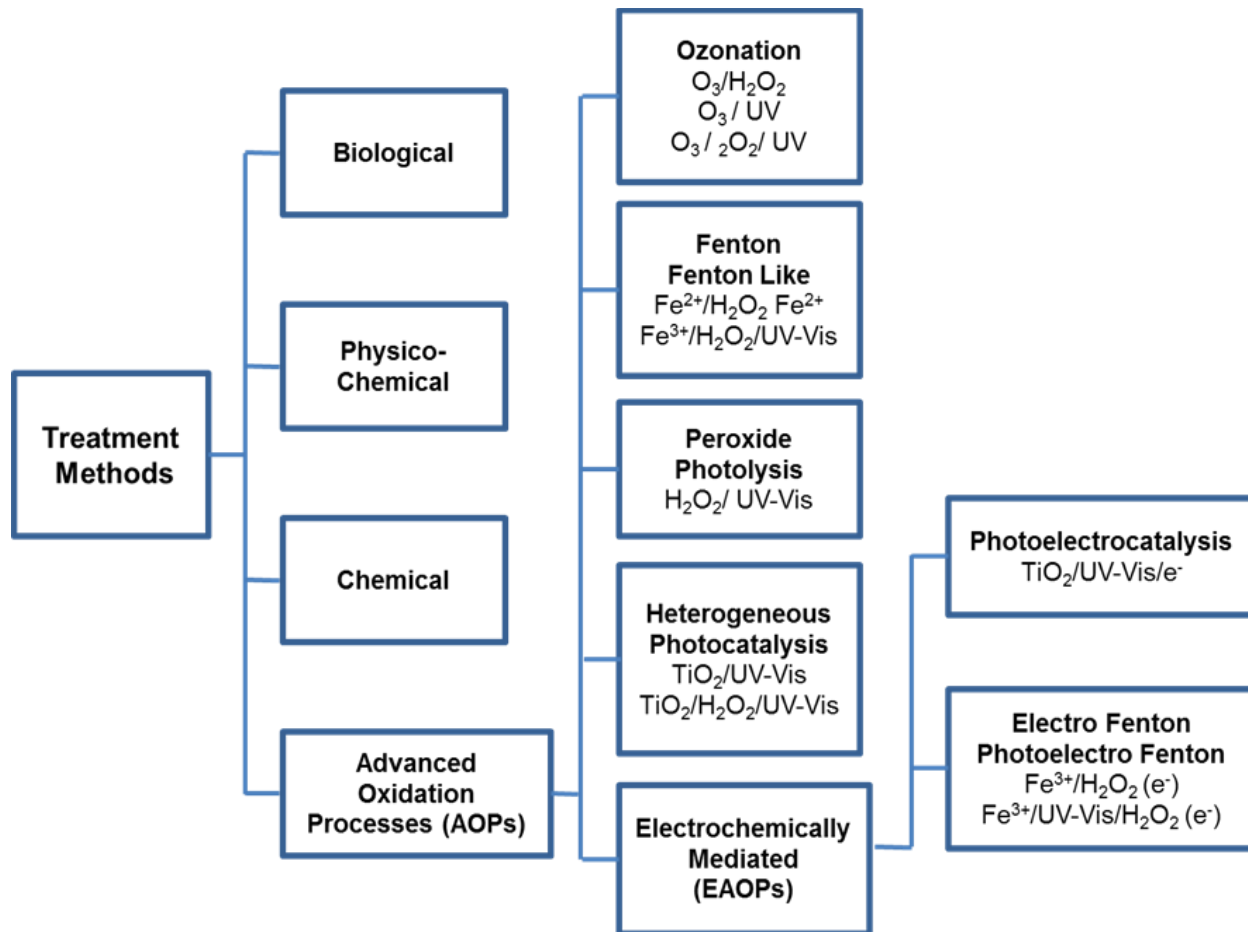


Figure 1.2: A depiction of the different classes of treatment methods with specificity to the Advanced Oxidation umbrella (Gökhan Eğilmez, Gürsel A. Sür,Özgüner, 2012).

2 CHAPTER 2: LITERATURE REVIEW

2.1 COMPARISON OF WATER TREATMENT TECHNOLOGIES

Many different technologies are available in the field of water purification. Most of which are very well established and used, in one of the three stages of water purification, depending on their ability to remove different types of pollutants. In the first two stages; systems like deposition, sedimentation and flocculation are used to remove the coarse part of organic pollutants. Tertiary purification technologies like reverse osmosis, micro-filtration, advanced biological treatments, chlorination, ozonation and UV treatment which are also called advanced oxidation processes(AOP), are used to removed pollutants that are available in trace amounts (250ppm – 1000ppm) (Rand and Company, 2006). It is at this last level of purification that titanium dioxide photocatalysis has a potentially important role in the future.

Titanium dioxide photocatalysis is said to have the potential to detoxify industrial wastewater to a lower limit of 100ppm TOC and completely mineralise pollutants ($0.01\text{ppm} < \text{TOC} < 100\text{ppm}$) in water for drinking and industrial purposes where low volumes are required per unit time (Vezzoli, 2012).

Interest towards titanium dioxide photocatalysis and AOPs has increased greatly, due to the advantages this technology offers. The more well-established technologies like reverse osmosis, membrane filtration and adsorption usually suffer from high energy consumption, necessary to overcome the pressure drop generated by the filtration media, with their major drawback being that they do not oxidise pollutants. In conventional filtration technologies, pollutants are removed from the liquid phase and concentrated in a retentate, which requires to be disposed of safely (Rand and Company, 2006).

Biological transformation using microorganisms is one of the prevalent options for the remediation of pollution caused by these toxic compounds. However, advanced biological treatments have demonstrated their inability to destroy refractory compounds coming from both industry and households; they are only effective on biodegradable compounds that can be attacked by the specific microbial system.

Another limiting factor is lag which is a phenomenon inherent to microbial kinetics. Lag can be described as a delayed response of the microbial population to a sudden change in the environment. A lag phase can occur in both growth and inactivation processes. In case of growth conditions, the lag phase is an adjustment period during which bacterial cells modify themselves in order to take advantage of a new environment and also to initiate exponential growth (Mandal *et al.*, 2010).

During the process of disinfection, strong chemical oxidants such as chlorine, ozone and hydrogen peroxide are commonly used which may result in the formation of persistent harmful disinfection by-products, depending on the pollutants found in the water. Titanium dioxide photocatalysis also produces harmful by-products however; these can be easily photocatalysed if the reaction is allowed to continue for a longer time. These chemical oxidants are hazardous and toxic and therefore require strict and costly safety measures in order to be utilized in treatment plants (Vezzoli, 2012).

Ultraviolet light in the C spectrum (UVC) is another important disinfection technology. It is an energy rich light with wavelength in the 200-400nm range. It is very versatile and has been demonstrated to effectively and efficiently disinfect water without the addition of hazardous chemicals. However, this treatment requires a great number of costly UVC germicidal lamps that have to be periodically replaced and consume large amounts of energy. In order for the treatment to be successful and achieve the inactivation of bacteria, viruses and spores, it is important that the right amount of UVC light is delivered to the pathogens. For this reason, reactors have to be carefully designed to overcome the issues posed by short penetration depth of the wavelength of light and to ensure sufficient exposition to the radiation.

UVC for wastewater treatment

Ultraviolet in sewage treatment is commonly replacing chlorination. This is in large part because of concerns that reaction of the chlorine with organic compounds in the waste water stream could synthesize potentially toxic and long lasting chlorinated organics and also because of the environmental risks of storing chlorine gas or chlorine containing chemicals. Individual waste streams to be treated by UVGI must be tested to ensure that the method will be effective due to potential interferences such as suspended solids, dyes, or other substances that may block or absorb the UV radiation. According to the World Health Organization, "UV units to treat small batches (1 to several litres) or low flows (1 to several litres per minute) of water at the community level

are estimated to have costs of US \$20 per mega litre, including the cost of electricity and consumables and the annualized capital cost of the unit."

Large-scale urban UV wastewater treatment is performed in cities such as Edmonton, Alberta. The use of ultraviolet light has now become standard practice in most municipal wastewater treatment processes. Effluent is now starting to be recognized as a valuable resource, not a problem that needs to be dumped. Many wastewater facilities are being renamed as water reclamation facilities, whether the wastewater is discharged into a river, used to irrigate crops, or injected into an aquifer for later recovery. Ultraviolet light is now being used to ensure water is free from harmful organisms.

Efficiency of the process

The effectiveness of germicidal UV depends on the length of time a microorganism is exposed to UV, the intensity and wavelength of the UV radiation, the presence of particles that can protect the microorganisms from UV, and a microorganism's ability to withstand UV during its exposure.

In many systems, redundancy in exposing microorganisms to UV is achieved by circulating the air or water repeatedly. This ensures multiple passes so that the UV is effective against the highest number of microorganisms and will irradiate resistant microorganisms more than once to break them down.

UV water treatment devices can be used for well water and surface water disinfection. UV treatment compares favourably with other water disinfection systems in terms of cost, labour, and the need for technically trained personnel for operation. Water chlorination treats larger organisms and offers residual disinfection, but these systems are expensive because they need special operator training and a steady supply of a potentially hazardous material. Finally, boiling of water is the most reliable treatment method but it demands labour, and imposes a high economic cost. UV treatment is rapid and, in terms of primary energy use, approximately 20,000 times more efficient than boiling.

UV disinfection is most effective for treating high-clarity, purified reverse osmosis distilled water. Suspended particles are a problem because microorganisms buried within particles are shielded from the UV light and pass through the unit unaffected. However, UV systems can be coupled with a pre-filter to remove those larger organisms that would otherwise pass through the UV

system unaffected. The pre-filter also clarifies the water to improve light transmittance and therefore UV dose throughout the entire water column. Another key factor of UV water treatment is the flow rate, if the flow is too high, water will pass through without sufficient UV exposure. If the flow is too low, heat may build up and damage the UV lamp.

A disadvantage of Ultraviolet germicidal irradiation (UVGI) is that while water treated by chlorination is resistant to reinfection (until the chlorine off-gasses), UVGI water is not resistant to reinfection. UVGI water must be transported or delivered in such a way as to avoid reinfection.

Advanced oxidation processes such as titanium dioxide photocatalysis, $\text{H}_2\text{O}_2/\text{UV}$, $\text{H}_2\text{O}_2/\text{O}_3$, O_3/UV and Fenton's reactions have led the way as the innovative water treatment technologies. The rationales of these AOPs are based on the insitu generation of highly reactive transitory species (i.e H_2O_2 , O_2^- , OH^\bullet , e^- , O_3) for the mineralization of refractory organic compounds, water pathogens and disinfection by-products. Titanium dioxide photocatalysis stands out as the most effective AOP and has been extensively used in water and wastewater treatment studies with great benefits arising because it is cost effective due to the 'recycle' of the catalyst against the consumption of chemicals like ozone and hydrogen peroxide. It is thermally stable, non-toxic; it is chemically and biologically inert with the possible use of solar light.

Advanced oxidation processes (AOPs) has great potential for wastewater treatment, but still limited in application due to their high cost for extensive reagent and energy demand, and restricted working conditions (e.g. narrow pH range).

A study (Li et al, 2016) found that AOPs based on pre-magnetization Fe^0 (Pre- Fe^0) were found to be highly efficient at wider pH conditions, partly solved the above problems. After pre-magnetization, Fe^0 was supposed to be easier to be corroded, which remarkably improved processes (e.g., Pre- $\text{Fe}^0/\text{H}_2\text{O}_2$, Pre- $\text{Fe}^0/\text{K}_2\text{S}_2\text{O}_8$) efficiency several to >100 folds and valid for many refractory contaminants (e.g. dyes, phenols, organic acids), compared with that conventional processes without pre-magnetization.

Another study investigated the possibility of applying photo-catalytic treatment ($\text{UV}/\text{H}_2\text{O}_2/\text{TiO}_2$) to reduce the cytotoxicity and mutagenicity as well as the microbial load of soap and detergent wastewater. The microbial load; bacterial count and total coliform tests were performed under standardized conditions. Along with toxicity appraisal, the water quality parameter such as BOD,

COD, DO, pH, TDS and TSS were also measured before and after application of UV/H₂O₂/TiO₂ treatment. A considerable reduction in cytotoxicity and mutagenicity was achieved with the maximum degradation of pollutants. With the application of advanced oxidation treatment complete removal of cytotoxicity and mutagenicity was obtained and results indicate that the advanced oxidation process can be successfully used for toxicity removal, for the improvement of water quality parameters and hence the treated wastewater could possibly be used for irrigation purposes (Iqbal et al, 2014).

Another study (Plahuta et al, 2014) aimed to compare the efficiency of BPA removal from aqueous samples with photolytic, photocatalytic, and UV/H₂O₂ oxidation. The toxicity and oestrogenic activity of BPA were largely reduced in photolytically treated samples. Photocatalytic oxidation, however, either did not reduce BPA toxic and oestrogenic effects or even increased them in comparison with the baseline, untreated BPA solution. The findings suggest that chemical analysis is not sufficient to determine the efficiency of advanced oxidation processes in removing pollutants from water and needs to be complemented with biological tests (Plahuta et al, 2014).

Solar photocatalytic treatment of real wastewater

The artificial generation of photons required for the detoxification of polluted water is the most important source of costs during the operating of photocatalytic wastewater treatment plants. This constitutes one of the major drawbacks particularly for the rapid commercialization of photocatalytic water treatment units. Solar photons have been utilized with great success for many years now as an economically and ecologically sensible light source (Bahnemann, 2004). With a typical UV-flux near the surface of the earth of 20 – 30 Wm⁻² the sun puts 0.2 – 0.3mol photons m⁻²h⁻¹ in the 300 – 400 nm range at the process disposal (Bahnemann, 1994). Principally these photons are suitable for destroying water pollutants in photocatalytic reactors (Bahnemann, 2004). Over the last 15 years several reactors for the solar photocatalytic water treatment have been developed and tested.

Despite its obvious potential for the detoxification of polluted water, there has been little commercial or industrial use of photocatalysis as a technology so far. According to a review by Goswami (Goswami, 1997) the published literature shows only two engineering scale. Demonstrations for groundwater treatment in the US and one industrial wastewater treatment in Spain. Engineering scale field experiments have been conducted by the National Renewable

Energy Laboratory (NREL) at Lawrence Livermore National Laboratory (LLNL) treating ground water contaminated with trichloroethylene (TCE) (Mehos and Turchi, 1993). Other real wastewaters that have been treated successfully with solar photocatalysis include wastewater from 5-Fluorouracil manufacturing (Anheden et al.,1996) and biologically pretreated distillery effluents (Zaidi et al., 1995).

2.2 PHOTOCATALYSIS

The AOPs especially semiconductor photocatalysis have been the focus of intense study. Photocatalysis is a green technology which works to degrade organic and inorganic pollutants essentially to water and carbon dioxide. It is used in water and air purification.

Photocatalysis may be termed as a photoinduced reaction which is accelerated by the presence of a catalyst.

In the Quantum model, a beam of radiation is regarded as a stream of photons or quanta. A photon possesses specific energy (E) but has no mass. This energy is related to the frequency of radiation (ν) by the Planck's relation;

$$E=h\nu \tag{2.1}$$

where h is Planck constant (6.63×10^{-34} Js).

These types of reactions are activated by absorption of a photon with sufficient energy (equals or higher than the band-gap energy (E_{bg}) of the catalyst). The absorption leads to a charge separation due to promotion of an electron (e^-) from the valence band of the semiconductor catalyst to the conduction band, thus generating a hole (h^+) in the valence band as shown in **Figure 2.1**.

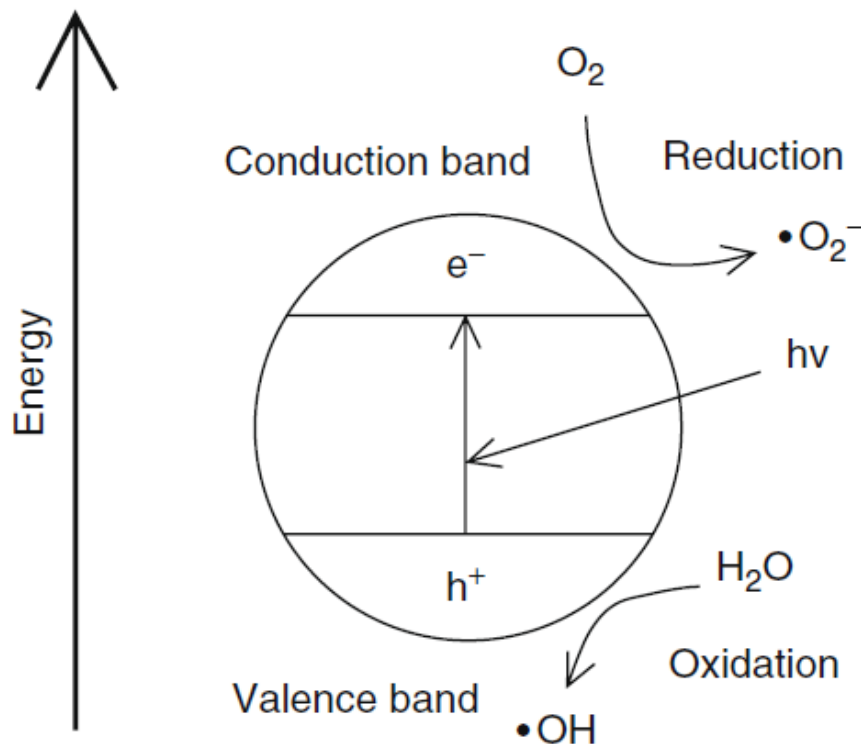


Figure 2.1: A schematic representation of the basic processes of photocatalytic water splitting on a semiconductor surface (Fujishima, Zhang and Tryk, 2008).

The recombination of the electron and the hole must be prevented as much as possible if a photocatalysed reaction must be favored. The ultimate goal of the process is to have a reaction between the activated electrons with an oxidant to produce a reduced product, and also a reaction between the generated holes with a reductant to produce an oxidized product. The photogenerated electrons could reduce the pollutant or react with electron acceptors such as O_2 adsorbed on the Ti(III)-surface or dissolved in water, reducing it to superoxide radical anion $O_2^{\bullet-}$. The photogenerated holes can oxidize the organic molecule to form R^+ , or react with OH^- or H_2O oxidizing them into OH^{\bullet} radicals. Together with other highly oxidant species (peroxide radicals) they are reported to be responsible for the heterogeneous TiO_2 photodecomposition of organic substrates. The resulting OH^{\bullet} radical, being a very strong oxidizing agent (standard redox potential +2.8 V) can oxidize most organic pollutants to the CO_2 and H_2O , destroy the cellular membrane of bacteria and deactivate viruses. Hydroxyl radicals have an oxidation potential much higher than

that of chlorine or ozone which is the most used chemicals for water purification and have already been linked to health problems in high concentrations.

Table 2.1: Common oxidants and their oxidation potentials.

<i>Oxidant</i>	<i>Oxidation potential (eV)</i>
<i>OH[•]</i>	2.27
<i>O₃</i>	2.07
<i>H₂O₂</i>	1.77
<i>Cl₂</i>	1.50
<i>Cl</i>	1.36
<i>O₂</i>	1.23

2.3 MECHANISM OF TITANIUM DIOXIDE PHOTOCATALYSIS

The relevant reactions at the semiconductor surface causing the degradation of pollutants can be expressed as follows:

Photoexcitation



Charge-carrier trapping



Electron-hole recombination



Photoexcited e^- scavenging



Oxidation of hydrolysis



Photodegradation by OH^{\cdot}



Direct photoholes



Protonation of superoxides



Co-scavenging of e⁻



Formation of H₂O₂



Equations 2.3 and 2.4 represent the surface trapped valence band electron (e⁻_{TR}) and conduction band hole (h⁺_{TR}), respectively. It was reported that these trapped carriers are usually TiO₂ surface bounded and do not recombine immediately after proton excitation (Nan *et al.*, 2010). In the absence of electron scavengers, the photoexcited electron recombines with the valence band hole in nanoseconds with simultaneous dissipation of heat energy. Therefore, the presence of electron scavengers is crucial for prolonging the recombination and successful functioning of photocatalysis.

Equation 2.6 shows how the presence of oxygen allows the formation of superoxide radical (O₂^{•-}) but prevents the recombination of electron-hole pair. The superoxide radical is further protonated to form the hydroxyperoxyl radical (HO₂[•]) and subsequently H₂O₂ as illustrated in Equation 2.11 and 2.12, respectively. The HO₂[•] radical is also reported to have scavenging property and thus, the co-existence of these radical species can doubly prolong the recombination time of the h⁺_{TR} in the entire photocatalysis reaction (Nan *et al.*, 2010). It should also be noted that all these occurrences are attributed to the presence of DO and water molecules.

2.4 SEMICONDUCTORS

Semiconductors (such as TiO_2 , ZnO , Fe_2O_3 , CdS , and ZnS) can act as sensitizers for light-induced redox-processes due to the electronic structure of the metal atoms in chemical combination, which is characterized by a filled valence band, and an empty conduction band as shown in **Figure 2.2**. Upon irradiation, valence band electrons are promoted to the conduction band leaving a hole behind. These electron–hole pairs can either recombine or can interact separately with other molecules. The holes may react either with electron donors in the solution, or with hydroxide ions to produce powerful oxidizing species like hydroxyl (oxidation potential 2.8 V) or superoxide radicals. (Kisch, 2013)

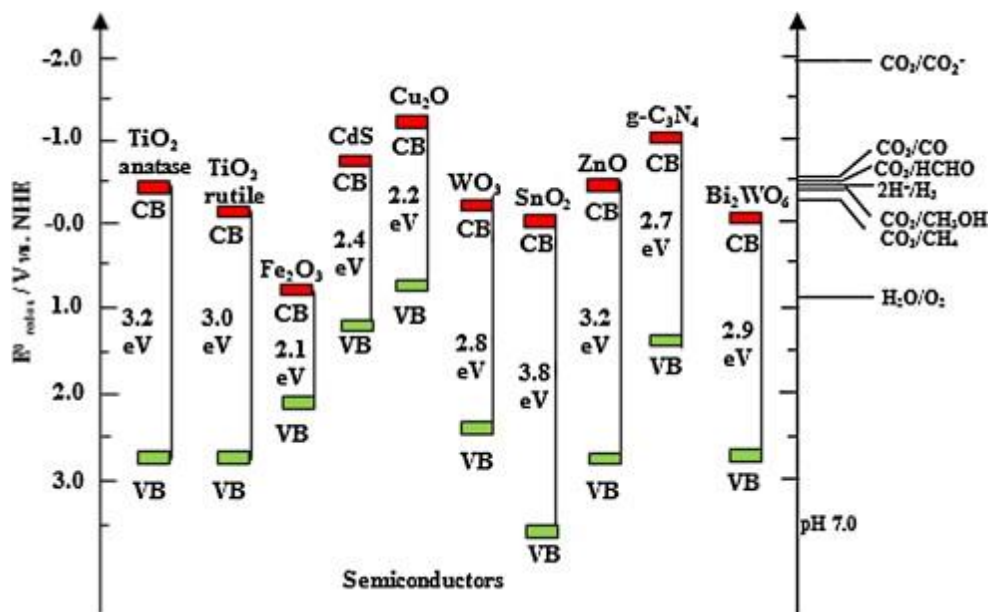


Figure 2.2: The position of different semiconductor band gap (Ola and Maroto-Valer., 2015).

In other words, semiconductor materials are materials whose valence band and conduction band are separated by an energy gap or band-gap. When a semiconductor molecule absorbs photons with energy equal to or greater than its bandgap, electrons in the valence band can be excited and jump up into the conduction band, and thus charge carriers are generated. In order to have a photocatalysed reaction, the $e^- - h^+$ recombination, subsequent to the initial charge separation, must be prevented as much as possible (Kisch, 2013; Fujishima and Zhang, 2006)

After excitation, the separated electron and hole can follow several pathways. The semiconductor can donate electrons to reduce an electron acceptor on its surface, usually oxygen in an aerated solution, while holes can oxidise an electron donor. Electron-hole recombination can happen either in the bulk or on the surface of the particles. **Figure 2.3** shows some of the de-excitation pathways for the exciton pairs. The photoinduced electron transfer to the adsorbed species or to the solvent results from migration of electrons and holes to the semiconductor surface.

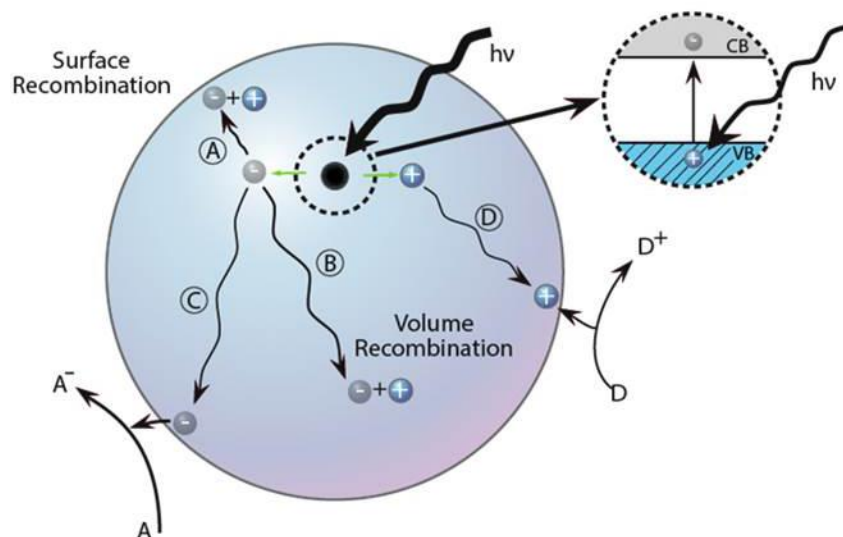


Figure 2.3: Excitation, charge recombination and reaction paths occurring on semiconductor surface (G. Cacciato *et al*, 2016).

Among all these semiconductors, the most widely used semiconductor catalyst in photoinduced processes is titanium dioxide (TiO_2). Though TiO_2 has the disadvantage of not being activated by visible light, but by ultraviolet (UV) light, it is advantageous over the others in that it is chemically and biologically inert, photo-catalytically stable, relatively easy to produce and to use, able to efficiently catalyze reactions, cheap and without risks to environment or humans.

2.5 TITANIUM DIOXIDE (TiO₂) PHOTOCATALYSIS

Titanium dioxide (TiO₂) or titania is a very well-known and well-researched material due to the stability of its chemical structure, biocompatibility, physical, optical and electrical properties. It exists in four mineral forms; anatase, rutile, brookite and titanium dioxide (B) or TiO₂(B). Anatase type TiO₂ has a crystalline structure that corresponds to the tetragonal system (with dipyramidal habit) and is used mainly as a photocatalyst under UV irradiation.

Rutile type TiO₂ also has a tetragonal crystal structure (with prismatic habit). This type of Titania is mainly used as white pigment in paint. Brookite type TiO₂ has an orthorhombic crystalline structure. TiO₂ (B) is a monoclinic mineral and is a relatively new comer to the Titania family. TiO₂, therefore is a versatile material that has applications in various products such as paint pigments, sunscreen lotions, electrochemical electrodes, capacitors, solar cells and even as a food coloring agent and in toothpastes (Fujishima, Rao and Tryk, 2000; Fujishima, Zhang and Tryk, 2008).

Table 2.2: The table reports the structural properties of the TiO₂ crystalline forms (Ola, O. and Maroto-Valer, M. M.,2015).

<i>Properties</i>	<i>Crystalline forms</i>		
	<i>Anatase</i>	<i>Rutile</i>	<i>Brookite</i>
<i>Crystalline structure</i>	Tetragonal	Tetragonal	Rhombohedral
<i>Lattice constants (nm)</i>	$a = b = 0.3733$ $c = 0.9370$	$a = b = 0.4584$ $c = 0.2953$	$a = 0.5436$ $b = 0.9166$ $c = 0.5135$
<i>Bravais lattice</i>	<i>Simple, Body centred</i>	<i>Simple, body centred</i>	<i>Simple</i>
<i>Density (g/cm⁻³)</i>	3.83	4.24	4.17
<i>Melting point (°C)</i>	<i>Turning into rutile</i>	1870	<i>Turning into rutile</i>
<i>Boiling point (°C)</i>	2927	–	–
<i>Band gap (eV)</i>	3.2	3.0	–
<i>Refractive index (n_g)</i>	2.5688	2.9467	2.8090
<i>Standard heat capacity, C^op</i>	55.52	55.60	–
<i>Dielectric constant</i>	55	110–117	78

The possible application of TiO₂ as a photocatalyst in a commercial scale water treatment facility is due to several factors:

- Photocatalytic reaction takes place at room temperature.
- It can be activated only under UV light of wavelength <387 nm irradiation due to its large band gap of 3.2 eV.
- Photocatalytic reactions do not suffer the drawbacks of photolysis reactions in terms of the production of intermediate products because organic pollutants are usually completely mineralized to non-toxic substances such as CO₂, and water.
- The photocatalyst is inexpensive and can be supported on various substrates such as, glass, fibers, stainless steel, inorganic materials, sand, activated carbons (ACs), and allowing continuous re-use.
- Photogenerated holes are extremely oxidizing and photogenerated electrons reduce sufficiently to produce superoxides from dioxygens.
- The effectiveness of TiO₂ photocatalyst can be enhanced by doping metal and non-metal ions into it.

2.6 APPLICATIONS OF UV/TiO₂ PHOTOCATALYSIS

Table 2.3: The table shows the classes of organics that have been successfully photomineralised.

<i>Alkanes</i>	<i>Phenols</i>
<i>Haloalkanes</i>	<i>Halophenols</i>
<i>Aliphatic alcohols</i>	<i>Aromatic carboxylic acids</i>
<i>Aliphatic carboxylic acids</i>	<i>Polymers</i>
<i>Alkenes</i>	<i>Surfactants</i>
<i>Haloalkenes</i>	<i>Herbicides</i>
<i>Aromatics</i>	<i>Pesticides</i>
<i>Haloaromatics</i>	<i>Dyes</i>
<i>Nitrohaloaromatics</i>	<i>Hormone</i>

The application of illuminated semiconductors for the remediation of contaminants has been used successfully for a wide variety of compounds such as alkanes, aliphatic alcohols, aliphatic carboxylic acids, alkenes, phenols, aromatic carboxylic acids, dyes, PCBs, simple aromatics, halogenated alkanes and alkenes, surfactants and pesticides **Table 2.3**) as well as for the reductive deposition of heavy metals e.g. Cr(VI) from aqueous solution to surfaces (Hoffmann *et al.*, 1995; Wang *et al.*, 2008).

2.7 PATHWAY ANALYSIS

Effective utilization of reactive species generated in-situ by photonic excitation of solid catalyst particles for the degradation of primary organic pollutants in water has been demonstrated as an effective technology for the treatment of a variety of organic pollutants in water. Degradation of organic compounds in water is often accompanied by the formation of several intermediate compounds, some of which are feared to be more toxic than the original pollutant being treated.

Effective treatment is expected to mineralise the primary pollutant and intermediate products formed during the treatment process, or reduce the pollutant/intermediates to environmentally insignificant concentrations. Profiling the intermediates produced in the course of the degradation of pollutants in water provides valuable information on the degradative pathways and the degradability of the intermediates formed (Bamuza-Pemu and Chirwa, 2013).

Although data on photocatalytic degradation of phenol are commonly available in literature (Laoufi *et al*, 2008) very few studies have reported results on the degradation pathway analysis and occurrence of potentially harmful intermediates formed during the photocatalytic degradation process.

Aromatic rings are basic constituents of many kinds of organic pollutants, such as dyes, explosives, pesticides and pharmaceuticals. The release of these compounds could largely affect the environment and human health. Accordingly, aromatic compounds are the most frequently used model substrates to investigate photocatalytic mechanisms and to test the activity of photocatalysts. Before the complete mineralization of the aromatic compounds into CO₂ and H₂O, the photocatalytic degradation proceeds through many main intermediates with different functional groups. The hydroxylation, in which the hydrogen on the aromatics is replaced by the electron-donating hydroxyl (**Figure 2.4** process I), is regarded as an important process in the degradation of aromatic contaminants, especially at the beginning stage of the reaction. On the way of mineralization, the cleavage of the aromatic ring, sometimes the hydroxylated one, to aliphatic compounds represents another critical process (**Figure 2.4** process II). The most stable intermediates after cleavage of aromatic ring should be the aliphatic carboxylates. The oxidative decarboxylation of these intermediates would lead to the formation of CO₂ and H₂O (**Figure 2.4** process III) (Pang *et al.*, 2014b).

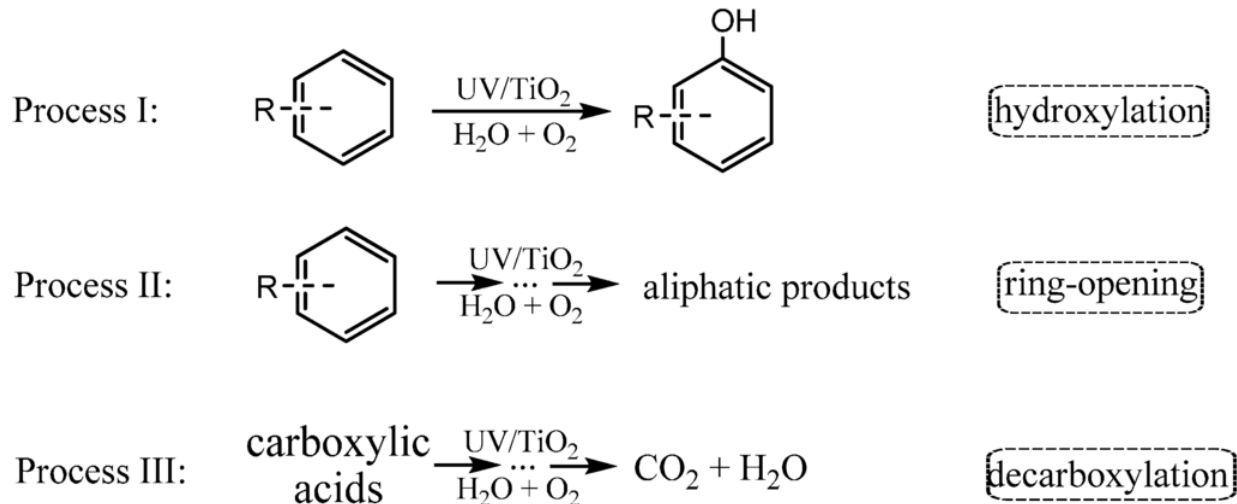


Figure 2.4: A representation of the three main processes of TiO₂ photocatalytic oxidation of aromatic compounds (Pang *et al.*, 2014b).

Photocatalytic reaction of benzene on TiO₂ is interesting for deepening the understanding of the photocatalytic reaction mechanism because it is one of the most fundamental organic materials. Clarification of the mechanism of this reaction is very important from both theoretical and practical aspects. A primary product of UV/TiO₂ photocatalytic degradation of benzene is phenol, which results from the reaction of HO[•] addition to the benzene ring. The TiO₂ photocatalysis of benzene involves HO[•] addition to form hydroxylated and polyhydroxylated adducts, which upon further oxidation can be converted into quinone type structures. Subsequent oxidation can also lead to ring open products, affording low molecular weight carboxylic acids and ultimately CO₂ (Bui *et al.*, 2010).

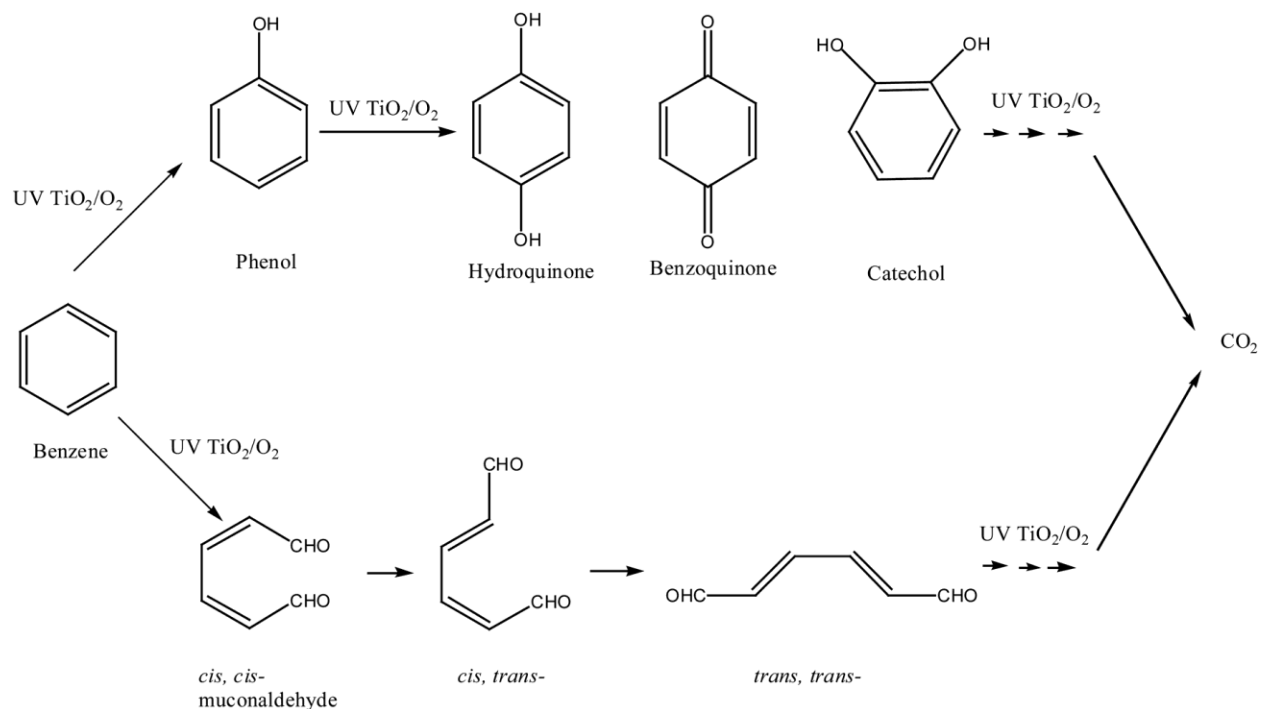


Figure 2.5: A schematic of the proposed pathways involved in the TiO₂ photocatalytic degradation of benzene.(Bui *et al.*, 2011).

In the degradation of phenol, several intermediates have been reported (**Figure 2.6**). The OH[•] radical attacks the phenyl ring of the phenol (a), yielding catechol

(b), resorcinol

(c), benzene-1,2,3-triol

(d) and hydroquinone

(e), then the phenyl rings in these compounds break up to give maleic acid

(f), then short-chain organic acids such as, 3-hydroxy propyl carboxylic acid

(g), 2-hydroxy propanal

(i), 2-hydroxy-ethanoic acid glycol acid

(j), finally CO₂ and H₂O. Even though H[•] produced during the attack of bonds by OH[•] participates in the process, it is scavenged by oxygen to form HO₂[•] radicals, which finally convert to [•]OH radicals.

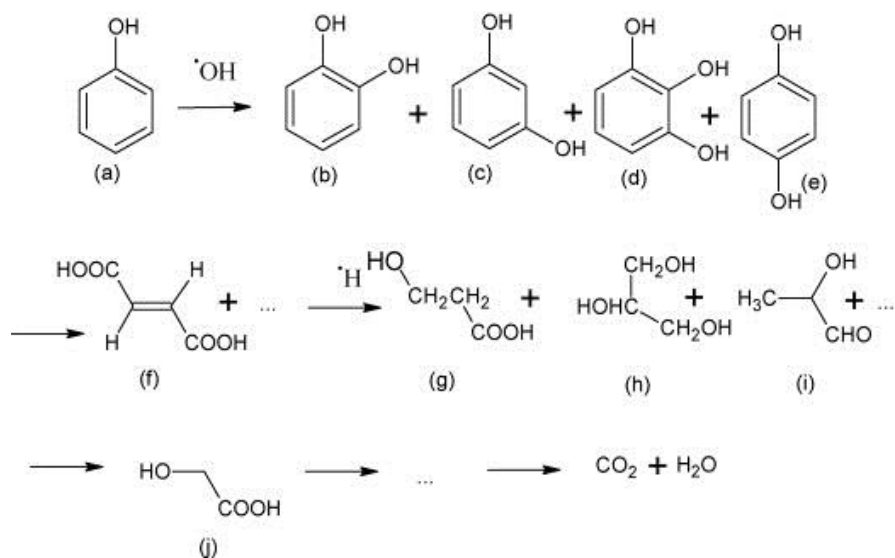


Figure 2.6: The postulated reaction pathway of phenol by the $\cdot\text{OH}$ radical (Gaya and Abdullah, 2008).

2.8 TiO_2 PHOTOCATALYTIC HYDROXYLATION OF AROMATICS

During the TiO_2 photocatalytic degradation of aromatic compounds, hydroxylation products are always the main detected intermediates. It is also accepted that the hydroxylation process is the primary one, and sometimes even the rate-determining step of the whole photocatalytic degradation reaction of aromatic compounds. Usually, the hydroxylation of aromatics is believed to be initiated by direct oxidation by $h\nu_{\text{vb}}^+$ followed by hydrolysis or the attack of $\cdot\text{OH}$ (formed from the oxidation of water by $h\nu_{\text{vb}}^+$) in the photocatalytic systems.

For substituted aromatic rings, different regioisomeric hydroxylated products (**Figure 2.7**), which usually exhibit different biological toxicity and secondary reactivity, can be formed during the photocatalytic hydroxylation (Li *et al.*, 2012). It is also noted that the selectivity of the attack to the aromatic ring in positions ortho-(o), meta-(m) and para-(p) is strongly dependent on the type of substituent (**Table 2.4**).

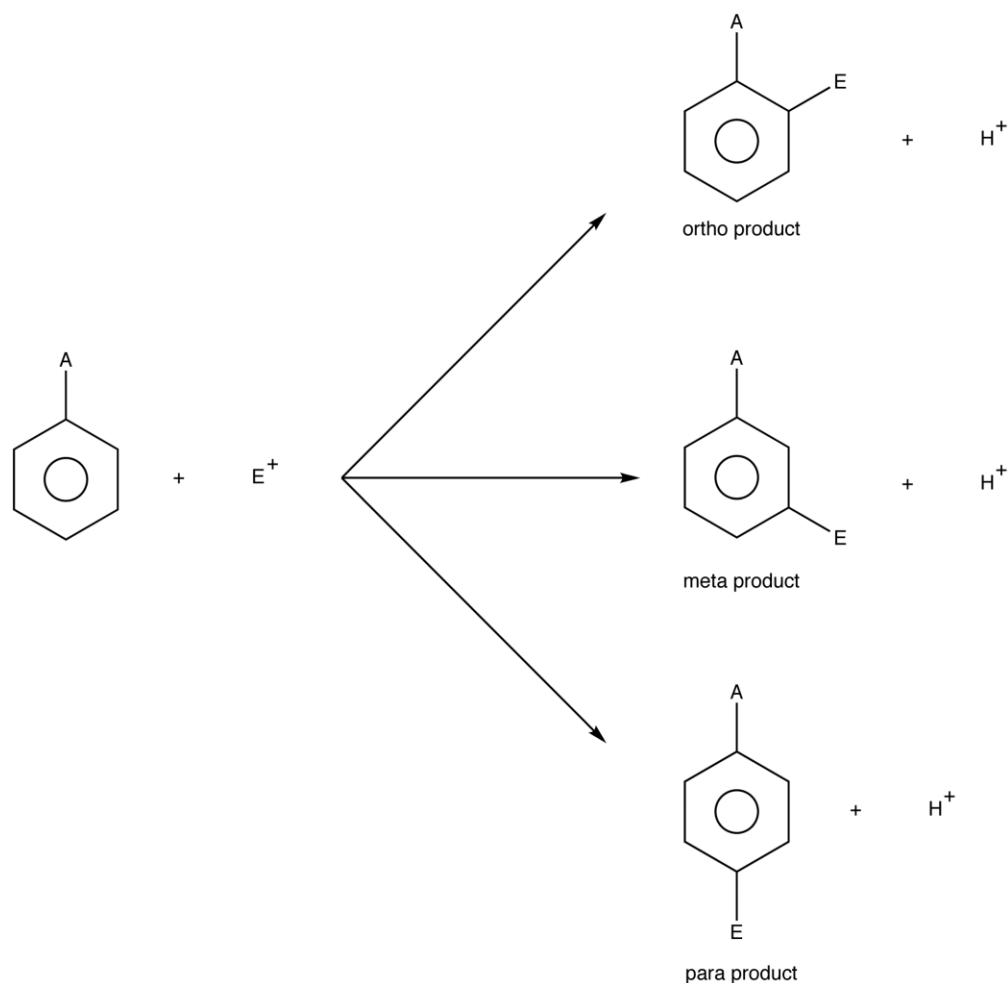


Figure 2.7: A representation of the different regioisomers of electrophilic (E^+) substitution of aromatic compounds (Palmisano *et al.*, 2006).

In a study, photocatalytic runs were performed in liquid–solid regime to oxidise aromatic compounds containing an electron donor group (phenol, phenylamine, and N-phenylacetamide) or an electron withdrawer group (nitrobenzene, cyanobenzene and 1-phenylethanone) in order to investigate the influence of the substituent on selective photocatalytic oxidation of aromatic compounds in aqueous TiO_2 suspensions (Palmisano *et al.*, 2006).

It is worth noting that the yields and o:m:p values reported in **Table 2.4** were calculated as average percentages, considering that during the first 45 min of irradiation time they did not change significantly. The yield data of monohydroxylated compounds obtained starting from aromatic substrates containing an electron donor group (EDG) indicate that the main products were ortho- and para- isomers, while the meta- isomer was not present or it was present only in very small amounts. Completely different is the behavior exhibited by the photocatalytic

oxidation when an electron withdrawer group (EWG) is present in the aromatic ring: no influence on the orientation of the monohydroxy substituent was observed, given that ortho-, meta- and para- isomers were all present in significant amounts (>20%) (Palmisano *et al.*, 2006).

This finding is confirmed by the intermediates found during photocatalytic oxidation of a large number of substituted aromatic compounds, using different kinds of TiO₂ under various experimental conditions (Bamuza-Pemu and Chirwa, 2012).

It is furthermore reported that the presence of both an EDG and an EWG gives rise to behaviour similar to that observed when only an EDG is present. In summary it was proved that the reaction of monohydroxylation of an aromatic ring occurs in all the three possible positions when a EWG is present, while only the formation of ortho and para-isomers virtually occurs when an EDG is present (**Table 2.4**).

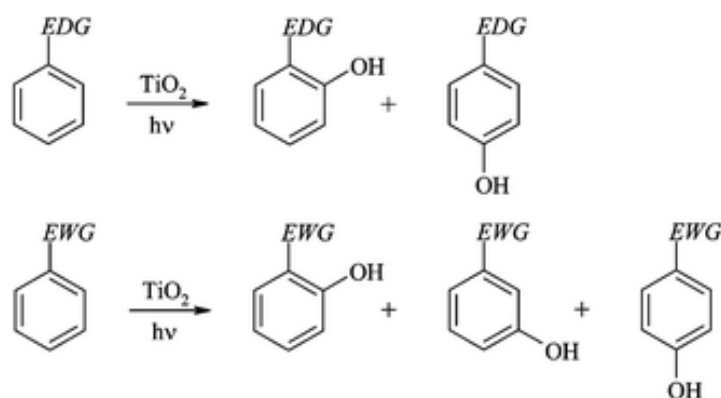


Figure 2.8: The main hydroxylated products obtained during the photocatalytic oxidation of aromatic compounds containing either an EDG or EWG (Palmisano *et al.*, 2006).

This gives perspective to produce monohydroxylated compounds with high conversions and yields starting from aromatics with an EDG, and also allows for the prediction of intermediate products through which the photo-oxidation of aromatic compounds evolves.

Table 2.4: The table reports the yields obtained for each aromatic compound and the ortho:meta:para ratios under irradiation (Palmisano *et al.*, 2006).

<i>Species</i>	<i>Group</i>	<i>Orientation</i>	<i>Conversion(%)</i>	<i>Total yield (%) in OH-derivatives</i>	<i>o:m:p Ratio</i>
<i>Phenol</i>	<i>-OH (EDG)</i>	<i>ortho, para</i>	<i>~70</i>	<i>~75</i>	<i>55:1:45</i>
<i>Phenylamine</i>	<i>-NH₂ (EDG)</i>	<i>ortho, para</i>	<i>~40</i>	<i>~50</i>	<i>50:0:50</i>
<i>N-Phenylacetamide</i>	<i>- NHCOCH₂(ED G)</i>	<i>ortho, para</i>	<i>~50</i>	<i>~60</i>	<i>20:3:77</i>
<i>Nitrobenzene</i>	<i>-NO₂ (EWG)</i>	<i>-</i>	<i>~50</i>	<i>~20</i>	<i>29:34:37</i>
<i>Cyanobenzene</i>	<i>-CN (EWG)</i>	<i>-</i>	<i>~60</i>	<i>~30</i>	<i>45:30:25</i>
<i>1-Phenylethanone</i>	<i>-COCH₃ (slightly EWG)</i>	<i>-</i>	<i>~55</i>	<i>~30</i>	<i>39:21:41</i>

Fig 2.9 shows the proposed reaction pathways for oxidation of phenol in the TiO₂ photocatalytic system in an argon atmosphere. The basic idea is that the initiation of phenol polymerization involves a surface reaction of adsorbed phenol to form phenoxy radicals, which can be further oxidized to dihydroxylic benzenes or to produce dimeric compounds. This pathway is proven by the detection of hydroquinone, resorcinol, biphenol and phenoxy phenol in the reaction suspension after brief illumination (Palmisano *et al.*, 2006). As these coupled phenol units have a lower oxidation potential than phenol, they are more readily oxidized to radicals. Chain propagation results when fresh phenol diffuses to the surface and reacts with the monomer, dimer or oligomer radicals. As the hydrophobicity of the polymer increases with chain propagation, adsorption of the phenolic polymer on TiO₂ is favored in the aqueous solution as water is a poor solvent for the phenolic polymer. Besides, photocatalytic oxidative polymerization of other monomers using semiconductor has also been documented (Ng *et al.*, 2012).

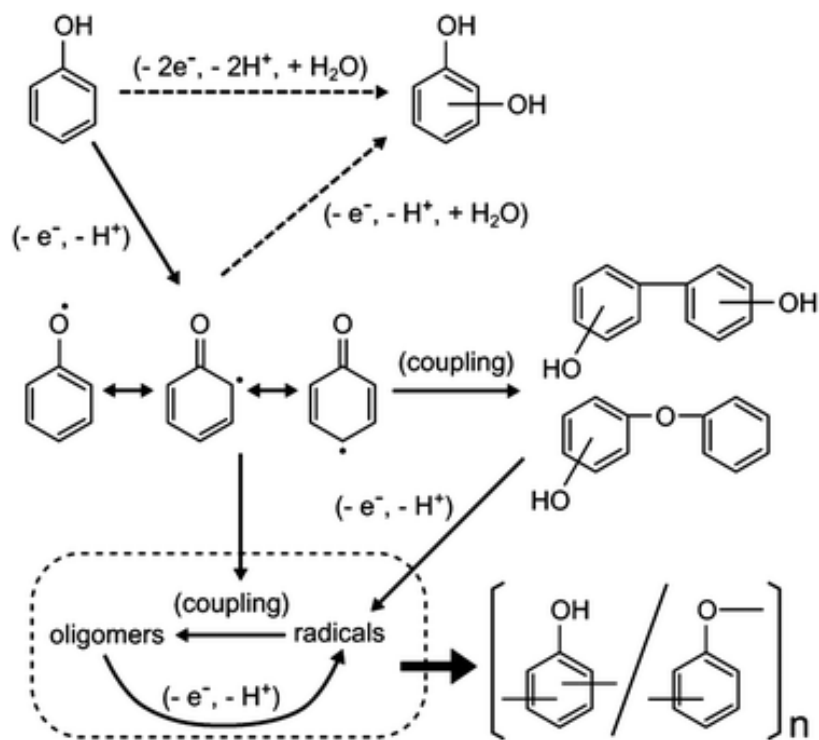


Figure 2.9: Representation of the postulated reaction pathways for oxidation of phenol in the TiO₂ photocatalytic system. (Ng *et al.*, 2012).

2.9 PHOTOCATALYTIC CLEAVAGE OF AN ARYL-RING ON TiO₂ SURFACE

Another essential step on the way to the complete mineralization of aromatic pollutants into CO₂ is ring opening, which involves the C-C bond cleavage of aryl rings and is more complex than the hydroxylation process. Accordingly, the understanding on the mechanism of cleavage of aryl ring is even poorer. Researchers believe that the ·OH radicals are the main active oxygen species in the ring-opening step due to their high oxidative ability (Pang *et al.*, 2014b). However, recent electrochemical studies suggest that the aromatic rings cannot be efficiently cleaved by the ·OH radicals in the absence of O₂, indicating the ·OH radicals are not a good active species for the cleavage of aryl rings. Other reports also argued that the reaction of the O₂-derived species, such as superoxide or singlet oxygen, with aromatics is the main pathway in photocatalytic ring-opening step (Pang *et al.*, 2014b). It is also considered that both the ·OH radicals and O₂ are both important in the aromatic ring cleavage, *i.e.*, ·OH radicals attack the aromatic ring, and the cleavage results from the reaction of the radicals formed by OH-attack and O₂. As a matter of fact, whether ·OH radical or O₂ ultimately breaks the C-C bond of aromatic ring is still experimentally under debate

and the mechanism of the ring-opening reaction in most reports remains somewhat speculative. Another popular mechanism in the ring-opening step for TiO₂ photocatalysis is that the superoxide radical anion, generated from the reduction of O₂ by e_{cb}⁻, reacts with substrate radical cation which is formed from oxidation of the substrate by h_{vb}⁺, to form a dioxetane intermediate, then homolytic cleavage of the C-C bond leads to the formation the muconaldehyde (figure 2.10) (Pang *et al.*, 2014b).

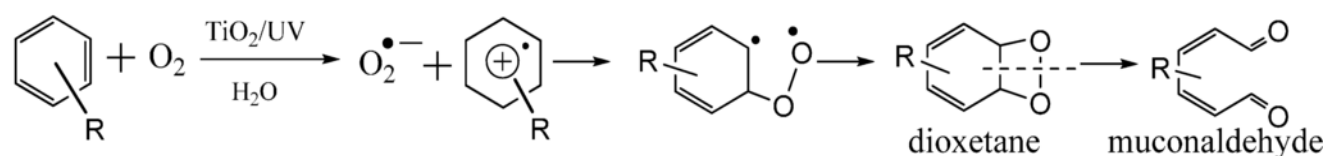


Figure 2.10: The proposed mechanism for TiO₂ photocatalytic cleavage of aryl-ring via a dioxetane intermediate (Pang *et al.*, 2014b).

In aqueous solution, the detected initial ring-opening products are always carboxylic acids or carboxylic acid derivatives, instead of the expected dialdehyde, probably because the aldehyde is an unstable intermediate and it can be rapidly converted into a stable carboxylic acid under photocatalytic conditions. Another possibility for the low yield of the aldehyde was attributed to the hydroxylation of the aromatic ring before the cleavage, while the ring cleavage still occurs via a dioxetane intermediate process. The muconaldehyde intermediate was detected during the cleavage of benzene rings by TiO₂ photocatalysis although its yield is also very low in aqueous solution. Unfortunately, the origin of O atoms introduced into the muconaldehyde could not be tracked due to the fast oxygen exchange between carbonyl groups of the muconaldehyde and water. In order to track the ring-open pathway by avoiding the oxygen exchange between the products and the solvent, the *ortho*-dihydroxybenzenes were used as model substrates, because the oxidative cleavage of *ortho*-dihydroxy-benzenes would form directly the muconic acid which cannot exchange its oxygen atom with H₂O (Pang *et al.*, 2014b). Therefore, the behaviours of oxygen in the ring-opening products can be definitely tracked by the ¹⁸O-labeling methods in the aqueous TiO₂ photocatalytic system.

Among the numerous *ortho*-dihydroxyl substituted benzenes, 3,5-di-*tert*-butylcatechol (DTBC) is an ideal molecular probe for the ring-cleavage, because its substituents can distinguish the ring-opening position and the steric effect of bulky *t*-butyl groups also can induce the primary ring-

opening reaction with unexpectedly high yields. Moreover, the pathway for oxidative cleavage of aromatic ring of DTBC has been extensively studied in the systems of catechol oxygenases and its artificially synthesised iron-containing analogues (Pang *et al.*, 2014b).

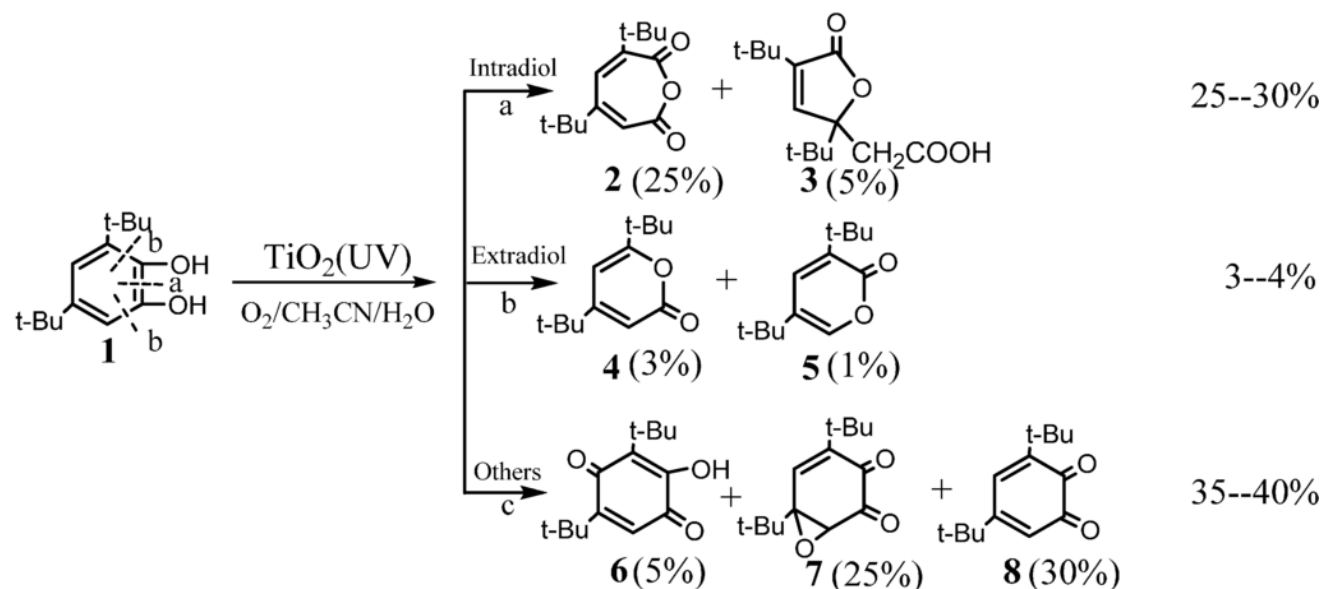


Figure 2.11: A representation of the structures of the main intermediate products of photocatalytic cleavage of 3,5-di-tert-butylcatechol (DTBC) by TiO₂, with the main products divided into three groups (a, b and c) and the values in brackets indicating the highest (Pang *et al.*, 2014b).

Figure 2.11 illustrates the main oxidation products generally divided into three groups:

- Products 2 and 3 are the primary ring-opening products without the loss of a carbon atom, and they are generally intradiol products, which means that the O-atom was inserted into the C-C bond between the two *ortho* hydroxyls;
- Products 4 and 5 have a loss of one carbon relative to their matrix and are generally extradiol products because the O-atom is inserted into the C-C bond out of the two hydroxyls; and
- Products 6–8 are the products by simple oxidation of the DTBC in which no aromatic C-C bond is completely broken. The yields of these products are known to change over a wide range, dependent on the reaction conditions, oxidation systems and reaction mechanisms.

2.10 TiO₂ PHOTOCATALYTIC DECARBOXYLATION OF CARBOXYLIC ACIDS

The observed initial ring-opening products of aromatic compounds in aerated aqueous solutions are always carboxylic acids or carboxylic acid derivatives. Thus decarboxylation of these carboxylic acids is one of the most important steps for complete mineralization of organic pollutants. The most accepted mechanism for decarboxylation is through the Photo-Koble reactions, which is initiated by the hole ($h_{\nu b}^+$) oxidation of the carboxylic acids to release the CO₂ and alkyl radicals. In the presence of O₂, the alkyl radicals react with O₂ to form the peroxy radicals, and then decompose to hydroxylated and carbonylated intermediates via quaternion peroxide intermediates by the Russell mechanism.

2.10.1 Schmitt Reaction (Kolbe Process)

A reaction for adding a carboxyl group onto the benzene ring of a phenol, figure 2.12. This reaction is carried out for the industrial synthesis of salicylic acid to be converted into aspirin.

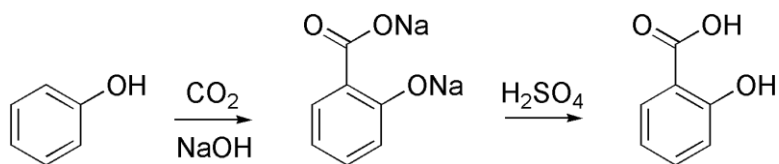


Figure 2.12: The carboxylation of phenol to salicylic acid for the industrial synthesis of aspirin (Hermann Kolbe, 1860; R.Schmitt, 1885).

The mechanism for the Kolbe-Schmitt reaction begins with deprotonation of phenol by hydroxide ion (a strong base) to give phenoxide (the conjugate base of phenol). Phenoxide (an alkoxide and enolate nucleophile) adds to carbon dioxide to give a carboxylate. Aqueous sulfuric acid (a strong acid) protonates the carboxylate. Acid-catalyzed tautomerization then restores aromaticity.

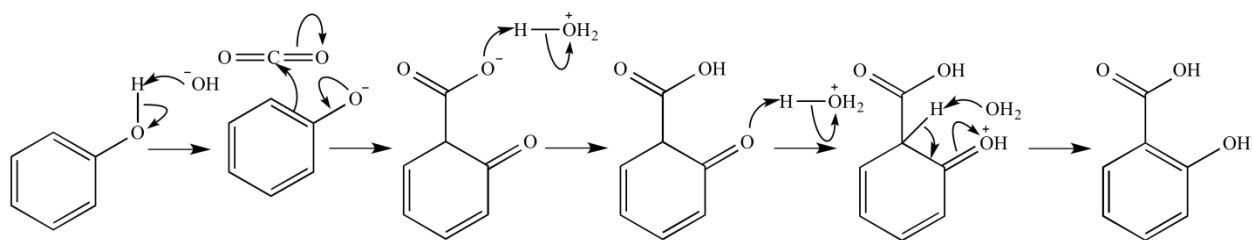


Figure 2.13: A detailed reaction mechanism of the formation of salicylic acid by phenol carboxylation. (Hermann Kolbe, 1860; R.Schmitt, 1885).

2.10.2 Russell Mechanism

Figure 2.13 illustrates the proposed Russell mechanism for the bimolecular reaction of primary and secondary peroxy radicals ($\text{ROO}\cdot$) involving a cyclic mechanism from a linear tetraoxide intermediate (ROOOOR) and the corresponding products: alcohol (ROH), ketone (RO) and O_2 ; or alcohol (ROH), excited ketone (RO^*) and O_2 .

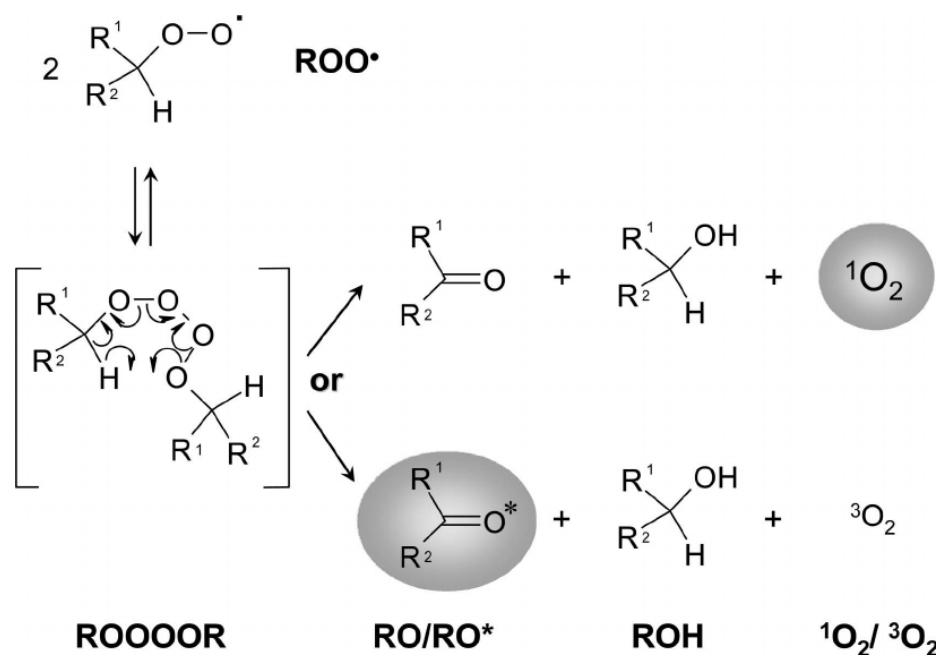


Figure 2.14: A schematic diagram of the Russell Mechanism (Miyamoto *et al.*, 2014).

2.11 ISOTOPIC LABELLING FOR STUDYING REACTION MECHANISM

Isotopic labeling is used to monitor the fate of a molecule or a fragment thereof through the use of detection methods that specifically distinguish the isotope used against a natural abundance background. There are many applications for the specific labeling of molecules with radioactive or stable isotopes. The technique can be used to prepare substrates for the study of reaction mechanism, in either an artificial or a biological medium. It can also be used to trace the movement of a molecule, or its degradation or metabolic product, in vivo, in vitro, or in the environment. In the medical field, a variety of imaging techniques have been developed that rely on materials labeled with radioactive isotopes. The use of radiolabeled compounds is also of critical importance in the drug development process for use as radioligands in lead discovery, as metabolic tracers in development, and in phase IV clinical studies. They play a similar role in the compound development process for crop protection chemicals, used in metabolic investigations and environmental fate studies.

A study used ^{13}C isotope labeling to establish different pathways involved in the formation of reaction products, muconaldehyde and phenol (**Figure 2.5**). It was found that muconaldehyde could be readily oxidized to the corresponding carboxylic acids, with extensive oxidation leading to CO_2 as final product. The reaction pathways leading to muconaldehyde account for 60–70% and pathways via phenol account for 30–40% of benzene consumption (Bui *et al.*, 2010).

Another study used the oxygen-18 isotopic labeling method to investigate the oxidation process on the three representative photocatalytic reactions as shown in **Figure 2.4**. The results show that the oxygen atoms of molecular oxygen can incorporate into the corresponding products in aqueous solution in all three of these reactions, but the detailed incorporation pathways are completely different in each case (Li *et al.*, 2012). For the hydroxylation process, the O atom in O_2 is shown to be incorporated through activation of O_2 by conduction band electrons. In the cleavage of aryl rings, O atoms are inserted into the aryl ring through the site-dependent coordination of reactants on the TiO_2 surface. A new pathway for the decarboxylation of saturated carboxylic acids with pyruvic acid as an intermediate was identified, and the O_2 is incorporated into the products through the further oxidation of pyruvic acid by active species from the activation of O_2 by conduction band electrons (Pang *et al.*, 2014b).

2.12 FACTORS AFFECTING THE OPERATION OF A PHOTOCATALYTIC REACTOR

2.12.1 Catalyst Loading

Concentration of TiO_2 in the photocatalytic water treatment system affects the overall photocatalysis reaction rate in a true heterogeneous catalytic regime, where the amount of TiO_2 is directly proportional to the overall photocatalytic reaction rate (Gaya and Abdullah, 2008). A linear dependency holds until certain extent when the reaction rate starts to aggravate and becomes independent of TiO_2 concentration.

This is attributed to the geometry and working conditions of the photoreactor where the surface reaction is initiated upon light photon absorption (Bamba *et al.*, 2008). When the amount of TiO_2 increases above a saturation level (leading to a high turbidity state), the light photon absorption coefficient usually decreases radially.

The excess TiO_2 particles can create a light screening effect that reduces the surface area of TiO_2 being exposed to light illumination and the photocatalytic efficiency. Therefore, any chosen photoreactor should be operated below the saturation level of TiO_2 photocatalyst used to avoid excess catalyst and ensure efficient photons absorption. In this sense, both catalyst loading and light scattering effect can be considered as a function of optical path length in the reactor.

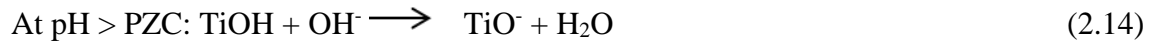
2.12.2 Reaction pH

In heterogeneous photocatalytic water system, pH is one of the most important operating parameters that affect the charge on the catalyst particles, size of catalyst aggregates and the positions of conductance and valence bands. Due to the nature of TiO_2 catalyst used, any variation in the operating pH is known to affect the isoelectric point or the surface charge of the photocatalyst used. Many reports have used the point of zero charge (PZC) of TiO_2 to study the pH impact on the photocatalytic oxidation performance (Chong *et al.*, 2009b,c; Ochuma *et al.*, 2007; Chin *et al.*, 2006; Toor *et al.*, 2006).

The PZC is a condition where the surface charge of TiO_2 is zero or neutral that lies in the pH range of 4.5 - 7.0, depending on the catalysts used. At PZC of TiO_2 , the interaction between the photocatalyst particles and water contaminants is minimal due to the absence of any electrostatic force. When operating $\text{pH} < \text{PZC} (\text{TiO}_2)$, the surface charge for the catalyst becomes positively

charged and gradually exerted an electrostatic attraction force towards the negatively charged compounds.

Such polar attractions between TiO_2 and charged anionic organic compounds can intensify the adsorption onto the photon activated TiO_2 surface for subsequent photocatalytic reactions (Xu and Langford, 2000; Gogniat *et al.*, 2006). This is particularly significant when the anionic organic compounds present in a low concentration level. At $\text{pH} > \text{PZC} (\text{TiO}_2)$, the catalyst surface will be negatively charged and repel the anionic compounds in water. Different pH will affect the surface charge density of the TiO_2 catalyst (Rincón and Pulgarin, 2004), according to the following water equilibrium equations (Eqs. 12 and 13);



2.12.3 Temperature

Numerous studies have been conducted on the dependence of photocatalytic reaction on the reaction temperature (Muradov *et al.*, 1996; Fu *et al.*, 1996; Chen and Ray, 1998; Rinco'n and Pulgarin, 2003; Evgenidou *et al.*, 2005). Although heat energy is inadequate to activate the TiO₂ surface, the understanding on such dependency could be extrapolated when operating the process under natural sunlight illumination. Most of the previous investigations stated that an increase in photocatalytic reaction temperature (>80°C) promotes the recombination of charge carriers and disfavours the adsorption of organic compounds onto the TiO₂ surface (Gaya and Abdullah, 2008). At a reaction temperature greater than 80°C, the photocatalytic reaction is interpreted with Langmuir-Hinshelwood (L-H) mechanism where the adsorption of the reactants is disfavoured resulting in KC becomes "1". This will reduce the L-H expression (Eq. 2.16) into the apparent rate equation

$$r = -\frac{dC}{dt} = k_r \theta_x = \frac{k_r KC}{1+KC} \quad (2.13)$$

$r = \frac{1}{4} k_{\text{apparent}} C$. Where;

k_r – limiting rate constant of reaction at maximum coverage under given experimental conditions.

K – equilibrium constant for adsorption of substrate onto catalyst.

C – substrate concentration at time t during degradation, mg/L.

r – rate of reaction, mg/L

All these drastically reduce the photocatalytic activity of TiO₂ when the reaction temperature rises. The desorption of degraded products from the TiO₂ surface is the rate-limiting step when temperatures rise. On the contrary, a low temperature below 80°C actually favours adsorption which is a spontaneous exothermic phenomenon, resulting in getting KC of L-H model $\ll 1$, enhancing the adsorption of final reaction products. A further reaction in temperature down to 0°C will cause an increase in the apparent activation energy. As a consequence, the optimum reaction temperature for photomineralisation is reported to be in the range of 20-80°C (Malato *et al.*, 2009).

2.12.4 Dissolved Oxygen

Dissolved oxygen (DO) plays an important role in TiO₂ photocatalysis reaction to assure sufficient electron scavengers present to trap the excited conduction-band electron from recombination (Chong *et al.*, 2009b). The oxygen does not affect the adsorption on the TiO₂ catalyst surface as the reduction reaction takes place at a different location from where oxidation occurs (Malato *et al.*, 2009). Other roles for DO may involve in the formation of other reactive oxygen species (ROS) and the stabilization of radical intermediates, mineralization and direct photocatalytic reactions. The total amount of DO in a reactor depends on a few technical considerations. For a photoreactor, the total delivered DO not only acts as an electron sink but also provides sufficient buoyant force for complete suspension of TiO₂ particles. Photoreactor sparging with pure oxygen in TiO₂ slurry reactor is usually a cost-ineffective solution, as the amount of DO being held-up is a function of the photoreactor geometry. The difference between the two sparging media of air and oxygen is usually not very drastic as the mass transfer of oxygen to the close vicinity of the surface is the rate dependent step (Habibi *et al.*, 2005).

2.12.5 Contaminants and Their Loading

Previous investigations (Skaf *et al.*, 2016) have reported the dependency of the TiO₂ photocatalytic reaction rate on the concentration of water contaminants. Under similar operating conditions, a variation in the initial concentration of the water contaminants will result in different irradiation time necessary to achieve complete mineralization or disinfection. Owing to the photonic nature of the photocatalysis reaction, excessively high concentration of organic substrates is known to simultaneously saturate the TiO₂ surface and reduce the photonic efficiency leading to photocatalyst deactivation (Nan *et al.*, 2010).

Not all organic substrates will have such profound effect on the irradiation time, and this also depends on the corresponding chemical nature of the targeted compounds for TiO₂ photocatalysis reaction. In example, 4-chlorophenol will undergo a degradation pathway with constant evolution of intermediate(s) product (i.e. hydroquinone and benzoquinone) while oxalic acid will undergo direct transformation to carbon dioxide and water (Bahnemann, 2004). In the case of 4-chlorophenol, such evolution of intermediate(s) will further prolong the irradiation time necessary for total mineralization owing to the direct competition over unselective TiO₂ surfaces. In the development of mathematical model that represents the kinetics of mineralization while relating to the TiO₂ loading required, commonly used water quality parameters such as chemical oxygen

demand (COD), total organic carbon (TOC) or dissolved organic carbon (DOC) could be more appropriate to account for such competitiveness of intermediate(s) with its predecessor compounds. Also organic substrates with electron-withdrawing nature such as benzoic acid and nitrobenzene were found to strongly adhere and more susceptible to direct oxidation than those with electron donating groups (Bhatkhnade *et al.*, 2004).

2.12.6 Light Intensity

The photonic nature of the photocatalysis reaction has outlined the dependency of the overall photocatalytic rate on the light source used. Light intensity is one of the few parameters that affect the degree of photocatalytic reaction on organic substrates. Fujishima *et al.* (2000), indicated the initiation of TiO₂ photocatalysis reaction rates is not highly dependent on light intensity, where a few photons of energy (i.e. as low as 1 mW cm⁻¹) can sufficiently induce the surface reaction. To achieve a high photocatalytic reaction rate, particularly in water treatment, a relatively high light intensity is required to adequately provide each TiO₂ surface active sites with sufficient photons energy required. However, when using the nominal TiO₂ particles without modifications, the surface reaction is restricted to photons with wavelengths shorter than the absorption edge of approximately 400 nm. The organic conversion in the presence of UV wavelength ($\lambda < 400$ nm) in many studies obeyed the linear proportionality correlation to the incident radiant flux (Nan *et al.*, 2010).

2.12.7 Turbidity

Turbidity often refers to the insoluble particulates that are present in the targeted water.(Rand and Company, 2006) The presence of such insoluble particulate matters are highly detrimental to the TiO₂ photocatalysis based process, as they can affect the optical properties and further impede the penetration of UV light by strong scattering and absorption of the rays (Bamuza-Pemu and Chirwa, 2013). This will cause a variation in the predicted use of TiO₂ loading, UV penetration path and light intensity. Also, excessive levels of turbidity can reduce the photomineralisation of the pollutants present in water owing to the shielding effects that attenuate the light penetration causing those pollutants to flee from the treatment.

2.13 REACTOR DESIGN CHALLENGES

Several factors impede the efficient design of a photocatalytic reactor. The problem of scaling up multiphase photocatalytic reactors is considerably more complex than that of scaling up conventional chemical reactors or homogeneous photoreactors. The need to utilise a solid catalyst makes the entire problem quite complicated as another phase is added to the system. Besides the requirement for good contact between reactants and catalysts, it is also necessary to achieve efficient exposure of the catalyst to light irradiation (Kobayakawa *et al.*, 1998; Li *et al.*, 2014).

In fact, in a photocatalytic reactor, besides the conventional reactor complications, such as reactant-catalyst contacting, flow patterns, mixing, mass transfer reaction kinetics, catalyst installation, temperature control, etc., an additional engineering factor related to the illumination of the catalyst becomes relevant. Without photons of appropriate energy content, the catalyst shows no activity. The problem of photon energy absorption has to be considered regardless of reaction kinetics mechanisms. The illumination factor is of utmost importance since the amount of catalyst that can be activated determines the water treatment capacity of the reactor (Hänel *et al.*, 2010; Vaiano *et al.*, 2015). The high degree of interaction between the transport processes, reaction kinetics and light absorption leads to a strong coupling of physicochemical phenomena and no doubt, it is the major obstacle in the development of a photocatalytic reactor.

The central problem in a photocatalytic reactor is focused on a uniform distribution of light to a large surface area of the catalyst. For the particular photoreactor geometry, scale-up in the axial and/or radial directions is constrained by the phenomenon of opacity, light scattering, depth of radiation penetration and local volumetric light absorption. The arrangement of the light source/reactor system influences the reactor design in such a strong way that independent consideration is not possible. Moreover, the need for at least one of the reactor walls to transmit the chosen radiation imposes the utilization of transparent materials, such as glass for the reactor construction, and thus imposes size limitations, sealing problems, and breakage risks (Nan *et al.*, 2010; Vezzoli, 2012).

Photocatalytic reactions are promoted by solid photocatalyst particles that usually constitute the discrete phase distributed within a continuous fluid phase in the reactor. Therefore, at least

two phases, i.e. liquid and solid, are present in the reactor. The solid phase could be dispersed (SPD) or stationary (SPS) within the reactor. SPD photoreactors may be operated with the catalyst particles and the fluid phase(s) agitated by mechanical or other means. Depending on the means of agitation, the photoreactor resembles slurry or fluidized bed reactors. In numerous investigations, an aqueous suspension of the catalyst particles in immersion- or annular-type photoreactors has been used (Nan *et al.*, 2010). However, the use of suspensions requires the separation and recycling of the ultrafine catalyst from the treated liquid and can be an inconvenient, time-consuming, expensive process. In addition, the depth of penetration of UV light is limited because of the strong absorption by both catalyst particles and dissolved organic species. The above problems could be avoided in SPS photoreactors in which the photocatalyst particles are immobilized onto a fixed transparent surface, such as the reactor wall or a fibre mesh, or are supported on particles, such as glass or ceramic beads, that are held in fixed positions in the photoreactor. However, the immobilization of the catalyst on a support generates a unique problem. The reaction occurs at the liquid-solid interface and usually only a part of the catalyst is in contact with the reactant. Hence, the overall rate may be limited to mass transport of the pollutant to the catalyst surface (Behnajady *et al.*, 2007). In addition, the rate of reaction is usually slow because of the low concentration level of the pollutant and therefore, there is a need for a reactor whose design provides a high ratio of illuminated immobilized catalyst to illuminated surface and the possibility of total reactor illumination.

The development of a reliable knowledge base is still in its initial stage related to the catalyst preparation and its activation, chemistry and kinetic networks of the pollutant degradation, intrinsic reaction kinetics that at times is mass-transfer-controlled, the process of photon energy absorption, and reactor design.

3 CHAPTER3: METHODS AND MATERIALS

3.1 BATCH EXPERIMENTS

3.1.1 Chemical Reagents

Phenol reagent was purchased from Merck (Johannesburg, South Africa). HPLC grade acetonitrile was purchased from Glassworld (99.9 % purity). All solutions were prepared using ultrapure water produced in a Milli-Q, Millipore Direct Q3 Unit (supplied by Microsep, Johannesburg, South Africa). Hydrochloric acid (32%) and sodium hydroxide pellets were purchased from Glassworld. Methanol GC grade was purchased from Glassworld (99.9% purity). Rutile TiO₂ (99.5%), Anatase TiO₂ (99.8%) and P-25 Degussa TiO₂ were purchased from Sigma-Aldrich Pty Ltd.

3.1.2 Experimental Methods

Degradation studies were conducted in a batch reactor as shown in **Figure 3.1** with photons for catalyst activation supplied by a medium pressure 400 W UV lamp immersed in the pollutant solution housed in a double jacket quartz sleeve, which served as the cooling system for the lamp. Temperature control in the reactor was achieved by circulating cold water through the outer cavity of the quartz sleeve. The reactor contents in all batches were aerated at a flow rate of 10 mL/min. Thorough mixing of the contents of the reactor was achieved by continuous agitation with a magnetic stirrer. The experimental reaction time was set at 60-100 minutes. Aliquots of 2ml were withdrawn from the reactor at timed intervals using a micro-syringe for further analysis.

Particulate matter was removed by filtration through a 0.45µm syringe filter (Millipore) before analysis. Degradation intermediates formed were monitored by High Performance Liquid Chromatography (HPLC) and GC-MS analysis.

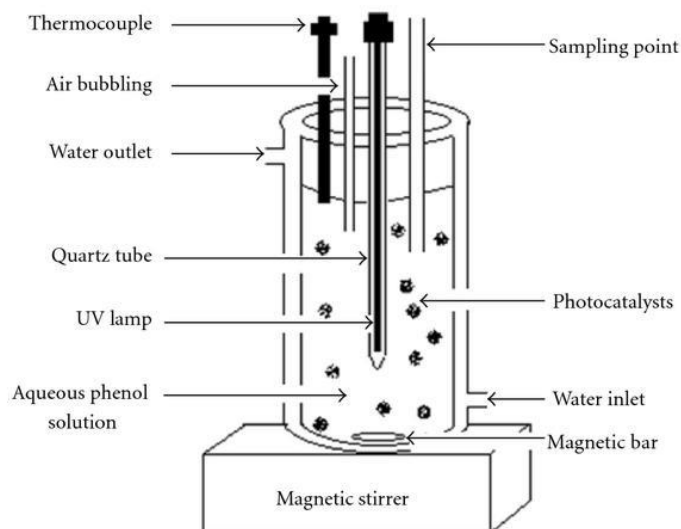


Figure 3.1: Experimental set-up of photocatalytic batch reactor (Adopted from Wang C. *et al*, 2004).

3.1.3 Analytical Methods

Concentrations of the phenol were monitored on a Waters HPLC (Waters 2695 separation module with a photo diode array – Waters 2998 PDA detector. Phenol and the intermediate compounds were separated on Synergi Fusion-RP C18 (150 x 4.6 mm, 4 μ m) column (Phenomenex) and Empower software for data analysis. A binary mobile phase consisting of 60% acetonitrile (A) and 40% water (B) was used for elution of compounds at a flow rate of 1.2 mL/min at 25°C, injection volume was 10 μ L with B operated in the isocratic mode. Concentration of phenol was determined from calibration curves of phenol standards.

The progress of degradation of phenol was also monitored by gas chromatographic analysis on a Perkin Elmer Clarus 600T Gas Chromatograph-Mass Spectrometer (GC-MS) equipped with headspace sampler. The GC-MS comprised of Clarus 600T GC, Clarus 600T Mass spectrometer, and Turbomatrix 40 trap headspace sampler equipped with a trap for a line extraction and concentration of sample constituents.

TiO₂ Characterisation by X-ray Fluorescence

The samples were roasted at 1000° C to determine Loss on Ignition (LOI). 1g roasted sample was then placed together with 6g of Li₂B₄O₇ into a Pt/Au crucible and fused The ARL Perform'X

Sequential XRF instrument was used for the analyses. Analyses were executed using the Quantas software. The software analysed for all elements in the periodic table between Na and U, but only elements found above the detection limits were reported. The results were also monitored and filtered to eliminate the presence of some of the flux, wetting and oxidising agents' elements. Blank and certified reference materials were analysed with each batch of samples and the columns in bold represents one of these.

3.1.4 Degradation Studies

The photocatalytic degradation of phenol in the presence of titanium dioxide (TiO₂) nano-particles and UV light was investigated, with emphasis on the effects of; solution pH, catalyst load, initial phenol concentration, dissolved oxygen and UV radiation intensity.

All the experiments were carried out using the same cylindrical annular batch photoreactor. The reactor has an internal volume of 1L with the UV lamp positioned on the axis inside a quartz immersion well. Illumination was provided by a 400 W medium pressure mercury lamp (Phillips HPA 400/30s) held in the immersion wall. The reactor was maintained at isothermal condition by passing chilled water through the cooling jacket of the immersion well. Oxygen was continuously sparged.

Phenol was selected as a model pollutant for the photocatalytic degradation experiments because it is a non-volatile, common contaminant in industrial wastewater. The initial concentration of phenol in dispersion was fixed at 100 mg/L and the initial pH of the dispersion was 8.3 and was adjusted by addition of sulphuric acid and/or sodium hydroxide. All experiments were performed at a solution temperature of 300 K for a reaction time of 60- 100 minutes, with samples taken for analysis every 10 min.

3.1.5 Total Organic Carbon (TOC) Analysis

Since the overall goal of the water treatment process was the complete destruction of the organic pollutant, (i.e. the conversion to carbon dioxide, water and the oxidised inorganic anions of any heteroatoms present). The rate of disappearance of Total Organic Carbon was a key performance indicator, and a Shimadzu TOC-V analyser was used to determine the extent of mineralization in the samples.

3.1.6 Titanium Dioxide Characterization

Powder X-ray diffraction (XRD)

XRD measurements were performed on a Bruker D8 Advance diffractometer with 2.2 kW CuK α radiation ($\lambda=1.54060$ nm) fitted with a LynxEye detector with a 3.7° active area. Samples were scanned in reflection mode in the angular range 2° to 70° 2 θ at a rate of 0.01° s⁻¹. The generator settings were 40 kV and 40 mA. Data processing and analysis were carried out using the Bruker Diffrac^{Plus} EVA evaluation program. Quantitative XRD analyses were performed according to the Rietveld method using Diffrac^{Plus} TOPAS software.

X-ray fluorescence (XRF) is a non-destructive analytical technique and was used to determine the elemental composition of the three TiO₂ powder forms. XRF analysers determine the chemistry of a sample by measuring the fluorescent (or secondary) X-ray emitted from a sample when it is excited by a primary X-ray source.

Scanning Electron Microscope (SEM)

The morphology of the three TiO₂ powders was obtained using a JEOL JSM 5800 scanning electron microscope (SEM). The samples were coated five times with carbon. A SEM auto-coating unit E2500 (Polaron Equipment Ltd) sputter coater was used.

Brunauer-Emmett-Teller (BET) analysis was employed to provide precise specific surface area evaluation of the three TiO₂ powder by nitrogen multilayer adsorption measured as a function of relative pressure using a fully automated analyzer. The technique encompasses external area and pore area evaluations to determine the total specific surface area in m²/g yielding important information in studying the effects of surface porosity. Pathway Analysis Photocatalytic degradation was conducted using a carbon-13 isotope labeled phenol. The experiment was conducted using the abovementioned batch reactor system. Experiments were run for 100 minutes, with samples taken in 10 minute time intervals using a micro-syringe. Samples were then centrifuged for 10 minutes to separate the catalyst particles from the phenol solution. Samples were monitored by GC-MS analysis.

4 CHAPTER 4: CHARACTERISATION OF TITANIUM DIOXIDE

4.1 INTRODUCTION

Among the photocatalysts, TiO₂ is believed to be the most promising presently known material because of its superior photoreactivity, nontoxicity, long-term stability, and low price. The photocatalytic activity of TiO₂ depends on various parameters, including crystallinity, impurities, surface area, and density of surface hydroxy groups; however, the most significant factor is its crystal form. TiO₂ is usually used as a photocatalyst in two crystal structures: Rutile and Anatase. The photoreactivity of P-25 Degussa, consisting of anatase and rutile (4/1 w/w), exceeds that of pure anatase in several reaction systems. However, the origin of the high photocatalytic activity of P-25 remains unclear.

The size of TiO₂ particles has been demonstrated to influence their photocatalytic activity, although there appears to be some disagreement in that Rivera *et al.* observed that the photocatalytic degradation rate increases linearly with increasing anatase crystallite size whereas Anpo *et al.* have reported that for anatase particles in the range of 4–50 nm, photocatalytic activity increased with decreasing TiO₂ particle diameter, an observation which they attributed to size quantization.

It seems obvious that a fundamental understanding of the factors affecting photocatalytic activity is necessary to make more efficient use of existing catalysts and provide design criteria for new catalyst preparation, thus it remains a subject of great interest.

4.2 X-RAY DEFRACTION (XRD)

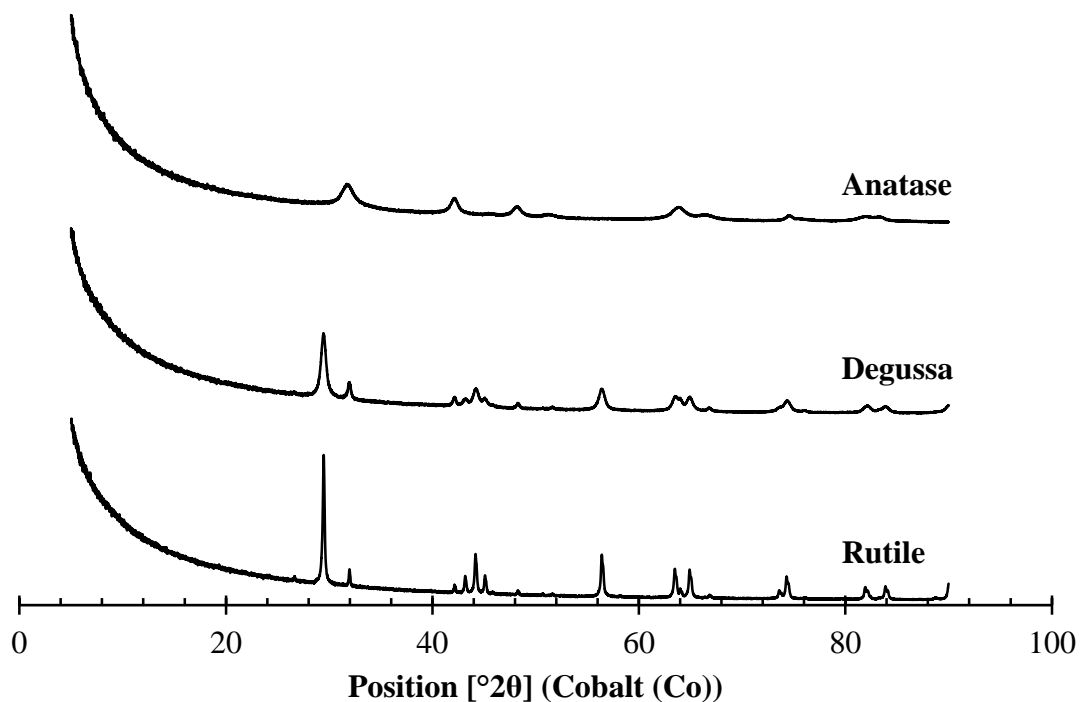


Figure 4.1: An X-ray diffraction pattern for TiO₂ in the Anatase, Rutile and Degussa form.

The XRD patterns for the three samples are illustrated in **Figure 4.1**. The sharp diffraction peaks in the XRD patterns as well as the low impurity peaks indicate that the synthesised compounds have high crystallinity and purity. The small peak intensities in the XRD pattern are attributed to the presence of fine grains. Degussa was revealed to contain 87.3% Anatase and 12.7% Rutile.

4.3 X-RAY FLUORESCENCE (XRF)

Table 4.1: The table shows the chemical composition of the three powders of TiO₂.

SARM49

	Certified	Analysed	ANATASE	DEGUSSA	RUTILE
SiO₂	99.6	99.40	0.52	0.02	10.80
TiO₂	0.01	0.00	98.40	96.70	75.70
Al₂O₃	0.05	0.01	<0,01	<0,01	0.11
Fe₂O₃	0.05	0.01	0.06	0.05	0.33
CaO	0.01	0.01	<0,01	<0,01	0.12
Na₂O	0.05	0.02	<0,01	<0,01	1.44
K₂O	0.01	0.01	<0,01	<0,01	0.23
P₂O₅	0	0.03	0.06	<0,01	<0,01
Cr₂O₃	0	0.00	<0,01	<0,01	0.82
NiO	0	0.01	<0,01	<0,01	0.37
SO₃	0	0.00	0.03	<0,01	<0,01
LOI	0	0.10	0.86	3.19	9.97
Total	100	99.61	99.94	99.96	99.89

Table 4.1 reveals the purity of the three powders of TiO₂. The anatase form being the most pure at 98.4%, followed by Degussa at 96.7% and Rutile at 75.7%. It is notable that rutile being the least pure, contains significant amounts of impurities than that of the other two powders. This may be a contributing factor to the relatively poor photocatalytic performance of rutile.

4.4 PARTICLE SIZE DISTRIBUTION (PSD)

Table 4.2: The table shows the Brunauer-Emmett-Teller (BET) surface area and the specific area for each of the three powder forms of TiO₂.

<i>Catalyst</i>	<i>D(10) μm</i>	<i>D(50) μm</i>	<i>D(90) μm</i>	<i>BET Surface Area (m²/g)</i>
<i>Anatase</i>	0.07	0.708	2.85	8.23
<i>Rutile</i>	0.94	3.14	10.2	119.495
<i>Degussa</i>	0.726	2.54	7.91	55.96

It can be seen in **Table 4.2**, that rutile and degussa have a much higher surface area than anatase. Because the photocatalytic degradation of phenol occurs on the surface of the catalyst, rutile and Degussa show greater potential for the photodegradation of phenol. However, this is not the case. Experiments show that anatase has a much higher photoactivity than that of rutile in several reaction systems. This can be attributed to their energy gap differences as shown in **Figure 2.2**. Anatase and rutile have a bandgap of 3.2eV and 3.0eV, respectively.

4.5 SCANNING ELECTRON MICROSCOPY (SEM)

SEM analysis was carried out to investigate TiO₂ morphology. The image shown in **Figure 4.2** presents the SEM images for anatase, degussa and rutile. The SEM shows nanoparticle structures with a large surface area, which enhances sensitivity. The particle morphology generally shows an irregular or near spherical shape. The primary particle size is in the nano range. The powders are highly agglomerated.

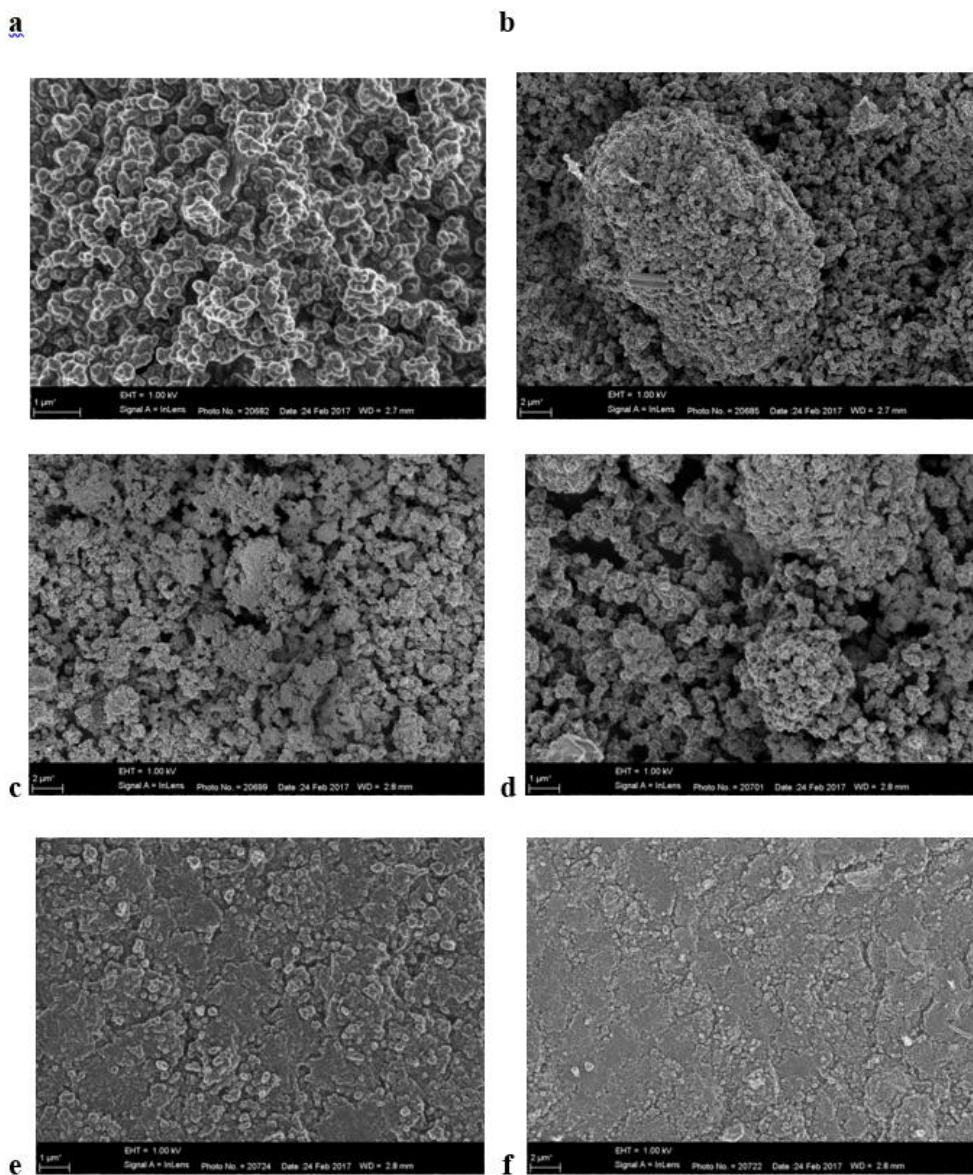


Figure 4.2: SEM images of Anatase (a&b), Degussa (c&d) and Rutile (e&f).

4.6 A COMPARISON BETWEEN THE THREE TiO₂ POWDER FORMS AND THEIR EFFECT ON THE PHOTOCATALYTIC ACTIVITY.

An experimental initial catalyst concentration of 20mg/L was used throughout all experiments **Figure 4.3**. Experiments were ran in triplicates and average values are reported. Experiments were carried out as described in **Figure 3.1**. Results show that rutile was highly effective at an initial phenol concentration of 10mg/L. The photocatalytic activity decreased with increasing phenol concentration. Anatase showed the highest phenol degradation at an initial phenol concentration of 20mg/L. A similar trend was observed with Degussa.

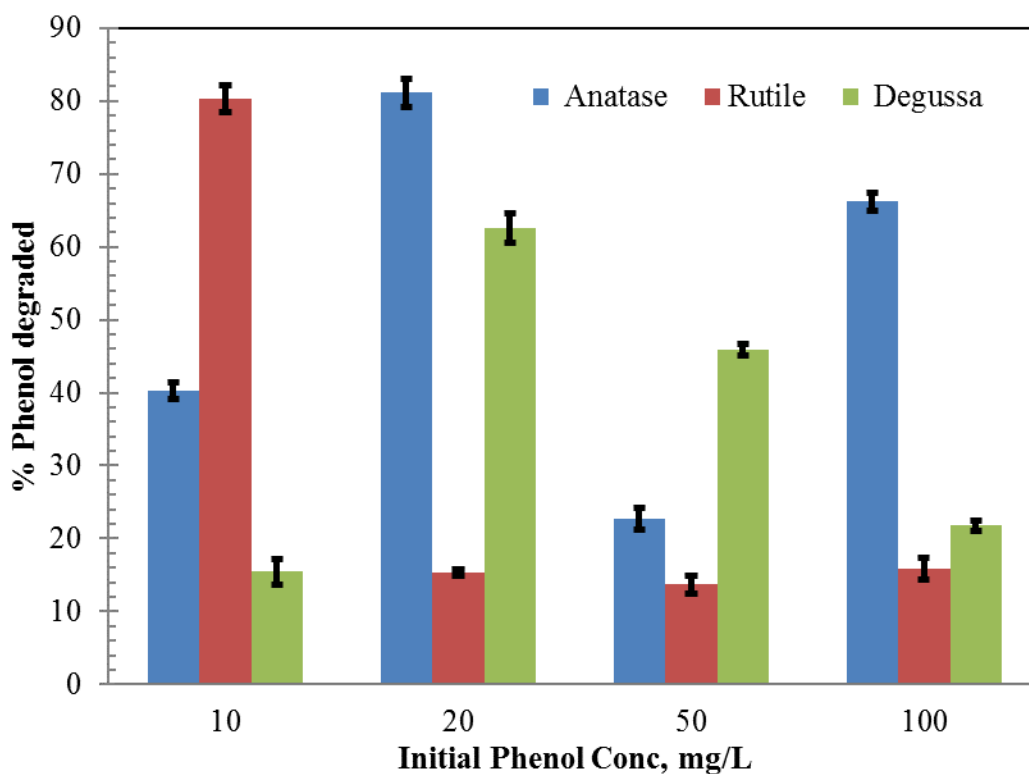


Figure 4.3: Effect of initial phenol concentration on the photocatalytic performance of the three powder forms of TiO₂ is depicted in the graph at a constant catalyst concentration of 20mg/L.

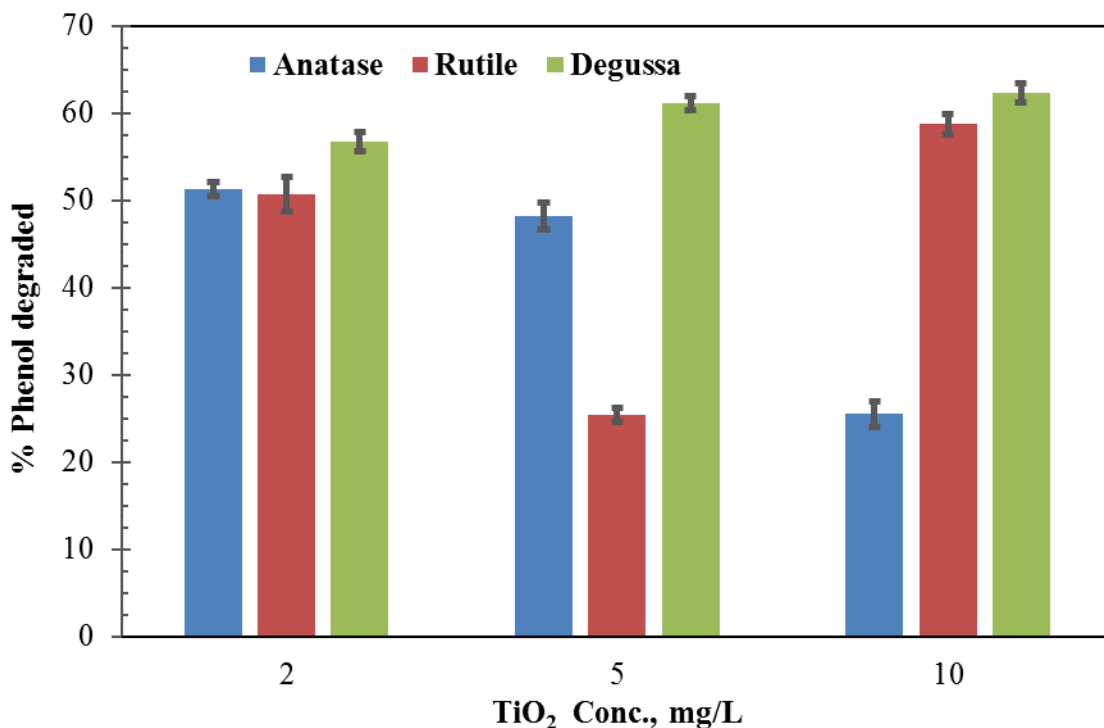


Figure 4.4: The ideal initial phenol concentration for each TiO₂ powder as observed in **Figure 4.3** was kept at constant and the TiO₂ concentration was varied from 2 – 10mg/L, and results are depicted in the graph.

In the case of anatase, a significant decrease in phenol removal is observed with increase in TiO₂ concentration from 2mg/L to 10 mg/L. This can be attributed to the clouding of the solution by the catalyst and therefore resulting in the inhibition of the reaction by the blocking of UV light from reaching the catalyst surface. Degussa showed a gradual increase in phenol removal with increasing TiO₂ concentration from 2- 10 mg/L as expected, considering that it has optimum phenol removal at an initial phenol concentration of 20mg/L in **Figure 4.4**. It is understood that there is direct correlation between organic pollutant and surface coverage of TiO₂ photocatalyst. Greater phenol removal is observed with increase in catalyst concentration and this can be attributed to the availability of free active sites for photocatalysis (Gaya and Abdullah, 2008). Rutile showed no trend, however, high photoactivity was obtained at a catalyst concentration of 10 mg/L.

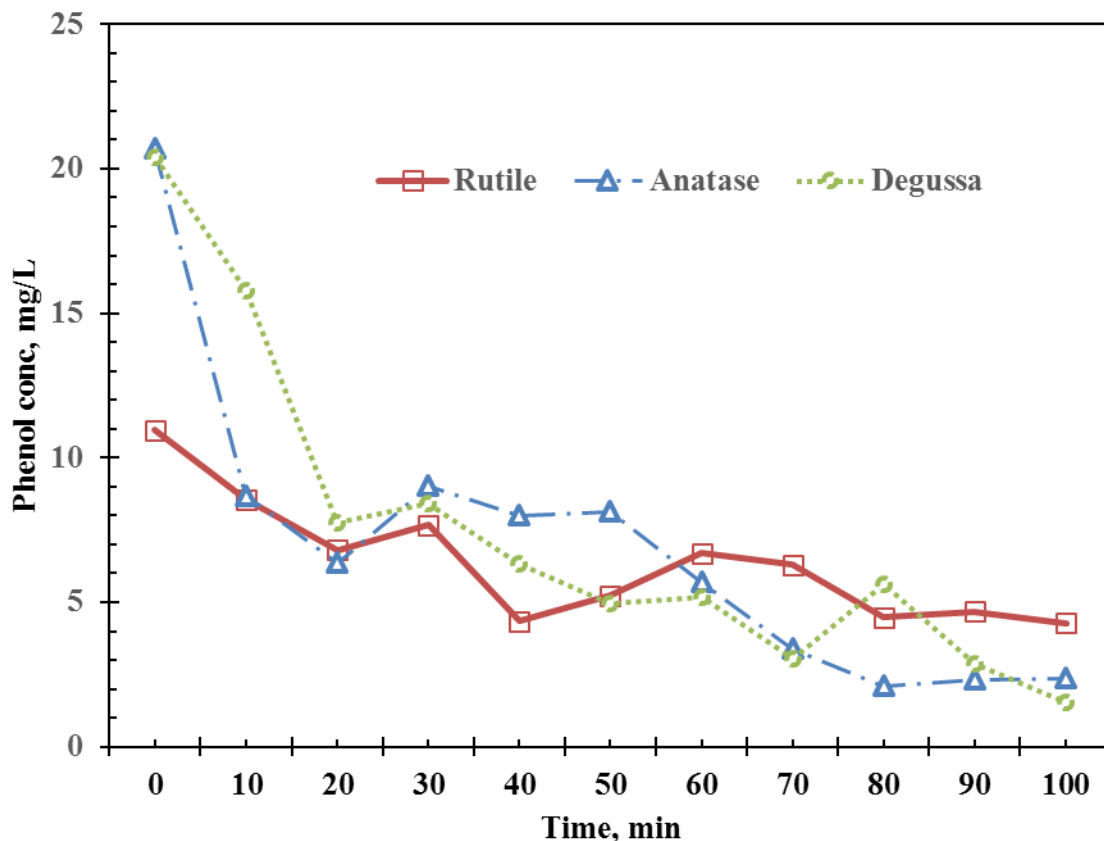


Figure 4.5: The degradation profile for the three powder forms of TiO₂ at their ideal initial phenol and catalyst concentrations.

Kinetics experiments were conducted to obtain the degradation profile for the three powder forms of TiO₂. The effect of initial phenol concentrations on phenol removal were experimented (**Figure 4.3**) the optimum initial phenol concentrations were obtained for each of the three powders.

Figure 4.5 shows the kinetics of photodegradation in all three cases. The highest phenol degradation rate (1.6mg/L.min) in the first 10 minutes is observed with anatase. The reaction rates decreased gradually reaching 0.01mg/L.min, with increasing contact time.

In the case of Degussa, the highest phenol degradation rate (1.14mg/L.min) was obtained in the first 20 minutes and gradually declined to a final reaction rate of 0.02mg/L.min in 100minutes.

Rutile showed slightly different behavior, with a rapid phenol degradation rate between 30 – 40minutes, and gradually decreased to 0.09mg/L.min in 100minutes.

Table 4.3: The table shows the average phenol degradation rates for each TiO₂ powders over a 100 minutes reaction time.

<i>TiO₂ Catalyst</i>	<i>Reaction rate (k – mg/L.min)</i>
<i>Degussa</i>	0.1881
<i>Anatase</i>	0.1825
<i>Rutile</i>	0.067

4.6.1 DISCUSSION

There is direct correlation between organic pollutant and surface coverage of TiO₂ photocatalyst. Morita *et al.* 2016 reported that the number of photons striking the photocatalyst actually controls the rate of the reaction. The latter is an indication that the reaction takes place only in the adsorbed phase of the semiconductor particle. A very important parameter influencing the performance of photocatalyst in photocatalytic oxidation is the surface morphology, namely the particle size and agglomerate size. Numerous forms of TiO₂ have been synthesized by different methods to arrive at a photocatalyst exhibiting desirable physical properties, activity and stability for photocatalytic application.

Evidently, there is a clear connection between the surface properties, the rational development of improved synthesis routes and the possible usefulness of the material prepared in application. For instance, smaller nano-particle size is reported to give higher conversion in gaseous phase photomineralisation of organic compounds over nano-sized titanium dioxide.

4.6.2 CONCLUSION

Anatase generally has higher activity than rutile. More interesting is the fact that the activity of P-25 (Degussa), which consists of 87.3% anatase and 12.7% rutile exceeds that of pure anatase in a number of reaction systems. Degussa has frequently been used as a benchmark for photocatalysts and has indeed proven success in the degradation of recalcitrant organics including phenol. Based on these results, Degussa was used for all experiments thereafter.

5 CHAPTER 5 PHENOL DEGRADATION STUDIES

5.1 EFFECT OF INITIAL PHENOL CONCENTRATION

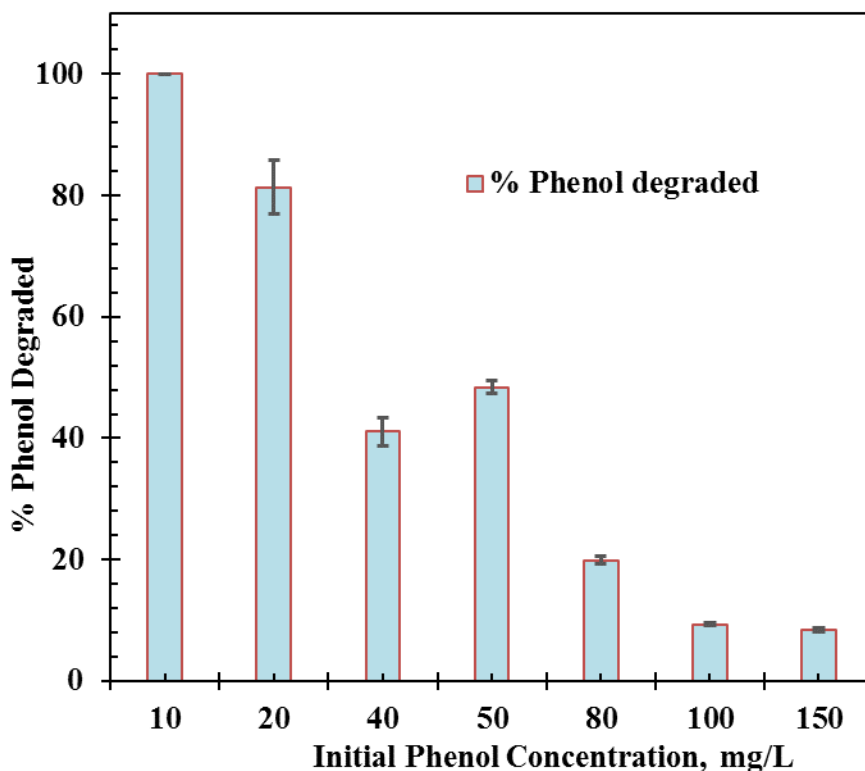


Figure 5.1: The graphs depicts the effect of initial phenol concentration on the degradation efficiency expressed as percentage.

Results revealed a maximum phenol removal was achieved with an initial phenol concentration of 10mg/L. An experimental TiO_2 concentration of 10mg/L was used. Phenol removal decreased with increasing initial phenol concentration. A 100% phenol degradation was achieved in less than 60minutes for 10mg/L initial phenol. All batches were carried out for 60minutes. Higher initial phenol concentration required longer reaction times for complete degradation.

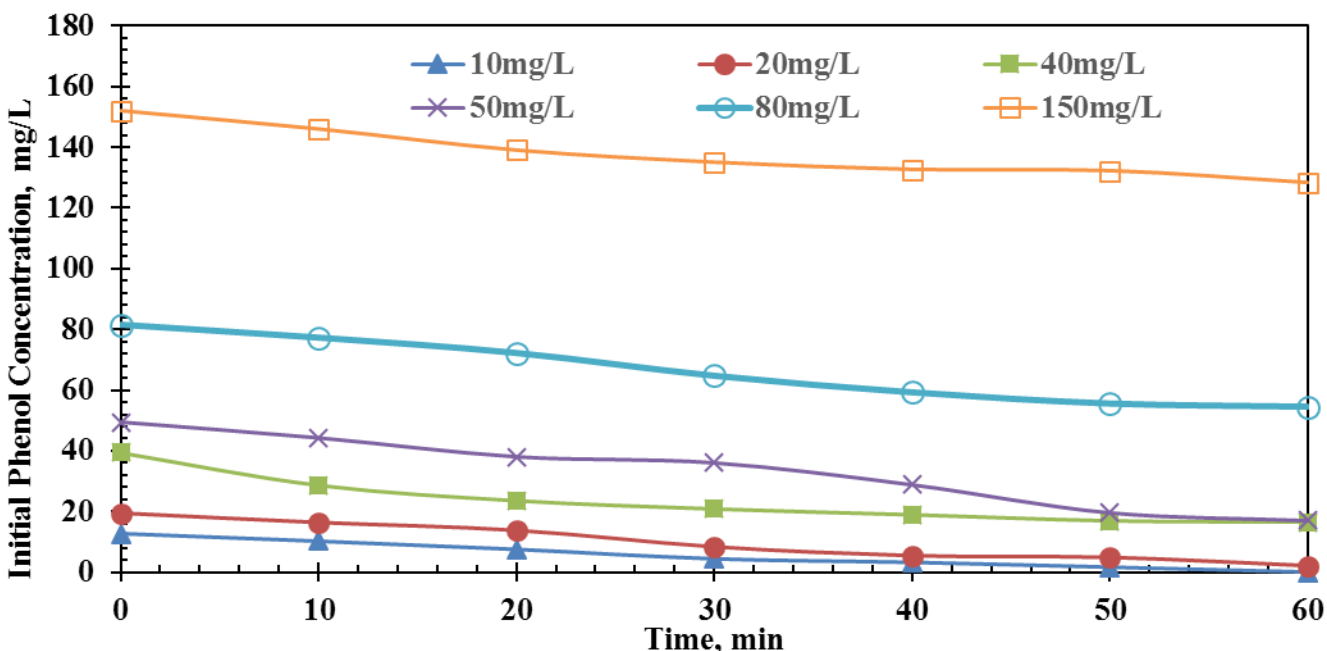


Figure 5.2: The graph depicts the phenol degradation profile for different initial phenol concentrations at a constant TiO₂ concentration of 20mg/L.

Degradation efficiencies are governed by the availability and effective contact of reactive species in solution and on the catalyst surface with pollutant species. Phenol is relatively soluble in water and its main reaction zone for photocatalytic degradation is believed to be in the bulk liquid. The sharp decrease in phenol concentration beyond initial phenol concentration of 10mg/L can be attributed to the fact that high concentration of pollutant in water saturates the TiO₂ surface. This leads to a reduction in the photonic efficiency and deactivation of the photocatalyst especially as formation of reactive radical species ($\cdot\text{OH}$ and $\text{O}_2^{\cdot-}$) remain constant at a particular catalyst concentration (20mg/L) and light intensity (Fujhima et al., 2000). The degradation profile of phenol at different initial concentrations over a constant catalyst concentration (20mg/L) can be seen in **Figure 5.2**.

5.2 TOC ANALYSIS

Table 5.1: The table reports NPOC results (mg/L) with change in initial phenol concentration (mg/L).

<i>Initial Phenol Conc, mg/L</i>	<i>NPOC Degraded (mg/L)</i>	<i>% NPOC Degraded</i>
10	0.012	1.15
20	0.010	1.11
30	0.007	0.7
50	0.0009	0.089
100	0.0142	1.42

TOC analysis showed there was no significant difference in the Non-purgable Organic Carbon (NPOC) amounts before and after photocatalysis (**Table 5.1**), although results from HPLC and GC-MS analysis showed significant amounts of phenol removal. This was attributed to the simultaneous formation of degradation intermediates during the course of phenol photocatalysis, therefore longer reaction times were required in order to achieve significant differences in NPOC.

The time it takes to reach full mineralisation depends on a number of factors such as the type of catalyst being used, the pollutant loading, pH of solution, irradiation intensity and the catalyst concentration. A study (Alalm and Tawfik, 2014) showed the optimal solution pH was 5.2 in which 94.5% degradation of phenol was achieved after 150 minutes of irradiation. Further rising of the initial pH led to a decrease in degradation efficiency of phenol. The optimum dosage of TiO₂ was 2 g/L which achieved a 94.5% degradation of phenol in 150 minutes of irradiation. Increasing the dosage more than 2 g/L reduced the degradation efficiency due to the increasing of turbidity in the solution, which detracts the amount of light reaching the semiconductor active sites (Alalm and Tawfik, 2014). Furthermore, increasing the catalyst loading may cause agglomeration of particulates, which decreases the active sites on the semiconductor surface. Another study (Rahmani, 2008) reported the removal efficiencies of UV, TiO₂ and UV/TiO₂ photocatalytic oxidation system with various operation conditions had a range of 1.8%-19.64%, 2.38%-17.8%

and 34.65%-82.91%, respectively. It was found that increasing of TiO₂ concentration and contact time and pH , increasing the amount of phenol that oxidized in combined system and maximum removal coefficients obtained in pH=11 , 9 hour contact time and 0.2 gr of TiO₂.

5.3 EFFECT OF TiO₂ CONCENTRATION

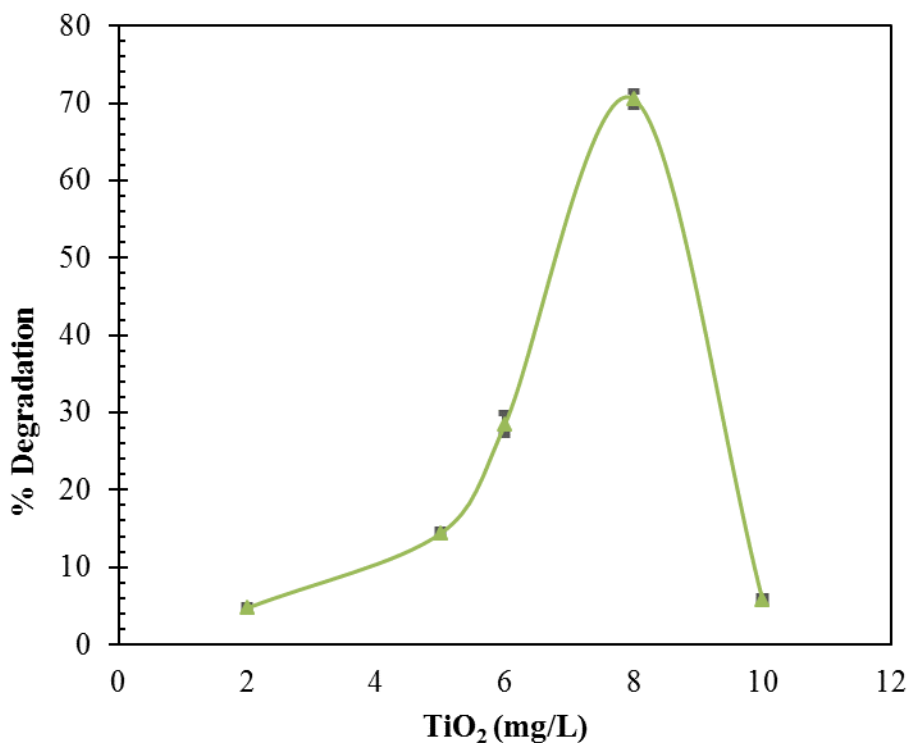


Figure 5.3: The graph shows the % phenol degradation for TiO₂ (2mg/L – 10mg/L).

Degradation efficiency was tested on pre-determined TiO₂ concentrations, in the range of 2mg/L to 10mg/L at a constant phenol concentration of 100mg/L. The highest degradation was obtained at a TiO₂ concentration of 8mg/L as shown in **Figure 5.3**. The degradation efficiency gradually increased from 2% to 14% at a TiO₂ concentration of between 0mg/L to 5mg/L. There was a rapid increase in the degradation efficiency from 29% to 71% between TiO₂ concentration of 6mg/L at a TiO₂ loading of 8mg/L and 10mg/L respectively. This can be attributed to the fact that the amount of TiO₂ is above saturation level, the light photon adsorption co-efficient decreases radially and the excess photocatalyst creates a light screening effect that leads to the reduction in the surface area exposed to irradiation and thus reduces the photocatalytic efficiency of the process.

5.4 EFFECT OF DISSOLVED OXYGEN

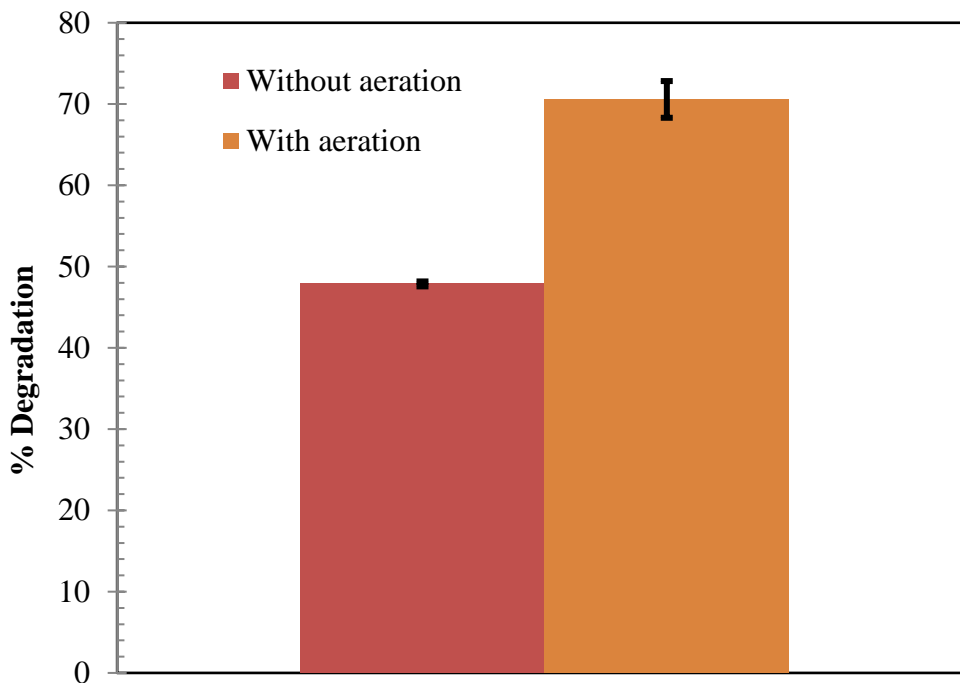


Figure 5.4: The graph shows the % phenol degradation under aerobic and anaerobic conditions.

Reactions were carried out with an initial phenol concentration of 100mg/L and a TiO_2 concentration of 8mg/L. Experiments were run in triplicates and average results were reported. A phenol removal of 70.5% was achieved when the reactor was continuously bubbled with oxygen as depicted in **Figure 5.4**. The phenol removal amount reduced to 47.8% when the solution was not bubbled with oxygen. These results clearly show that continuous addition of oxygen to the reaction mixture is required to sustain the photocatalytic reaction and to effect complete degradation. Oxygen acts as the electron scavenger for the conduction band electrons, thereby preventing recombination of the electron-hole pair and thus promoting photocatalysis. Without subsequent addition of air/oxygen, the reaction rate is slow as the rate of DO addition by surface aeration is less than what is required by the reaction.

5.5 EFFECT OF pH

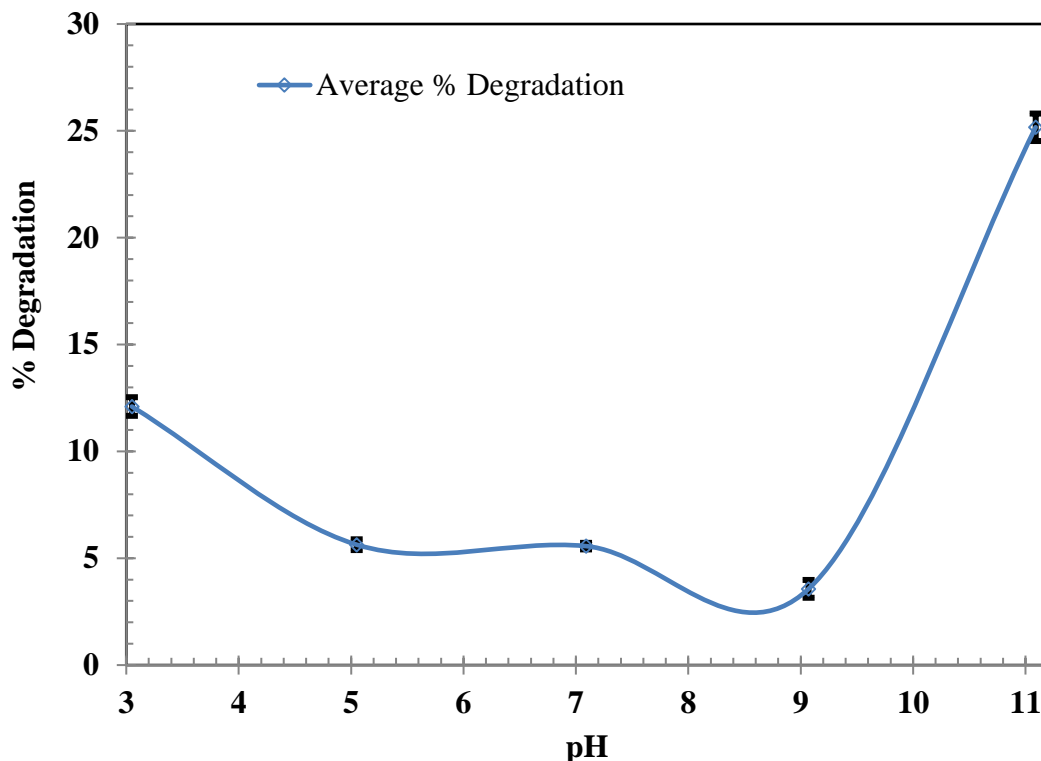


Figure 5.5: The graph shows the % phenol degradation with change in pH.

Figure 5.5 shows the effect of pH on the photocatalytic oxidation of phenol in the presence of TiO_2 under ultra-violet light irradiation. Evidently, the degradation reaction can proceed in a wide range of pH, the conversion of phenol changed with the pH of the solution and average results were reported.

For an initial solution containing phenol 100mg/L, 12.1% conversion of phenol at pH 3, 5.7% at pH 5, and 5.6% at pH 7 were observed within 1 h of irradiation. Overall, the conversion of phenol increased with the increase of pH when the reaction was conducted in alkaline media, and the conversion rate of phenol at the same irradiation time dropped to 3.6% at pH 9 and increased to 25.2% at pH 11. The increasing activity at higher pH attributed to the increasing concentration of phenolate ions. The stabilities of the transition states of phenol or phenolate and singlet oxygen determine the rate of photo-oxidation. The electronic interaction takes place between the calculated lowest unoccupied molecular orbital (LUMO) of singlet oxygen, located at -0.98 eV, and

calculated HOMO of phenolate, located at -2.69 eV, or of phenol, located at -9.81 eV. An increase in the difference between the energy of the LUMO of singlet oxygen and the energy of the HOMO of the organic substrate results in weaker electronic interaction. Therefore, phenol is less reactive than phenolate in the photo-oxidation process. The reaction time, 60 minutes, was a limiting factor and it did not paint a picture of the full reaction kinetics. Longer reaction time is to be investigated.

5.6 EFFECT OF CONTACT TIME AND INITIAL PHENOL CONCENTRATION

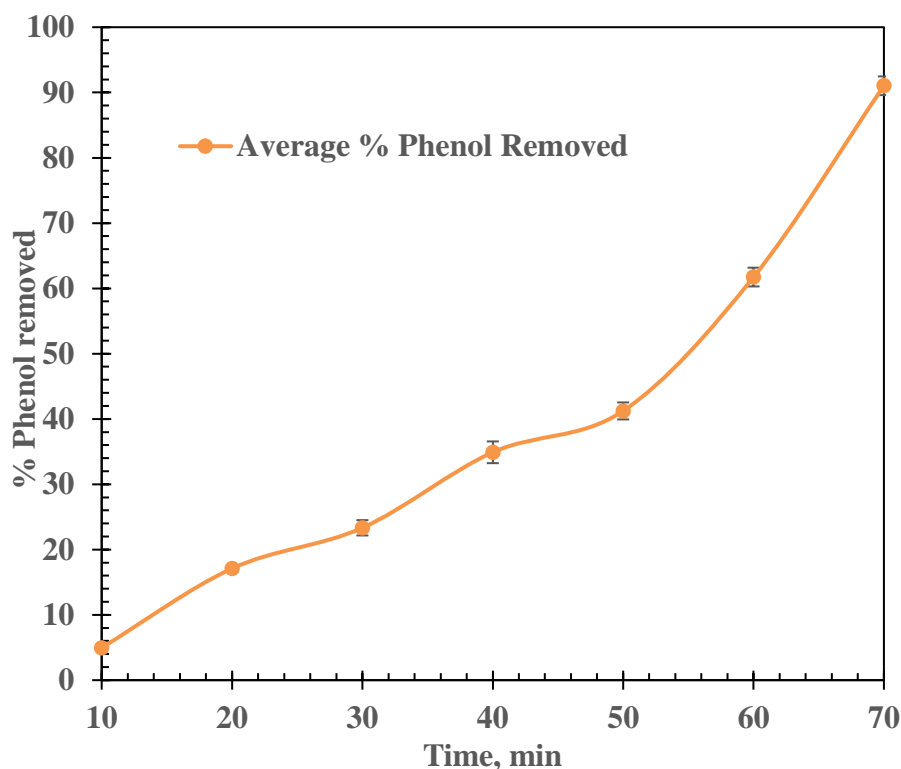


Figure 5.6: The effect of contact time and initial phenol concentration on the % phenol degradation are shown by the graph.

These results indicated that increasing contact time and reducing initial phenol concentration led to improvement in the removal percentage of phenol. **Figure 5.6** shows an increase in phenol removal with time with an initial phenol concentration of 30mg/L.

5.7 EFFECT OF UV LIGHT INTENSITY

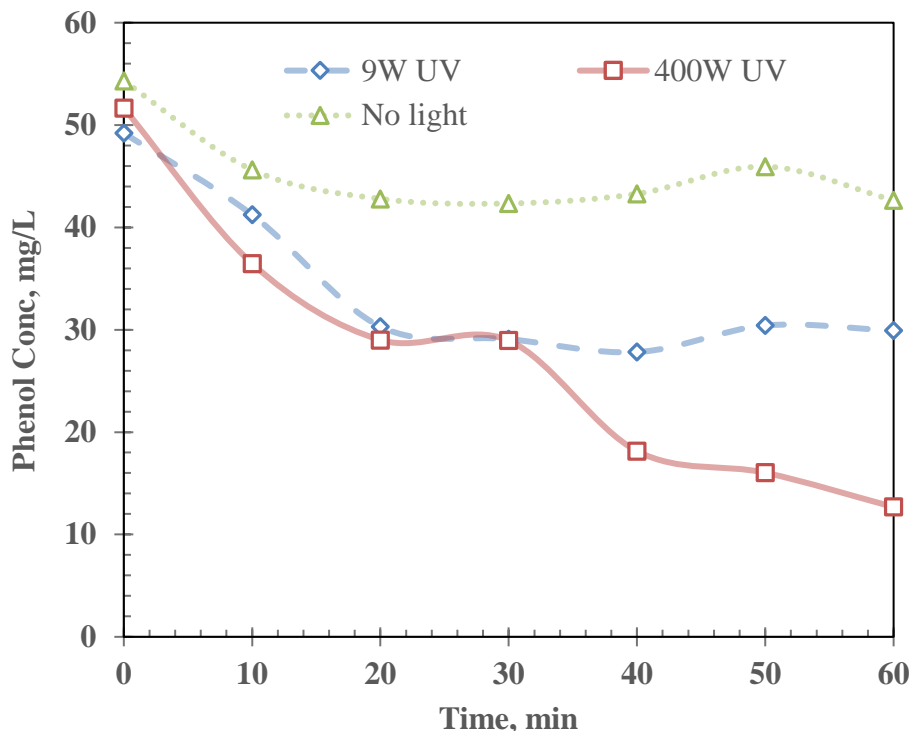


Figure 5.7: The graph shows the effect of UV light and its intensity on the photocatalytic degradation profile.

The reaction (**Figure 5.7**) was carried out with 100mg/L phenol at a constant TiO_2 concentration of 8mg/L. Experiments were run in triplicates and average results were reported. The amount of phenol degraded reduced from 70.6% to 11.1% when using the 400W and 9W UV lamps respectively. Higher light intensity resulted in higher phenol degradation. The conversion depended strongly on the incident light intensity, thus, increasing the light intensity from 9 W to 400W enhanced phenol degradation in a remarkable way. The photonic nature of the photocatalysis reaction has outlined the dependency of the overall photocatalytic rate on the light source used. These results are attributed to the fact that there were relative low amounts of photons in the reaction system at low light intensity; on the other hand, at high intensity, photons were present in excessive amounts leading to more reactive species generation and more destruction of phenol; this proved that higher catalyst activity occurred under high light intensity.

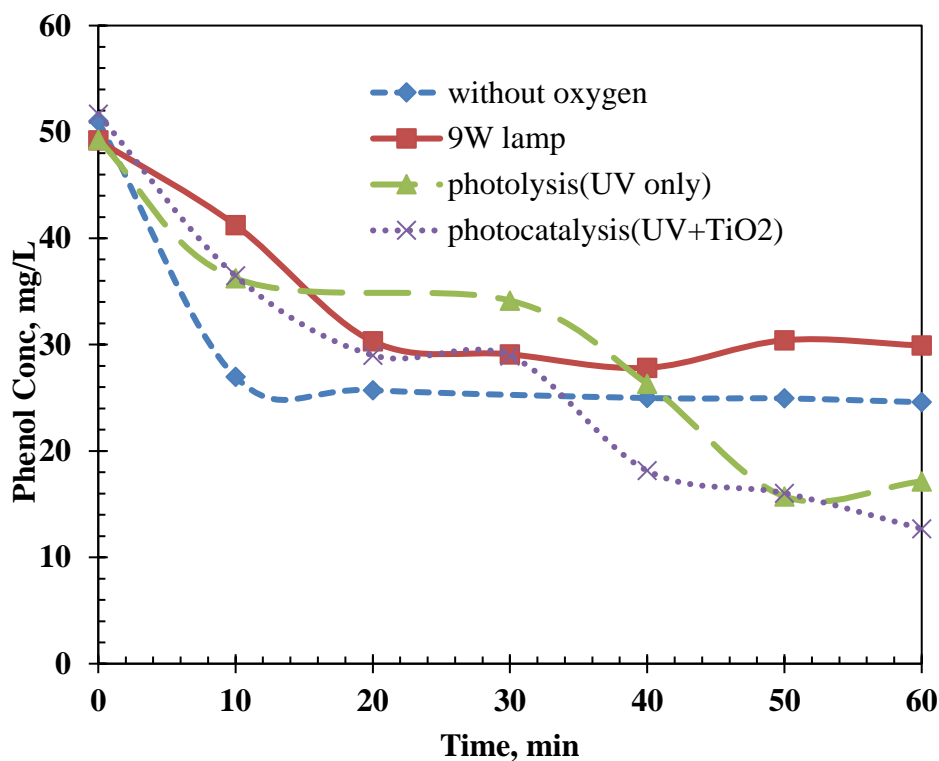


Figure 5.8: The graph shows the degradation profile for the different control conditions.

Different control conditions were experimented on and the results are depicted in **Figure 5.8**. Each of the control conditions had a significant effect on the photocatalytic activity. The least phenol degradation was observed when the reaction was illuminated with UV radiation of 9W. The removal of aeration also saw a great reduction in phenol removal. Photocatalysis and photolysis did not differ much in terms of overall phenol removal., however, the rate constant varied during the course of reaction.

5.8 CONCLUSION

Results showed that photo degradation is an effective method for the removal of phenol from wastewaters. The efficiency of the process depends strongly on the experimental conditions. The amount of catalyst, UV irradiation time, pH and light intensity were important parameters in the degradation process. The rate constants for the different parameters were evaluated and indicated

that titanium dioxide photocatalyst P-25 was very active in phenol degradation. Therefore, combined UV/TiO₂ process may be applied as an effective process for the removal of phenol from aquatic solutions such as industrial wastewaters and polluted water resources.

6 CHAPTER 6: PATHWAY ANALYSIS

6.1 INTRODUCTION

A chemical reaction mechanism may be thought of as a motion picture of all of the atoms (and their electrons) involved in the reaction, beginning before the reacting species approach each other and picturing their paths during the reaction. This includes which bonds are broken, which are formed, in what sequence/order, how many steps are involved and relative rates of each such steps and ending after the products have been formed (De Wolfe, 1963). Reaction mechanisms, therefore, must include descriptions of these movements with regard to spatial change and with regard to time. The overall route of change is called the course of the reaction, and the detailed process by which the change occurs is referred to as the reaction path or pathway. Reaction intermediates are formed in one step and then consumed in a later step of the reaction mechanism. The slowest step in the mechanism is called the rate determining or rate-limiting step. The overall reaction rate is determined by the rates of the steps up to (and including) the rate-determining step (Frost and Pearson, 1961). Such detailed knowledge of the course of a reaction can never be attained in actual practice, and a reaction mechanism is usually understood to mean all of the simple reactions involving molecules, radicals, and ions, that take place simultaneously or consecutively in producing the observed over-all reaction (De Wolfe, 1963).

The experimental elucidation of reaction mechanisms poses some very thorny problems. A knowledge of the stoichiometry of a reaction, or of the position of an equilibrium, yields no information on how the reaction occurs or how the equilibrium is attained. Chemical thermodynamics, dealing as it does with initial and final states, tells nothing about the paths connecting these states. Since the individual molecular collisions and interactions, comprising a mechanism cannot be observed directly, their occurrence and nature must be deduced from indirect evidence of various kinds. The most powerful tool for the experimental study of reaction mechanisms is chemical Kinetics. Kinetics deals with the rates at which chemical reactions occur, and with all of the factors, which influence these rates. No reaction mechanism can be considered more than a temporary working hypothesis until it is supported by kinetic data.

Much useful information regarding the mechanism of a reaction can be obtained by studying the effects of environmental changes on reaction rate. Changes in reaction rate produced by changes in solvent polarity, nucleophilicity, and ionizing power yield useful information on the role played by solvent molecules in a reaction (Leffler, 1956). There are, of course, many kinds of information other than rate data, which are useful in the study of mechanisms. Changes in rate caused by changing the isotopic composition of the solvent are also enlightening. Another widely used application of chemical kinetics is the study of rate changes produced by structural alterations in one or more of the reactants. The stereochemistry of product must be accounted while studying the mechanistic details of a reaction, which played a major role in developing our current understanding of organic reaction mechanisms. Nowadays, the stereochemical course of many reactions is known, although the mechanistic explanation may still be under debate. A knowledge of the effects of such changes on reactivity and on the rate equations of reactions is particularly useful in the study of organic reactions. Rate variations caused by structural alterations in the reactants yield information on the electronic and steric requirements of the reaction, which is pertinent to its mechanism (De Wolfe, 1963).

A special kind of structural change, which frequently causes meaningful rate changes, is isotopic substitution - the use of isotopes as labels in a reaction. One of its isotopes selectively replaces an atom in the reactant. These isotopes behave much like the ordinary atoms they replace, but they can be identified by their behavior. The reaction is carried out as usual, and the location or distribution of the isotopic label in the product(s) is determined. The probable mechanism can then be inferred. In this approach, the focus is on the identification of intermediates and products (Maitra and Chandrasekhar, 1997). For example, the effect on rate of replacing hydrogen by deuterium at or near the reaction site in an organic molecule affords valuable information on the mechanism of the reaction and on the structure of the transition state (Wiberg, 1955). The study of reaction mechanisms is complicated by the reversibility of most reactions (the tendency of the reaction products to revert to the starting materials) and by the existence of competing reactions (reactions that convert the starting material to something other than the desired products). Another complicating factor is the fact that many reactions occur in stages in which intermediate products are formed and then converted by further reactions to the final products.

The effects of catalysts and inhibitors on reaction rates are of fundamental importance in mechanisms studies. A knowledge of the kinds of things, which catalyse or inhibit a reaction usually, enables one to decide whether the reaction proceeds by a radical or a heterolytic mechanism. The influence of light and of solid surfaces on the rate of a reaction is also pertinent to its mechanism (Long and Paul, 1957).

There are, of course, many kinds of information other than rate data, which are useful in the study of mechanisms. Physical measurements involving absorption spectroscopy, nuclear magnetic resonance spectroscopy, electron paramagnetic resonance spectroscopy, and cryoscopy have been valuable in establishing the existence and structures of reactive intermediates (Leffler, 1956). Isotopic labelling often makes it possible to determine the role of individual atoms in reactions, and has been extensively used in establishing the positions of bond cleavages (De Wolfe, 1963). Isotopic exchange experiments have served to establish the existence of several reactive intermediates. A knowledge of the structures of all of the products of a reaction, and of its stereochemistry, frequently supports some mechanisms and eliminates others from consideration (Polo et al, 2008). Competition and crossover experiments may furnish valuable mechanistic clues.

The study of the detailed processes of reaction mechanisms is important for many reasons; including the help, it gives in understanding and monitoring chemical reactions. Many reactions of great commercial importance can proceed by more than one reaction path; knowledge of the reaction mechanisms involved may make it possible to choose reaction conditions favoring one path over another, thereby giving maximum amounts of desired products and minimum amounts of undesired products. Furthermore, based on reaction mechanisms, it is sometimes possible to find correlations between systems not otherwise obviously related.

In examining chemical reactions, it is useful to consider the following:

- Factors that influence the course of chemical reactions,
- Energy changes involved in the course of a typical reaction,
- Factors that reveal the mechanism of a reaction, and
- The classification of reaction mechanisms.

6.2 METHODS OF STUDYING REACTION MECHANISM

6.2.1 Study of Intermediates Formed

Intermediates are postulated in many mechanisms. Their presence or absence of is an essential information for proposing a fairly correct mechanism for a reaction.

The simplest variations are reaction time and temperature can yield different intermediates in a reaction. The evidence is provided by product analysis. Many reactions are proposed to proceed via the formation of intermediates such as carbocations, carbanions, free radicals, carbenes, nitrenes. The intermediate and its structure is determined and studied by several ways.

6.2.2 Isolation of an Intermediate

The intermediates can be isolated sometimes from a reaction mixture by stopping the reaction after a short time or by the use of very mild conditions. When subjected to the reaction conditions, if the isolated intermediate gives the same product and at a rate not slower than the starting compound, this constitutes strong evidence that the reaction involves that intermediate. Although it is not conclusive, since the compound may arise by an alternate path and by coincidence give the same product.

6.2.3 Detection of an Intermediate

If the intermediate cannot be isolated, then it can be detected by various spectroscopic techniques such as IR, ReactIR, NMR, or other spectra. For example during nitration of benzene, the formation of nitronium ion has been detected by Raman spectra of NO_2^+ .

ESR (Electron Spin Resonance) and CIDNP (Chemically Induced Dynamic Nuclear Polarization) are often used for the detection of free radical and triplet intermediates. Free radicals (as well as radical ions) can also be detected by isomerisation, without using spectroscopy. In this method, a double bond compound is added to the reaction mixture, and its fate traced. One possible result is cis–trans conversion. For example, cis-stilbene is isomerized to the trans isomer via a radical. Since the trans isomer is more stable than the cis, the reaction does not go the other way, and the detection of the isomerized product is evidence by the presence of the radical.

6.2.4 Trapping of an intermediate

Sometimes the mechanistic details of a reaction can be better understood by trapping the intermediate formed. For example, when a benzyne is an intermediate, the addition of a diene and the detection of the Diels–Alder adduct indicates the presence of benzyne as an intermediate.

6.2.5 Addition of a Suspected Intermediate

If a certain intermediate can be obtained by other means, then under the same reaction conditions it should give the same products. This provides us with a negative evidence, since if the desired product is not formed then the intermediate is wrongly interpreted. However, if the desired product is formed, then the intermediate is (in most cases) the correct one in proposing a suitable mechanism for a reaction.

6.2.6 Study of Catalyst

Catalysts perform their actions by providing an alternate pathway for the reaction. The knowledge of catalyst also provides sufficient information about the mechanism of a reaction. The proposed reaction mechanism for any reaction which uses catalysts should be compatible with it apart from being compatible with products and intermediates.

6.2.7 Stereochemical Evidence

A lot of information about the mechanism is revealed if the products of a reaction can exist in different stereoisomeric forms. The preferred isomer can lead a chemist to give a more trustworthy mechanism. For example, Walden discovered that (+) malic acid gives (-)- chlorosuccinic acid when treated with PCl_5 and the (+) enantiomer when treated with SOCl_2 , showing that the mechanisms of these apparently similar conversions could not be the same.

Much useful information has also been obtained about various important types of organic reactions like nucleophilic substitution, elimination, rearrangement, and addition reactions from this type of experiment.

6.2.8 Kinetic Evidence

The rate of a homogeneous reaction is the rate of disappearance of a reactant or appearance of a product. A study of which reactants influence the rate often gives a good deal of information about the mechanism of a reaction. The rate law of a reaction is an experimentally determined fact. The molecularity which is the number of molecules that come together to form the activated complex, also gives a good deal of information about the mechanism.

Kinetics investigations are the single most important group of techniques in mechanistic determinations. Various kinetics parameters like order of a reaction, rate law, rate constants, kinetic isotope effects, etc. summed up with other evidences provide great insights into the mechanisms to be proposed.

In practice, some methods are much more widely used than others are, and UV–vis spectrophotometric techniques are amongst these. A major recent development is the increasing exploitation of time-resolved IR spectrophotometry for kinetics, which has a major advantage over UV methods – in addition to kinetic data; it also provides readily interpretable IR spectroscopic information that allows some degree of structural characterisation of reactive intermediates.

6.2.9 Isotope Labelling

The commercial availability of a wide range of isotopically enriched organic compounds provides many opportunities to investigate reaction mechanisms using isotopic labelling. Isotopes are generally distinguished by three analytical means. The first of them makes use of radioactive isotopes, such as tritium (^3H), ^{14}C , ^{32}P etc. This is a highly sensitive technique, but special facilities are required to handle radioactive material. Mass spectroscopy can also be used to detect isotopes. This is also a highly sensitive technique. When the fragmentation pattern of a compound is known, mass spectral data provide a wealth of information. The third, and at present the most - frequently used technique is nuclear magnetic resonance. This technique requires an NMR active nucleus such as ^2H , ^{13}C , ^{18}O etc. and is relatively less sensitive. But the ease of operation more than compensates for its limitations (Maitra and Chandrasekhar, 1997).

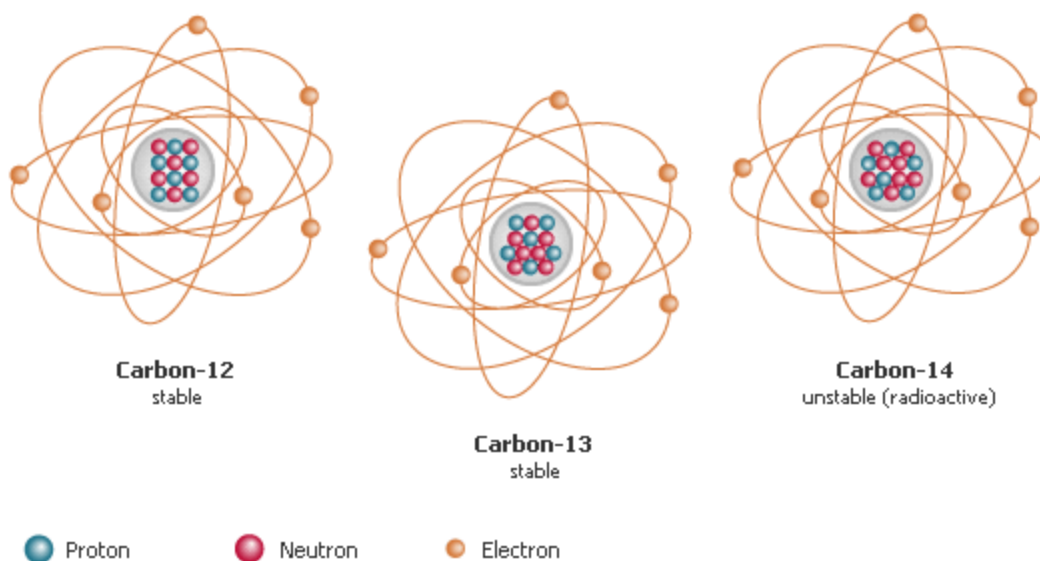


Figure 6.1: The three main isotopes of carbon (Adopted from Kuensting S., 2004).

By far the most common isotope of carbon is carbon-12 (^{12}C), which contains six neutrons in addition to its six protons as seen in **Figure 6.1**. The next heaviest carbon isotope, carbon-13 (^{13}C), has seven neutrons. Both ^{12}C and ^{13}C are called stable isotopes since they do not decay into other forms or elements over time. Carbon-14 contains six protons, eight neutrons, and six electrons; its mass number is 14. Out of these three isotopes of carbon, carbon-14 (^{14}C) is unstable and radioactive isotope with half-life of 5568 years (Godwin H., 1962).

Variations of $^{13}\text{C}/^{12}\text{C}$ in nature are very small. It is very difficult to measure absolute isotope abundances with a precision that is sufficient to detect small variations in isotope ratios. Measuring $^{13}\text{C}/^{12}\text{C}$ ratios relative to laboratory standards with a known isotope ratio, related to international standards, can be done with sufficient precision using stable isotope mass spectrometers (Maitra and Chandrasekhar, 1997).

There are a number of techniques by which reaction mechanisms can be investigated. In this study, the carbon-13 isotope labeling technique was used to track the reaction mechanism for phenol degradation over UV/TiO₂ photocatalysis.

Table 6.1: The physical properties of the carbon-12/carbon-13 isotopes (Man-Sung and Francois, 2006).

	<i>Carbon-12</i>	<i>Carbon-13</i>
<i>Atomic Weight</i>	12	13.003355
<i>Abundance</i>	98.93%	1.07%
<i>Mass Excess</i>	0MeV	3.13MeV
<i>Binding Energy</i>	7.680144MeV	7.47MeV
<i>Magnetic Moment</i>	0 μ	0.70 μ
<i>Spin</i>	0	1/2

6.3 METHODOLOGY

6.3.1 Experimental setup

The phenol solution was prepared and brought to equilibrium by the use of a magnetic stirrer. All batches were prepared using ultra-pure water. A 1L volume reactor was aerated using compressed air to ensure proper mixing as the experiment was taking place. Cold water was circulated in the annulus of the reactor in order to control the temperature of the solution as the experiment ran. A UV lamp inside a quartz tube was immersed just above the reactor using a retort stand. The reactor system was a closed system as UV light is very dangerous. The experiment was run for 100 minutes with samples taken periodically.

6.3.2 Chemicals

Phenol-1-¹³C (Fig 6.2) was purchased from Sigma-Aldrich and is a product of the USA.

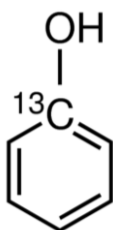


Figure 6.2: Chemical structure of the Phenol-1-¹³C.

Table 6.2: The physical properties of the C-13 isotope labeled phenol.

Chemical formula:	¹³ CC ₅ H ₆ O
Molecular weight:	95.10g/mol
Melting point:	40-42 °C
Boling point:	182 °C
Density:	1.082g/mol at 25 °C
Assay:	98% (CP)

6.3.3 Batch Studies

Experiments were run in triplicates and average values are reported. Carbon-12 phenol degradation experiments and Carbon-13 labeled phenol degradation experiments were ran separately for each batch and results were compared. Each batch was run for 100 minutes and samples were taken every 10 minutes using micro-syringe. Samples were then transferred into 0.5mL micro-centrifuge tubes where they were then centrifuged for 10 minutes to separate suspended catalyst from the solution before GC-MS analysis.

6.3.4 Analytical Methods

The phenol samples were analysed using a GC system comprising of a Clarus 600 GC, Clarus 600T mass spectrometer (MS), attached to a Turbomatrix 40 trap headspace sampler (PerkinElmer, South Africa division). The chemical separation component was the Elite 5MS GC system capillary column (30 m, 250 m) from PerkinElmer. Helium (He) carrier gas of 99.999 % purity and applied at a flow rate of 1 mL/min. MS interface comprised of an electron ioniser (EI) and a high performance mass analyser. This was used to measure the concentration of phenol during the course of photocatalysis.

6.4 RESULTS AND DISCUSSION

The degradation profile of phenol ^{12}C and the ^{13}C labeled phenol can be seen in **Fig 6.3**. It is evident that there was greater phenol removal with phenol ^{12}C than that of phenol ^{13}C under the same photocatalytic conditions; this can be attributed to kinetic isotope effects (KIE). KIE are rate changes due to isotopic substitution at a site of bond breaking in the rate-determining step of a reaction (Simmons et al., 2012). It is understood that ^{13}C contains a neutron more than ^{12}C and is considerably heavier than ^{12}C . This results in a slower reaction rate. The ground-state vibrational energy (or the zero-point vibrational energy) of a bond depends on the mass of the atoms and with the heavier isotope like ^{13}C , zero point energy is lowered thus, more energy is required to break a bond.

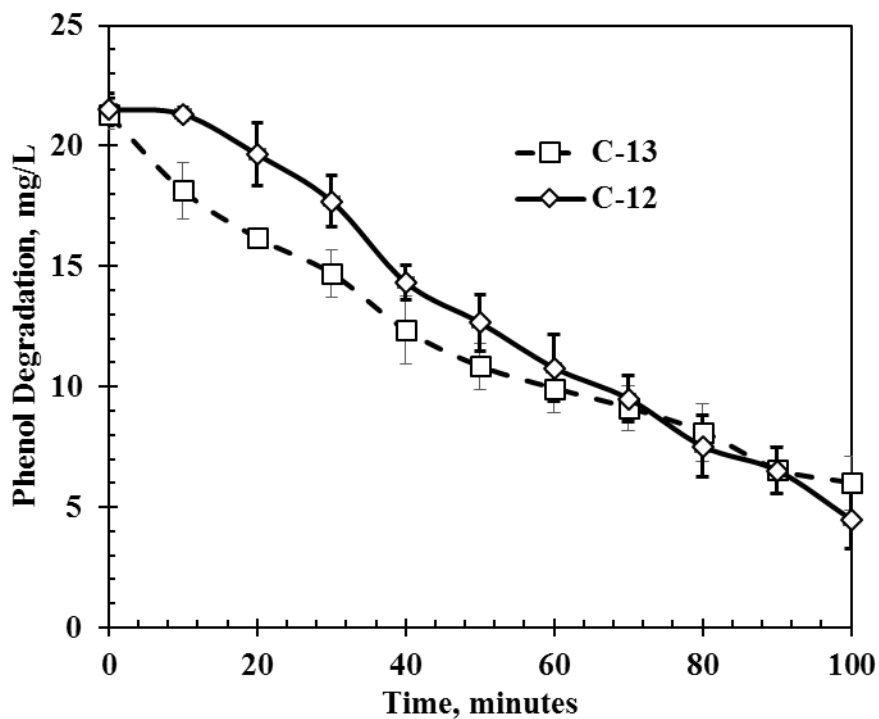


Figure 6.3 : The degradation profile of phenol-¹²C and phenol-¹³C over 100 minutes is depicted in the graph.

Isotope effects are perhaps one of the most powerful tools available to the mechanistic investigator based on the amount and different types of information one can obtain. An isotope effect can be defined as a change in the rate or equilibrium constant of a reaction upon substitution of a heavy atom for a light one at or adjacent to the position of bond cleavage in a molecule undergoing reaction (Cook, 1998). Isotopes provide an excellent tool for the study of reaction because they are isosteric and isoelectronic, and thus non-perturbing. However, isotope effects reflect changes in vibrational frequencies of reactants as they are converted to products in the rate-determining transition states.

There are two types of isotope effects termed primary and secondary. If a heavy atom is substituted for a light one in the bond undergoing cleavage, a primary kinetic isotope effect is observed on the rate of the reaction, expressed as the ratio of the rates with light and heavy atoms, k_L/k_H , where L and H refer to light and heavy, respectively. A primary deuterium (²H) kinetic isotope effect is observed (**Fig 6.4**) upon substitution of deuterium for protium in the pro-R position (1) of ethanol.

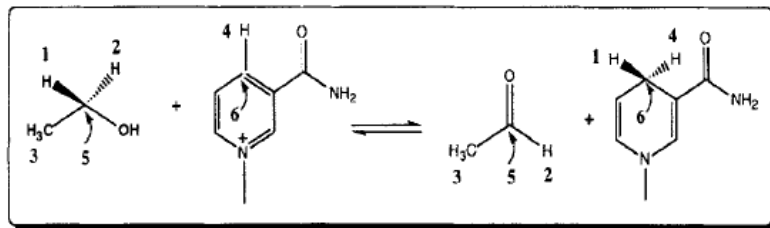


Figure 6.4: Overall reaction for oxidation of ethanol by **NAD'**. Numbers indicate positions of labelling in the reactants and products that will generate isotope effects as indicated in the text (Adopted from; Cook, 1998)

Primary ^{13}C kinetic isotope effects are obtained upon substitution at C-1 of ethanol (5) or the C-4 position of the nicotinamide ring (6) as the bond to the hydride at C-1 of ethanol is broken and the bond to the hydride at C-4 of the nicotinamide ring is formed. Primary kinetic isotope effects reflect changes in the symmetric and asymmetric stretching vibrations as bonds are broken and made (Cook, 1998). Kinetic isotope effects are related to changes in reduced mass that is the product of the atomic mass on both sides of a bond divided by the sum of the two masses. For example, a deuterium isotope effect on C-H bond cleavage, the reduced mass for $^{12}\text{C-H}$ is 0.923, while that for a $^{12}\text{C-D}$ is 1.714, and the ratio of the two is 1.85, similar to the increase in mass from H to D. Heavier atom effects will be much smaller. For example, the reduced masses for $^{12}\text{C-H}$ (0.923) to $^{13}\text{C-H}$ (0.929) gives a ratio of only 1.006 (Westheimer, 1961).

The magnitude of primary isotope effects depends on the nature of the transition state structure. In the case of a hydrogen or hydride transfer reaction, the magnitude of the primary deuterium or (^3H) tritium isotope effect reaches a maximum value as the hydrogen is symmetrically placed between the donor atom from which cleavage occurs and the acceptor atom to which a new bond is formed (Cook,1998). **Figure 6.5** shows a plot of the magnitude of the primary deuterium isotope effect (dotted line) vs. the chemical nature of the transition state, that is the amount of bond cleavage or bond formation. The isotope effect increases from a value of unity for a transition state where no bond cleavage occurs, goes through a maximum where the hydrogen is symmetrically placed between donor and acceptor, and decreases to unity where the new bond to the acceptor has been formed.

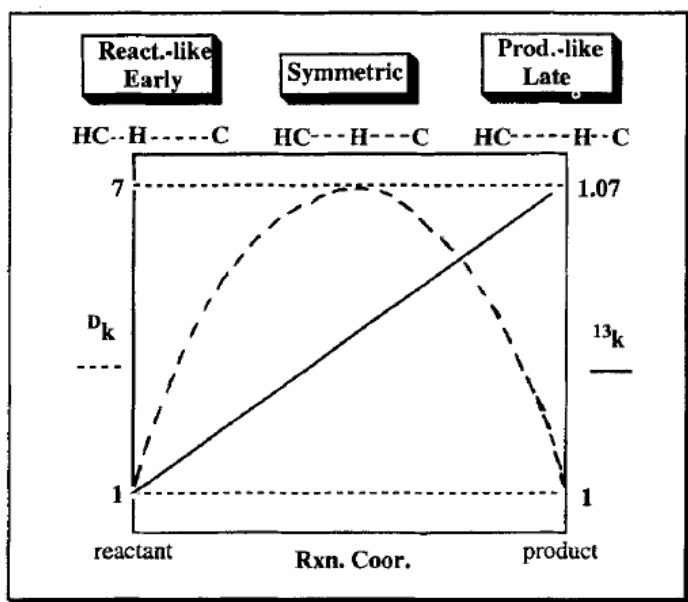


Figure 6.5: Dependence of primary kinetic isotope effects on reactant coordinate position. The deuterium isotope effect reaches a maximum value of 6-8 for a symmetric transition state. The ^{13}C isotope effect for breaking a bond to carbon increases monotonically to the maximum theoretical value of 1.07 until the bond is almost broken, and the isotope effect then decreases sharply to near one (1) (Adopted from Cook, 1998).

The reason for the low values of the deuterium effect for reactant-like or product-like transition states is the contribution of asymmetric stretching frequencies in the ground state that do not cancel in the transition state, while these effects do cancel in the symmetric case. For heavy atom effects, there is not always transfer of the heavy atom, rather a cleavage of the bond to the heavy atom. Thus, the transition state dependence of an ^{13}C isotope effect for a reaction where the bond to carbon is broken is also given in **Fig 6.5**. The isotope effect again starts at unity where no bond cleavage has occurred but increases monotonically to the maximum value of the isotope effect.

In all cases primary isotope effects are observed on the equilibrium constant for a given reaction, and reflect changes in bending vibrations in reactant and product, respectively. Dependent on whether the heavy atom is more stiffly bonded in reactant or product, the equilibrium isotope effect will be normal (> 1) or inverse (< 1), respectively. The equilibrium isotope effect is dependent only on the atoms that are directly bonded to the atom bonded to the heavy atom (Cleland, 1980). The primary deuterium equilibrium isotope effect for the reaction shown in **Fig 6.4** is 1.07. If a heavy

atom is substituted for a light one in a bond that does not undergo bond cleavage, but is bonded to or adjacent to an atom that undergoes bond cleavage, a secondary kinetic isotope effect is observed on the rate of the reaction. Secondary kinetic isotope effects predominantly reflect changes in bending vibrations at the substituted position as the reactant proceeds through the transition state to product (Weistheimer et al, 1958).

6.4.1 Photocatalytic degradation of phenol by UV/TiO₂

As degradation proceeded, other peaks were observed on the chromatogram from HPLC analysis as shown in **Figure 9A-1** and **Figure 9A-2**. These intermediates could not be identified. It can be concluded that these are degradation intermediates.

To investigate the reaction mechanism of phenol degradation, the evolution of intermediates during phenol decomposition was followed by GC-MS analysis. When TiO₂ was irradiated, the phenol concentration decreased exponentially. Several hydroxylation products were detected within the first 10 minutes as reported in Table 6.3. Hydroquinone, benzoquinone, 4,4-biphenol, catechol, benzene-1,2,3-triol and resorcinol were all detected within the first 10 minutes of irradiation.

TiO₂ catalyses the photocatalytic oxidation of phenol. A catalyst is a substance that can be added to a reaction to increase the reaction rate without being consumed in the process. Catalysts typically speed up a reaction by reducing the activation energy or changing the reaction mechanism. The first step in the photocatalytic degradation process is the formation of electron-hole pairs within the TiO₂ photocatalyst. Most of the electron-hole pairs are recombined producing heat energy. However, hydroxyl radicals (HO·) are formed in the presence of electron acceptor (dissolved O₂) while hole (h⁺) oxidises water or TiO₂ surface-active ⁻OH group. Dissolved O₂ reacts with the electron (e⁻) and generates superoxide ion (O₂⁻). Finally, the HO· reacts with either phenol or pollutant compounds until complete mineralization (Chowdhury et al., 2012). Photodegradation mechanism of phenol under UV light is presented as follows;





Overall reaction stoichiometry shows complete mineralisation of phenol with the involvement of HO^{\bullet} (Eq. (6.5)). A study (Devi and Rajashekhar, 2011) described the possible degradation mechanism for phenol under natural sunlight/UV light using nitrogen-doped TiO_2 . Phenol mineralisation went through the formation of dihydroxybenzene (catechol or resorcinol), pent 2-enedioic acid, and oxalic acid. In a parallel reaction path, benzoquinone and maleic acid were formed during the mineralisation (**Fig 6.6**). This pathway is in general agreement with results obtained from ^{13}C labelled phenol and ^{12}C phenol experiments as presented in **Table 6.3 - Table 6.5**.

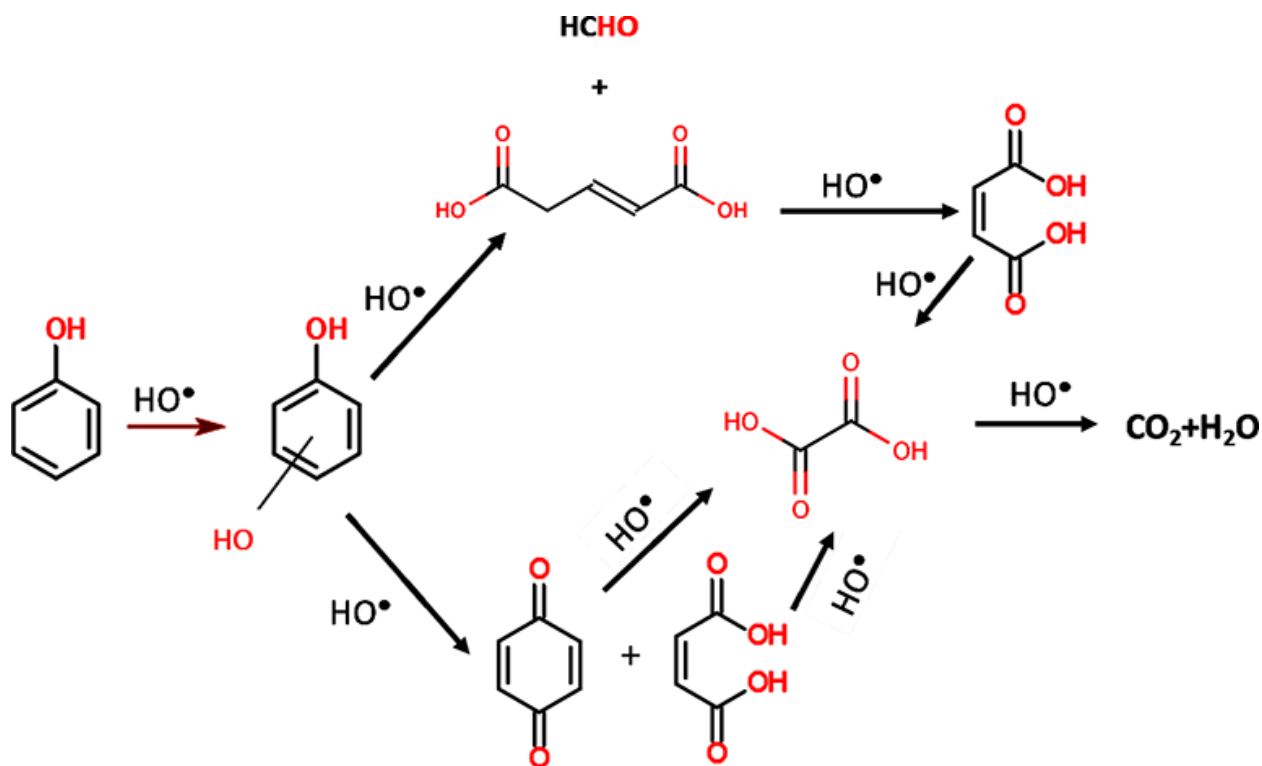


Figure 6.6: Phenol degradation mechanism (Devi and Rajashekhar 2011)

Usually, the hydroxylation of aromatics is believed to be initiated by direct oxidation by $h\nu_{\text{VB}}^+$ followed by hydrolysis or the attack of $\cdot\text{OH}$ (formed from the oxidation of water by $h\nu_{\text{VB}}^+$) in the photocatalytic systems. Various studies (Chen et al, 2002; Turchi, et al, 1989; Okamoto et al, 1985)

have reported the pathway of phenol degradation using TiO_2 as a photocatalyst. The results indicate that the degradation proceeds through the stepwise formation of intermediates. Catechol, hydroquinone, hydroxyhydroquinone and benzene-1,2,3-triol are the products of the initial stages of the degradation. These aromatic intermediates undergo further photocatalytic oxidation to ring cleavage to yield carboxylic acids and aldehydes, which give CO_2 and H_2O due to the decarboxylation as shown in **Fig 6.6**.

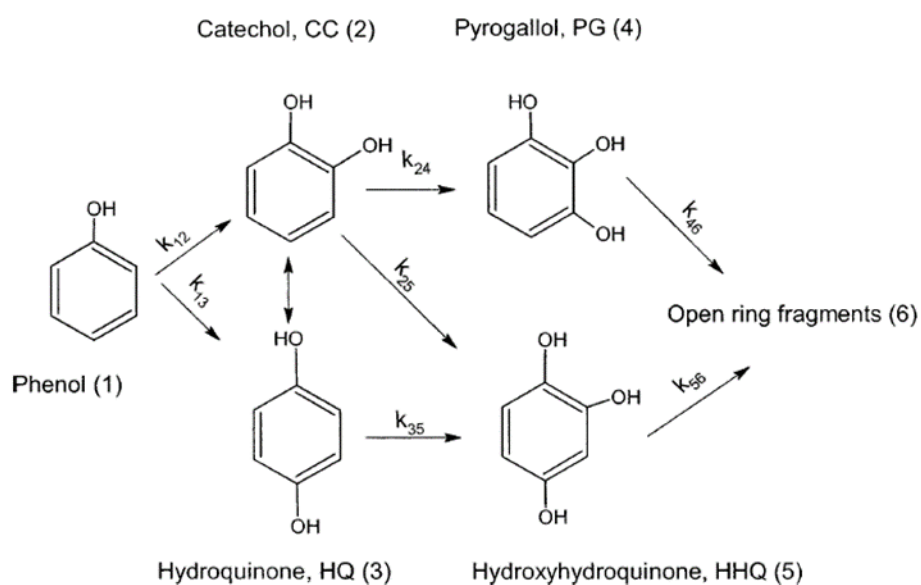


Figure 6.7: A scheme of phenol degradation with reaction pathways (Nagaveni et al., 2004)

The intermediates detected during photocatalytic experiments are recorded in **Table 6.3** and **Table 6.4**. The table shows a comparison of intermediates detected under the same photocatalytic conditions with the use of phenol ^{12}C and the ^{13}C labeled phenol, respectively. Their qualifier ions also referred to as their mass to charge (m/z) ratios identified each intermediate on chromatograms from GC-MS analysis. Qualifier ions are the fingerprint of a compound. The two reactions are comparable, each revealing the same intermediates as expected with the exception of 2-propylphenol in the case of phenol ^{13}C . This can be attributed to kinetic isotope effects. Perhaps a

different reaction pathway was taken and it could be a result of one product being favored over another.

Another study (Xiao-yan et al., 2005) carried out on the kinetics and pathways of the electrochemical (EC) degradation of phenol at three different types of anodes, Ti/SnO₂-Sb, Ti/RuO₂, and Pt. Although phenol was oxidised by all of the anodes, there was a considerable difference between the three anode types in the effectiveness and performance of EC organic degradation. It was argued that anodic property not only affects the reaction kinetics of various steps of EC organic oxidation, but also alters the pathway of phenol electrolysis. Several intermediates were detected by GC-MS analysis; their evolution was studied and is shown in **Fig 6.8**. Pathway (**Fig 6.9**) was postulated based on these experimental findings.

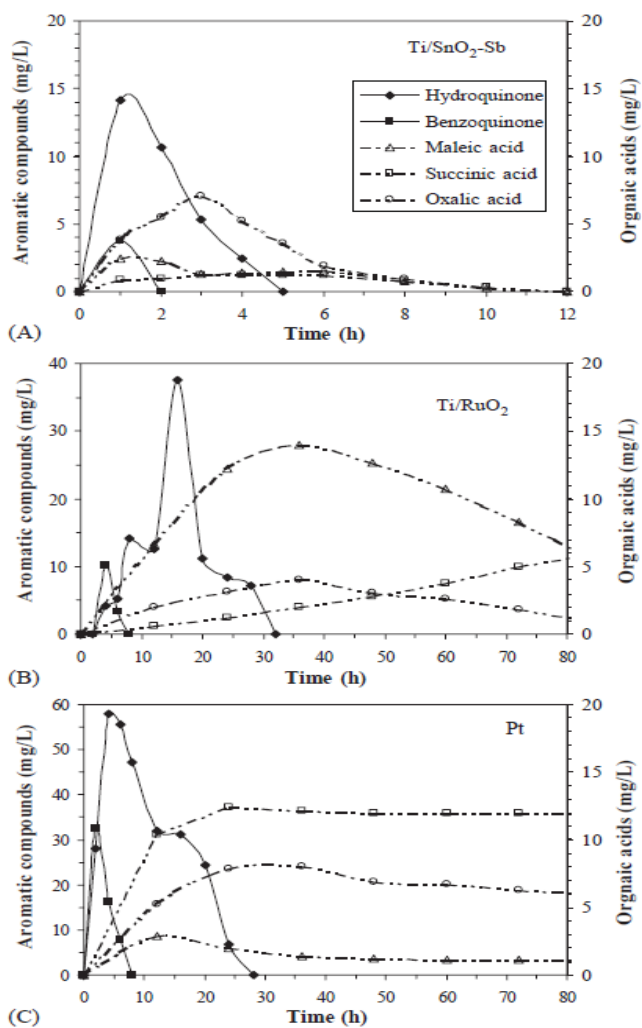


Figure 6.8: Intermediate products of EC phenol degradation on anodes (A) Ti/SnO₂-Sb, (B) Ti/RuO₂, and (C) Pt (Adopted from Xiao-yan et al., 2005).

The experimental results suggest that EC phenol oxidation on different anodes may follow different reaction pathways as seen by the evolution of intermediates in **Fig 6.8**. The major steps of the reaction pathway for EC phenol degradation are summarised in **Fig 6.9** with an emphasis on two modifications.

The first is the inclusion of polymerization via phenoxy radicals that attack either benzoquinone or hydroquinone. Polymerization is hardly a reversible reaction, and the polymeric products are likely to be more recalcitrant to EC degradation than phenol. For benzoquinone and hydroquinone, ring cleavage (I) and polymerization (II) are two parallel processes that occur simultaneously. This was in general agreement with carbon-13 kinetic isotope effect experiments. The reaction rate of phenol ¹²C and ¹³C labeled phenol experiments were compared. KIE calculations were carried out from the rate constants. KIE calculations revealed a primary kinetic isotope effect. A primary KIE revealed that the ¹³C isotope was labeled at a site of bond breaking in the rate determining step of the reaction. The conversion of hydroquinone to benzoquinone involved bond breaking at carbon position one (C-1) on the labeled phenol. If the aromatic ring is broken rapidly, then there is little accumulation of benzoquinone and an insignificant formation of polymeric compounds, which is the case with the Ti/SnO₂-Sb anode. In contrast, if ring cleavage is rather slow, then polymerization becomes more significant, which is in fact the case with the Ti/RuO₂ and Pt anodes (Xiao-yan et al., 2005).

Another pathway modification is the addition of a route from maleic acid to oxalic acid (IIIB) in parallel with the conventional route of maleic acid reduction to succinic acid (IIIA). For the Ti/RuO₂ and Pt systems, although the oxidation of maleic acid to oxalic acid might also take place, route IIIA is still the dominant process (Xiao-yan et al., 2005). With the Ti/SnO₂-Sb anode, maleic acid is rapidly converted to oxalic acid following route IIIB, whereas route IIIA is relatively slower and hence less important. These findings are in general agreement with the results obtained from carbon-13 tracking results. Maleic acid was part of the ¹³C pathway. It's appearance and disappearance was seen throughout photocatalytic experiments, however it could not be quantified. The intermediate oxalic acid is readily oxidised by anodic oxidation to CO₂ (Feng and Li, 2003).

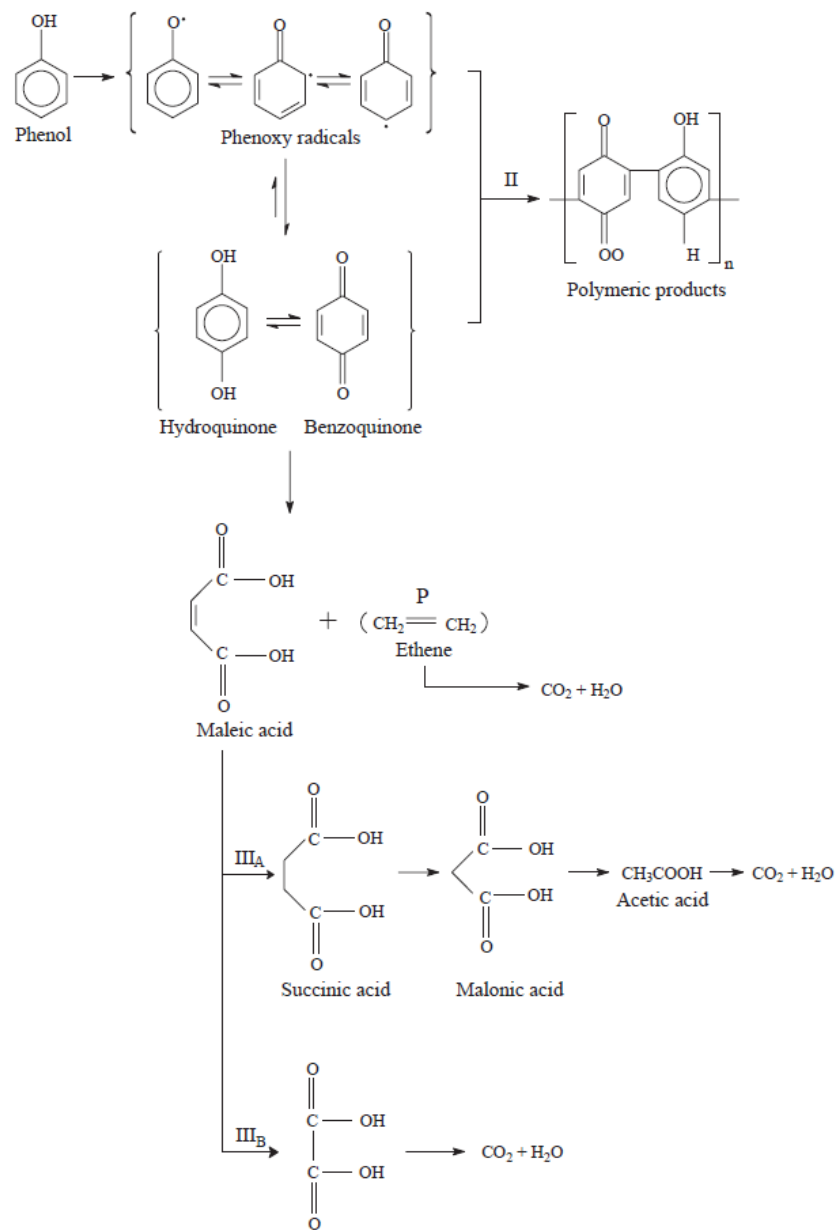


Figure 6.9: Reaction pathway of electrochemical phenol degradation (Adopted from Xiao-yan et al., 2005)

Table 6.3: The intermediates detected by GC-MS analysis during the cause of UV/TiO₂ photocatalytic degradation of phenol-¹²C.

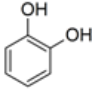
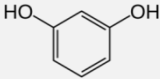

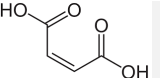
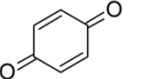
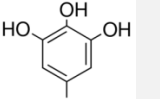
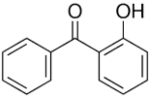
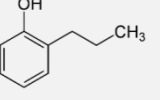
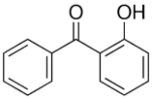
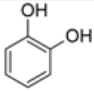
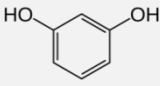
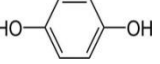
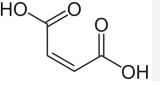
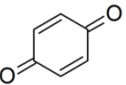
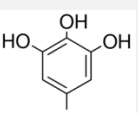
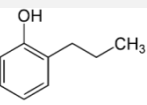
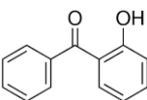
<i>Intermediate</i>	<i>Structure</i>	<i>Molecular Weight (g/mol)</i>	<i>Phenol C-12</i>
			<i>Mass/Charge (m/z) ratio</i>
<i>Catechol</i>		110.1	110; 111; 92; 82; 81; 64; 63; 53; 39; 27
<i>Resorcinol</i>		110.1	111; 110; 82; 81; 69; 64; 55; 53; 27; 39
<i>Hydroquinone</i>		110.1	111; 110; 82; 81; 55; 54; 53; 39; 27; 26;
<i>Maleic acid</i>		116.1	99; 98; 72; 55; 54; 53; 46; 45; 27; 26
<i>Benzoquinone</i>		108.1	109; 108; 82; 80; 54; 53; 52; 50; 26; 25
<i>Benzene-1,2,3-triol</i>		126.1	284; 228; 79; 78; 77; 65; 52; 51; 50; 39
<i>2-hydroxybenzophenone</i>		198.2	199; 198; 121; 97; 93; 105; 77; 65; 51; 39
<i>2-propylphenol</i>		136.2	136; 108; 107; 91; 79; 78; 77; 51; 39; 27
<i>2-hydroxybenzophenone</i>		198.2	199; 198; 121; 97; 93; 105; 77; 65; 51; 39

Table 6.4: The intermediates detected by GC-MS analysis during the course of UV/TiO₂ photocatalytic degradation of phenol-¹³C.

Phenol C-13

<i>Intermediate</i>	<i>Structure</i>	<i>Molecular weight</i>	<i>Mass/charge (m/z)ratio</i>
<i>Catechol</i>		110.1	110; 111; 92; 82; 81; 64; 63; 53; 39; 27
<i>Resorcinol</i>		110.1	111; 110; 82; 81; 69; 64; 55; 53; 27; 39
<i>Hydroquinone</i>		110.1	111; 110; 82; 81; 55; 54; 53; 39; 27; 26;
<i>Maleic acid</i>		116.1	99; 98; 72; 55; 54; 53; 46; 45; 27; 26
<i>Benzoquinone</i>		108.1	109; 108; 82; 80; 54; 53; 52; 50; 26; 25
<i>Benzene-1,2,3-triol</i>		126.1	284; 228; 79; 78; 77; 65; 52; 51; 50; 39
<i>2-propylphenol</i>		136.2	136; 108; 107; 91; 79; 78; 77; 51; 39; 27
<i>2-hydroxybenzophenone</i>		198.2	199; 198; 121; 97; 93; 105; 77; 65; 51; 39

The profile of intermediates under the same photocatalytic reaction over a 100 minute period are recorded in **Table 6.** Samples were collected at 10 minute intervals and taken for analysis, therefore the table reports intermediates detected in 10 minute intervals as indicated by (x), for phenol ¹²C and ¹³C labeled phenol experiments. It is evident that intermediates appeared and disappeared during the course of reaction. Photocatalysis is a complex reaction, one which consists of competing reactions where the starting material is converted to something other than the desired products. Photocatalysis is further complicated by the fact that it occurs in stages in which intermediate products are formed and then converted by further reactions to the final products. (Nagaveni et al., 2004) found that the concentration of the intermediates formed during the

degradation of phenol by P-25 Degussa increased initially with time followed by a decrease with time because of the competition of the primary (k_{12} , k_{13}) and secondary (k_{24} , k_{25} , k_{35}) hydroxylation steps as seen in **Fig 6.7**. A preliminary analysis of the data indicates that the photocatalytic degradation rate coefficients of the primary and secondary hydroxylation steps for phenol degraded by P-25 Degussa are 4×10^{-3} and 10^{-2} , respectively.

(Nagaveni et al, 2004) investigated the formation of intermediates in comparison to the phenol degradation with Degussa P-25 TiO₂. Two major peaks for catechol (CC) and hydroquinone (HQ) were detected and their concentration increased with decrease in phenol concentration over a reaction time of 180 minutes. The phenol conversion to open ring fragments was 34,5 %, with combined amounts of HQ, CC and unreacted phenol of 23.4 %, 22.3 % and 19.8 %, respectively.

Table 6.5: The evolution of intermediates detected during the course of phenol C-12 and phenol-C-13 degradation by UV/TiO₂ Photocatalysis.

		<i>Phenol-C-12</i>									
<i>Intermediate</i>	<i>Time, minutes</i>										
	10	20	30	40	50	60	70	80	90	100	
<i>Maleic acid</i>	x		x	x	x	x		x		x	
<i>Benzoquinone</i>	x		x	x	x			x		x	
<i>Resorcinol</i>	x	x		x	x	x		x	x	x	
<i>2-Hydroxybenzophenone</i>				x				x			
<i>Catechol</i>	x	x	x	x	x	x		x		x	
<i>Hydroquinone</i>	x	x	x	x	x	x		x	x		
<i>Benzene-1,2,3-triol</i>	x		x	x	x	x		x		x	
		<i>Phenol-C-13</i>									
<i>Intermediate</i>	<i>Time, minutes</i>										
	10	20	30	40	50	60	70	80	90	100	
<i>Maleic acid</i>	x			x	x	x		x		x	
<i>Benzoquinone</i>	x			x	x	x		x		x	
<i>Resorcinol</i>	x		x	x	x	x				x	
<i>Catechol</i>	x		x	x	x	x		x		x	
<i>Hydroquinone</i>	x		x	x	x	x		x		x	
<i>Benzene-1.2.3-triol</i>	x			x	x	x		x		x	
<i>2-propylphenol</i>	x		x	x	x			x		x	
<i>2-hydroxybenzophenone</i>	x		x	x	x	x		x		x	

6.5 CARBON-13 ISOTOPE TRACKING

6.5.1 METHOD DEVELOPMENT

The selective ion recording (SIR) function on the GC-MS was used for carbon-13 isotope tracking. SIR is a mass spectrometry scanning mode in which only a limited mass-to-charge ratio range is transmitted or detected by the instrument, as opposed to the full spectrum range. This mode of operation typically results in significantly increased sensitivity. This technique is most effective due to its inherent nature.

Photocatalytic degradation intermediates and their mass-to-charge ratios were identified from literature. This information was then recorded on the GC-MS library. SIR functions were created for each of the identified intermediates from literature. Carbon-13 mass-to-charge ratio was incorporated in all SIR functions. This would then allow for the tracking of ^{13}C in all intermediates detected. The intermediates generated during the degradation process were analysed by interpretation of their fragment ions in the mass spectra.

6.5.2 CARBON-13 TRACKING RESULTS OF PHENOL DEGRADATION BY UV/TiO₂ PHOTOCATALYSIS.

The movement of the Carbon-13 isotope during the course of degradation was followed. **Fig 9B.1** – **Fig 9B.7** show the chromatograms of the intermediates that contained the ^{13}C isotope. Chromatograms from phenol- ^{13}C labeled experiments contained a higher ^{13}C relative abundance of the mass/charge ratios than that of phenol- ^{12}C experiments. Carbon-13 was also detected in the unlabeled phenol due to its natural abundance. However, a much higher ^{13}C relative abundance is expected in the carbon-13 labeled phenol than that of the unlabeled phenol ^{12}C .

Experiments were run in parallel and are reported as such. The GC-MS chromatograms showed ^{13}C relative abundances were much higher in Phenol- ^{13}C experiments than that of phenol- ^{12}C , as expected. Hydroquinone, maleic acid and resorcinol were detected during ^{13}C tracking as presented in the

Table 6., these intermediates contained the carbon-13 isotope in the highest relative abundance. This revealed the movement of the isotope. Based on this information, the pathway (was postulated to describe the phenol degradation pathway by UV/TiO₂ photocatalysis.

A study (Su et al, 2012), followed the evolution of the reaction intermediates during the phenol photodecomposition process to explore how the nanoparticles participate in the catalytic cycle as demonstrated in **Fig 6.10**. When pristine TiO₂ was irradiated, the phenol concentration [P] declined exponentially. Significant accumulation of hydroquinone was observed within the first 30 minutes of irradiation while benzoquinone and catechol were only found in negligible amounts. The hydroquinone concentration ([H]) reached a maximum of ~100 μM, that is, 25 % of the phenol starting concentration. Only after the concentration ratio of [P]: [H] dropped below unity did [H] begin to decrease. This clearly showed that the decomposition of hydroquinone dictates the decay of the phenolic compounds over TiO₂. Similar observations have been reported previously (Chen et al., 2002; Palmisano et al., 1994; Nagaveni et al., 2004) implying that the hydroquinone pathway is the rate limiting step for phenol decomposition over TiO₂.

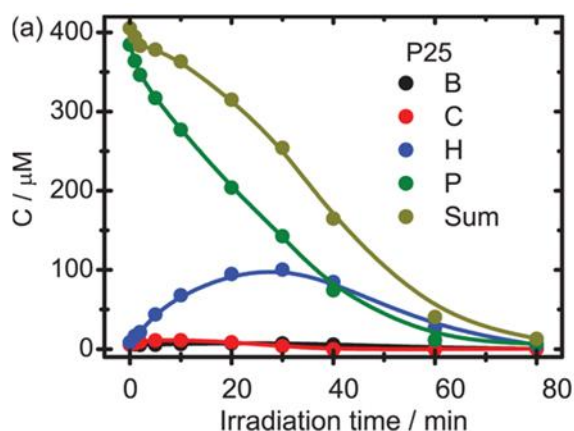


Figure 6.10: The evolution of phenol and hydroxylated phenolic intermediates derived from UV-vis spectra using TiO₂ P-25 Degussa. [B], [C], [H] and [P] indicate the benzoquinone, catechol, hydroquinone and phenol concentration curves, respectively (Adopted from Su et al, 2012).

Table 6.6: The intermediates detected from C-13 tracking results by UV/TiO₂.

<i>Phenol-C-13</i>	
<i>Intermediates</i>	Hydroquinone
	Maleic Acid
	Resorcinol

It is important to emphasize a logical point about the determination of reaction mechanisms. A proposed mechanism can never really be proven; rather, it is a case of alternative mechanisms being eliminated. Having in mind a mechanism that explains all the facts does not constitute proof that the mechanism is correct. That conclusion is possible only when all alternatives have been excluded. A key stage in a mechanistic investigation then is the enumeration of the various possible mechanisms and the design of experiments that distinguish between them. The principal basis for enumerating mechanistic possibilities is accumulated chemical experience with related systems and the inherent structural features of the system. A chemist approaching a mechanistic study must cast as broad as possible vision on the problem so as not to exclude possibilities.

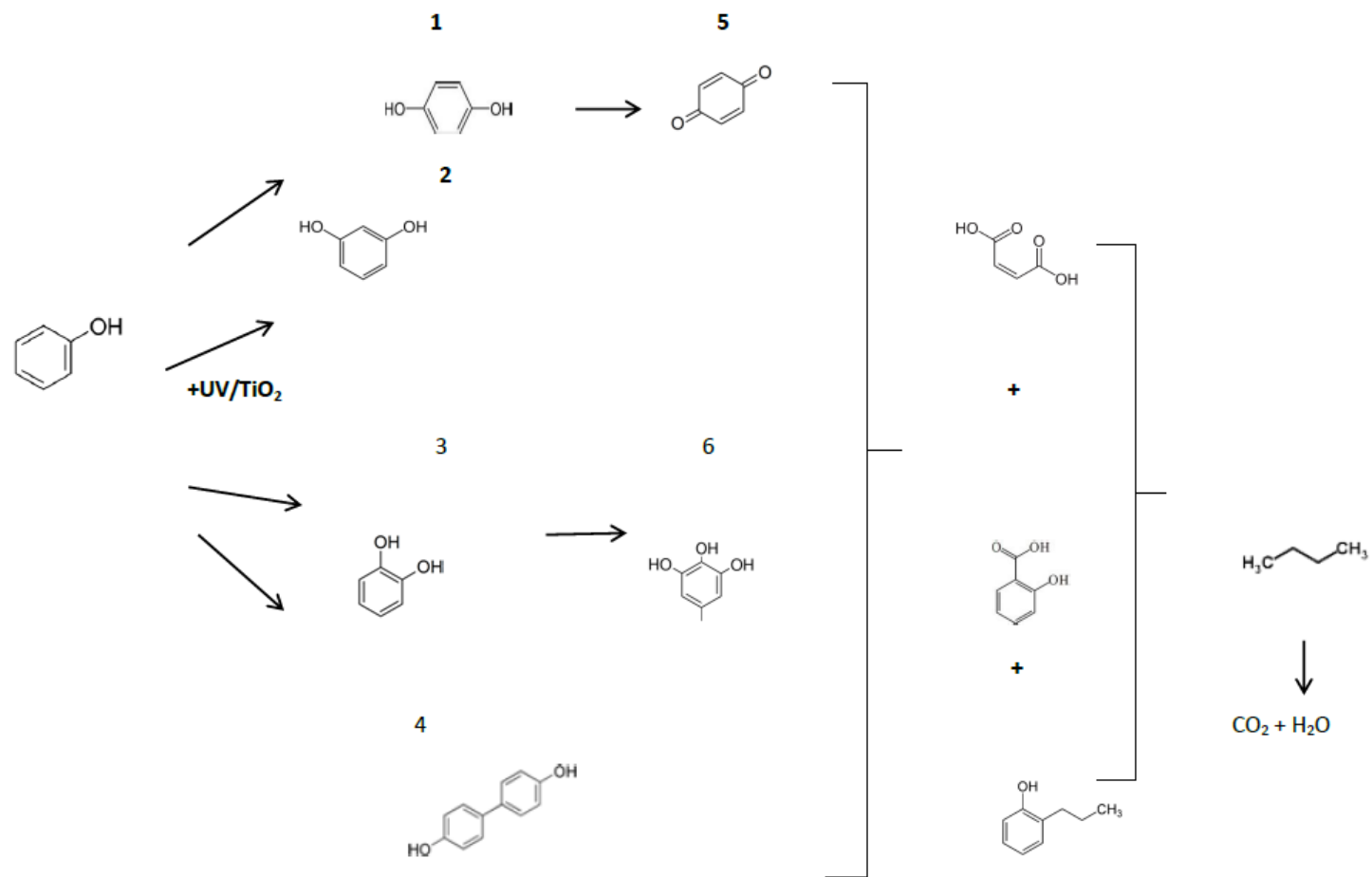


Figure 6.11: The postulated reaction pathway for the UV/TiO₂ photocatalytic degradation of phenol.

The UV/TiO₂ photocatalytic degradation pathway of phenol is postulated in **Fig 6.11**. During the photocatalytic degradation of phenol, several hydroxylation products were detected as depicted by compounds 1 – 6. These intermediates contain primary and secondary hydroxylation products. These hydroxylation products were detected within the first 10 minutes of photocatalysis. This confirms that hydroxylation is the primary step of photocatalysis. Hydroxylation products are believed to be initiated by direct oxidation by h_{ν}^{+} followed by hydrolysis or the attack of $\cdot\text{OH}$ (formed from the oxidation of water by h_{ν}^{+}) in the photocatalytic systems (Bui et al., 2010).

Different regioisomeric hydroxylated products were detected because phenol is a substituted aromatic ring. The phenol structure consists of a hydroxyl (-OH) group substituent on a benzene ring. The -OH substituent is an electron donating group (EDG) and therefore results in electrophilic substitution at the ortho (-o) and para (-para) positions (Palmisano et al., 2006). This was confirmed by the detection of degradation intermediates; hydroquinone, benzoquinone, catechol and benzene-1,2,3-triol. Subsequent oxidation of hydroxylation products is reported to lead to ring open products (Bui et al., 2010). This was confirmed by the detection of maleic acid.

The observed initial ring-opening products of aromatic compounds in aerated aqueous solutions are always carboxylic acids or carboxylic acid derivatives. Thus decarboxylation of these carboxylic acids is one of the most important steps for complete mineralization of organic pollutants (Pang et al., 2014). Further degradation by decarboxylation is reported (Pang et al., 2014) to lead to further ring breaking into smaller hydrocarbon chains until the compound reaches full mineralisation. However, these hydrocarbon chains were not detected during experiments because of short reaction times. The reaction did not reach full mineralisation.

6.5.3 Reaction Pathway under Anaerobic Condition (absence of electron scavenger)

The photocatalytic degradation reaction requires the use of electron acceptor to reduce the charge carrier recombination. Oxygen is the most common electron acceptor because of its availability, higher solubility, and nontoxic nature (Chowdhury et al.,2017). The photocatalytic reaction of phenols will terminate if sufficient oxygen is not available in the solution (Chen et al., 1999). A study by Chen and Ray (1998) showed the improvement of 4-Nitrophenol (4-NP) photo-degradation rate with increasing oxygen partial pressure. The photo-degradation rate constant reached approximately 70% of its maximum value at oxygen partial pressure of 0.2 atm. The effect of oxygen partial pressure on the photo-degradation of 4-NP is described by a non-competitive Langmuir kinetic equation as follows:

$$k_p \propto \frac{K_{O_2} p_{O_2}}{1 + K_{O_2} p_{O_2}}$$

where k_p is the kinetic constant for 4-NP degradation, K_{O_2} is the adsorption constant of dissolved oxygen on photocatalyst, and p_{O_2} is the partial pressure of dissolved oxygen.

Experimental conditions were manipulated to test whether the reaction pathway would be affected. Photocatalytic experiments were carried out without aeration. **Table 6.4** presents the intermediates detected with phenol ^{12}C and ^{13}C labeled phenol experiments under the same conditions. Results are comparable with the exception of benzene-1,2,3-triol. Carbon-13 labeled phenol experiments detected benzene-1,2,3-triol. This is attributed to KIE and the possibility of a different reaction pathway favouring one product over another. **Table 6.8** shows the evolution of intermediates over a 100 minutes period with samples taken at 10 minute intervals. The table shows the appearance and disappearance of specific intermediates represented by (x), during the course of photocatalytic degradation. This is attributed to competing primary hydroxylation and secondary hydroxylation reactions (Nagaveni et al, 2004).

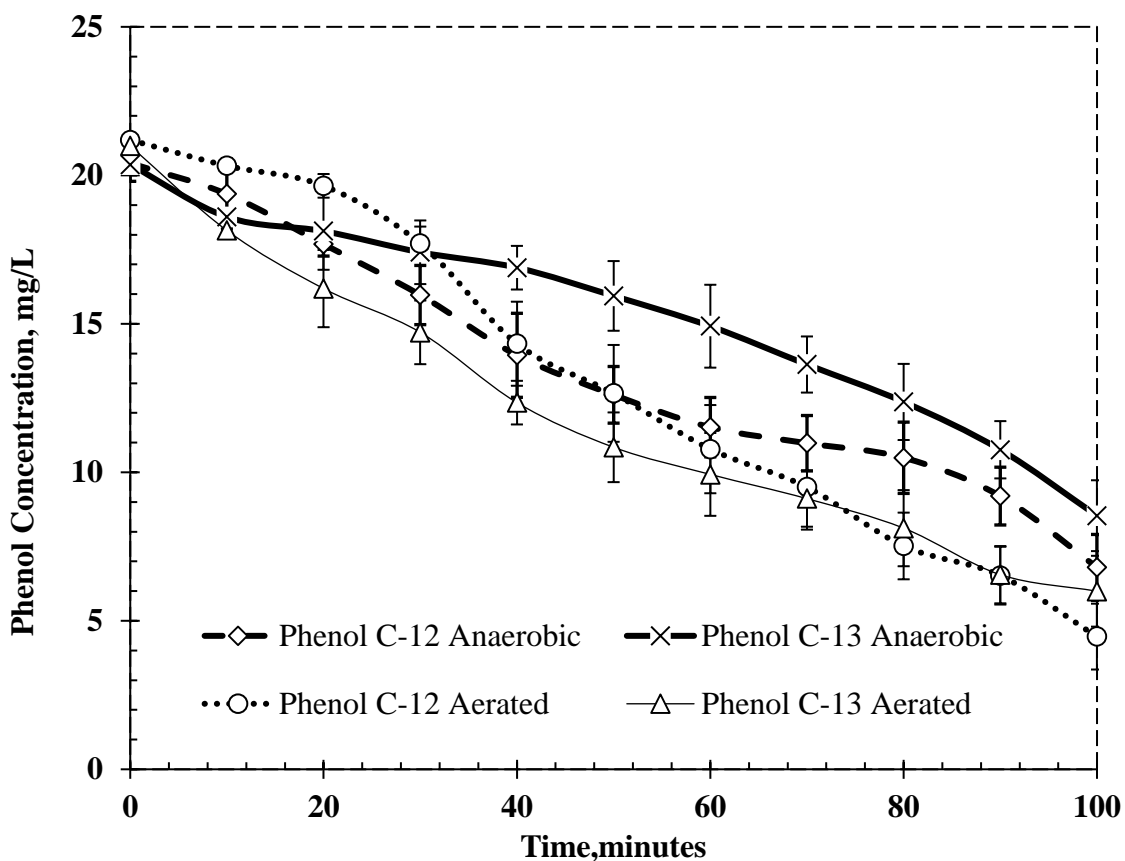


Figure 6.12: The UV/TiO₂ photocatalytic degradation profile of phenol-¹²C and phenol-¹³C labeled experiments with and without aeration.

The phenol removal profiles are shown in **Fig 6.12**. There is greater phenol removal with the aerated systems for both phenol-¹²C and phenol-¹³C labeled, than with the anaerobic systems. There is also a difference in phenol degradation between phenol ¹²C and the ¹³C labeled phenol. The ¹³C labeled phenol has an overall lower phenol removal than the ¹²C phenol due to obvious isotope effect (Simmons and Hartwig, 2012). Oxygen acts as the electron scavenger for the conduction band electrons (e^-_{CB}) thereby preventing recombination of the electron-hole pair and thus promoting photocatalysis (Chong et al., 2009). Without subsequent addition of oxygen, the reaction rate is slow as the rate of dissolved oxygen addition by surface aeration is less than what is required by the reaction. The results clearly show that addition of oxygen to the reaction mixture is required to sustain the photocatalytic reaction and to effect complete degradation in minimum time.

Table 6.4: The phenol photo degradation intermediates detected by GC-MS analysis for phenol-¹²C under anaerobic conditions (absence of electron scavenger).

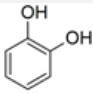
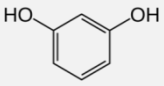
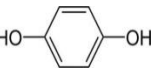
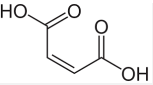
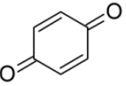
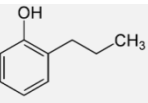
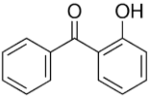
<i>Intermediate</i>	<i>Structure</i>	<i>Molecular weight</i>	<i>Phenol C-12</i>
			<i>Mass/charge (m/z) ratio</i>
<i>Catechol</i>		110.1	110; 111; 92; 82; 81; 64; 63; 53; 39; 27
<i>Resorcinol</i>		110.1	111; 110; 82; 81; 69; 64; 55; 53; 27; 39
<i>Hydroquinone</i>		110.1	111; 110; 82; 81; 55; 54; 53; 39; 27; 26;
<i>Maleic acid</i>		116.1	99; 98; 72; 55; 54; 53; 46; 45; 27; 26
<i>Benzoquinone</i>		108.1	109; 108; 82; 80; 54; 53; 52; 50; 26; 25
<i>2-propylphenol</i>		136.2	136; 108; 107; 91; 79; 78; 77; 51; 39; 27
<i>2-hydroxybenzophenone</i>		198.2	199; 198; 121; 97; 93; 105; 77; 65; 51; 39

Table 6.8: The phenol photo degradation intermediates detected by GC-MS analysis for phenol-¹³C under anaerobic conditions (absence of electron scavenger).

Phenol C-13

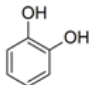
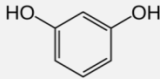
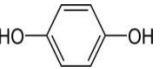
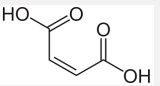
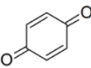
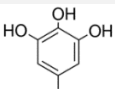
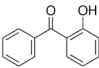
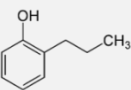
<i>Intermediate</i>	<i>Structure</i>	<i>Molecular Weight (g/mol)</i>	<i>Mass/Charge (m/z) ratio</i>
<i>Catechol</i>		110.1	110; 111; 92; 82; 81; 64; 63; 53; 39; 27
<i>Resorcinol</i>		110.1	111; 110; 82; 81; 69; 64; 55; 53; 27; 39
<i>Hydroquinone</i>		110.1	111; 110; 82; 81; 55; 54; 53; 39; 27; 26;
<i>Maleic acid</i>		116.1	99; 98; 72; 55; 54; 53; 46; 45; 27; 26
<i>Benzoquinone</i>		108.1	109; 108; 82; 80; 54; 53; 52; 50; 26; 25
<i>Benzene-1,2,3-triol</i>		126.1	284; 228; 79; 78; 77; 65; 52; 51; 50; 39
<i>2-hydroxybenzophenone</i>		198.2	199; 198; 121; 97; 93; 105; 77; 65; 51; 39
<i>2-propylphenol</i>		136.2	136; 108; 107; 91; 79; 78; 77; 51; 39; 27

Table 6.9: The intermediates detected during the course of phenol-C-13 degradation by UV/TiO₂ Photocatalysis under anaerobic conditions (absence of electron scavenger).

<i>Intermediate</i>	<i>Phenol-C-12</i>									
	<i>Time, minutes</i>									
	10	20	30	40	50	60	70	80	90	100
<i>Maleic acid</i>	x		x	x	x	x	x	x		
<i>Benzoquinone</i>	x	x	x	x	x	x		x	x	
<i>Resorcinol</i>	x	x	x	x	x	x	x	x	x	x
<i>2-Hydroxybenzophenone</i>	x		x			x	x			
<i>2-Propylphenol</i>	x		x	x		x	x		x	
<i>Catechol</i>	x		x			x	x	x	x	
<i>Hydroquinone</i>	x	x	x	x	x	x	x	x	x	x

<i>Intermediate</i>	<i>Phenol-C-13</i>									
	<i>Time, minutes</i>									
	10	20	30	40	50	60	70	80	90	100
<i>Maleic acid</i>	x		x	x		x	x			
<i>Benzoquinone</i>	x		x	x		x	x			x
<i>Resorcinol</i>	x		x	x	x	x	x	x	x	x
<i>Catechol</i>	x		x	x	x	x	x		x	x
<i>Hydroquinone</i>	x		x	x	x	x	x	x	x	x
<i>2-Propylphenol</i>	x	x	x	x	x	x	x	x		
<i>Benzene-1.2.3-triol</i>	x		x	x		x	x	x		x
<i>2-Hydroxybenzophenone</i>	x		x	x	x	x	x	x		x

6.5.4 Carbon-13 Tracking Results Of Phenol Degradation by UV/TiO₂ Photocatalysis Under Anaerobic Conditions.

Table 6.10: The intermediates detected from C-13 tracking results in the absence of electron scavenger.

	<i>Phenol-C-13</i>
<i>Intermediates</i>	Benzoquinone
	Maleic Acid
	Hydroquinone

Phenol can undergo either a direct ring-opening process via pathway 1 or an indirect ring cleavage process via pathways 2 or 3, where the hydroxylated phenolic intermediates and its oxidised form, mainly hydroquinone, and benzoquinone, are generated by the non-selective attack of •OH radicals

as depicted in **Fig 6.13**. All these intermediates can eventually be oxidized to CO₂ via various sub-intermediates following the ring opening processes (Sue et al., 2012).

The photo-induced electron-hole pairs can alternatively participate in the redox reaction via pathway 4 and 5. Eq 6.1 and 6.2 describe the reduction and oxidation half reactions for the conversion of benzoquinone to hydroquinone and benzoquinone to hydroquinone, respectively.

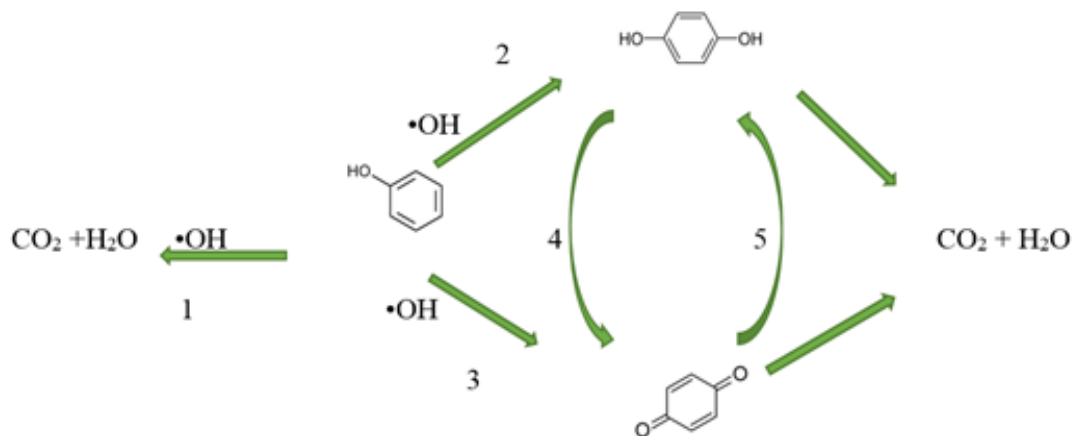


Figure 6.13: The proposed degradation pathway of Phenol.

Researchers believe that the $\cdot\text{OH}$ radicals are the main active oxygen species in the ring opening step due to their high oxidative ability (Pang *et al.*, 2014b). However, electrochemical studies suggest that the aromatic rings cannot be efficiently cleaved by the $\cdot\text{OH}$ radicals in the absence of O₂, indicating the $\cdot\text{OH}$ radicals are not a good active species for the cleavage of aryl rings (Pang *et al.*, 2014b).

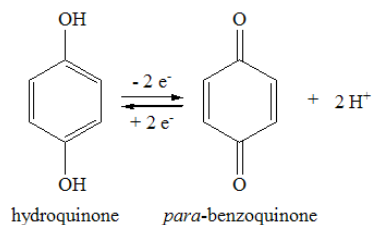
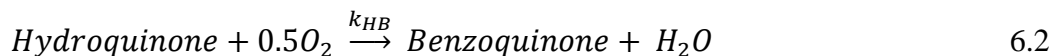
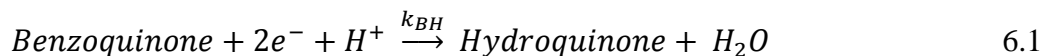


Figure 6.14: Conversion between hydroquinone and benzoquinone (Adopted from Shanmugam et al., 2007)



Where k_{BH} and k_{HB} are the rate constants for the conversion of benzoquinone-to-hydroquinone and hydroquinone-to-benzoquinone respectively.

6.1 EFFECT OF CATALYST ON REACTION

It is the collision of particles that causes reactions to occur and only some of these collisions are successful. This is because the reactant particles have a wide range of kinetic energies (KE), and only a small fraction of the particles will have enough energy (and the correct orientation) to actually break bonds so that a chemical reaction can take place. The minimum energy that is needed for a reaction to take place is called the activation energy (Masel, (2001).

Catalysts are substances that speed up a reaction by facilitating a particular mechanism sometimes by influencing an existing pre-reaction and sometimes by making a new process energetically favourable. A catalyst increases reaction rates in a slightly different way from other methods of increasing reaction rate. Catalysts typically speed up a reaction by reducing the activation energy or changing the reaction mechanism (Behr, 2002). This is achieved by orienting the reacting particles in such a way that successful collisions are more likely and by reacting with the reactants to form an intermediate that requires lower energy to form the product. Their presence or absence frequently determines the course a reaction may take, simply because one of a number of competing reactions is, or is not, favoured (Masel, Richard I. (2001).

Catalysts generally react with one or more of the reactants to form a chemical intermediate, which then reacts to form the final product. The chemical intermediate is sometimes called the activated complex. The catalyst provides alternative set of reaction steps, which we refer to as an alternative pathway. The pathway involving the catalyst requires less activation energy and is therefore faster (Behr, 2002).

Energy diagrams are useful to illustrate the effect of a catalyst on reaction rates. Catalysts decrease the activation energy required for a reaction to proceed (shown by the smaller magnitude of the activation energy on the energy diagram in **(Figure 6.15)**, and therefore increase the reaction rate

(Lindström and Petterson, 2003). With a catalyst, the average kinetic energy of the molecules remains the same but the required energy decreases (**Figure 6.16**).

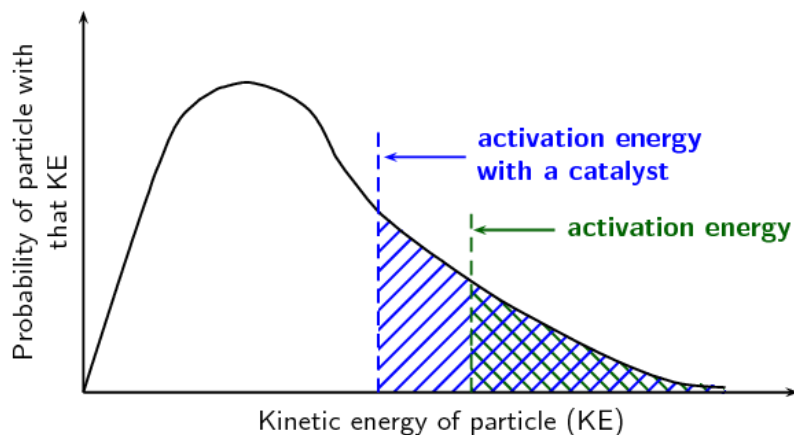


Figure 6.15: The proportion of particles that have enough energy to react is increased in the presence of a catalyst (Adopted from Behr, 2002)

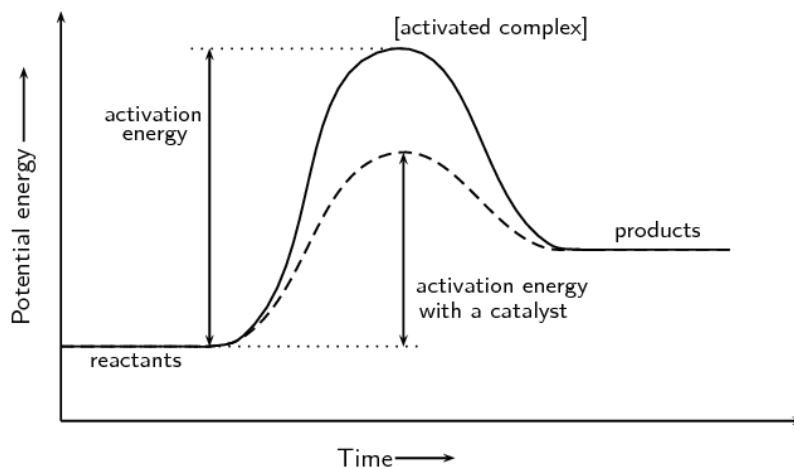


Figure 6.16: The effect of a catalyst on the activation energy of an endothermic reaction. The catalyst would act in the same way for an exothermic reaction (Adopted from Behr, 2002)

6.2 EFFECT OF UV LIGHT ON REACTION

Also important to the study of reaction mechanisms are the energy requirements of the reactions. Most reactions of mechanistic interest are activated processes—that is, processes that must have a supply of energy before they can occur. The energy is consumed in carrying the starting material of the reaction over an energy barrier. This process occurs when the starting material absorbs energy and is converted to an activated complex or transition state. The activated complex then proceeds to furnish the product of the reaction without further input of energy—often, in fact, with a release of energy (Sohn and Olivas-Martinez, 2014). Such considerations are important to an understanding of reaction mechanisms because the reaction pathway that any reaction follows is the one that requires the least energy of activation.

6.3 EFFECTS OF SOLVENT IN REACTION

In dissolving the reactants, the solvent may interact with any or all of the reactants, and it may be involved in the transition state for any reaction available for the system. If the solvent interacts more powerfully with the transition state than with the reactants, it facilitates the reaction. The solvent itself may of course be one of the reactants, and this circumstance introduces special problems because of the difficulty of distinguishing experimentally between its functions as a reagent and as an environment for the reaction. In this study, methanol was chosen as the solvent. Methanol is somewhat less polar than water so many organic compounds have a significantly higher solubility in methanol than in water. Thus, methanol elutes them quicker than water does.

6.4 KINETICS AND MODELLING

The most powerful tool for the experimental study of reaction mechanisms is chemical Kinetics. Kinetics deals with the rates at which chemical reactions occur, and with all of the factors, which influence these rates, No reaction mechanism can be considered more than a temporary working hypothesis until it is supported by kinetic data.

Like any other tool, chemical kinetics has certain fundamental limitations. Perhaps the most useful information furnished by a kinetic study of a reaction is its rate equation. This is an equation, derived from rate measurements, which describes the concentration dependence of a reaction. For a generalized reaction (Goulde, 1959):



$$\text{rate} = -dc_A/t = k a_A^l a_B^m a_C^n \dots$$

where a_A , a_B , etc., refer to the thermodynamic activities of species A, B, etc., and c_A , c_B , etc. refer to their concentrations. l , m , and n ...are the powers to which the activities or concentrations must be raised in order to describe the experimental observations. Since many reactions involve two or more steps, and since the slowest step (or steps), which determines the rate of the reaction, may not involve all of the starting materials, it is not generally possible to deduce the rate equation from the stoichiometric equation of the over-all reaction.

Changes in experimental conditions may alter the rate equation, but the altered form is usually more general, and includes the original equation as a special case. More useful in mechanisms studies than the observed kinetic order of a reaction is its molecularity. Molecularity is usually defined, by organic chemists, as the number of molecules (using the term to include ions and radicals) which undergo valency changes in the slowest step of the reaction (Livingstone, 1953).

The principal limitation of reaction kinetics in mechanisms studies is that the experimental rate equation cannot be depended upon to establish the molecularity of the rate-limiting step of the reaction. It will do so only if there is a single rate-limiting step, which is not preceded by rapid equilibrium steps, and if none of the reactants in the rate-limiting reaction is present in large excess (Livingstone,. 1953). These conditions are not always satisfied.

In summary, the rate equation may indicate the composition of the transition state of the rate-limiting step of a reaction. It will not do so if one of the reactants is present in large excess, or if

the reaction does not have a single rate-limiting step. The rate equation may also indicate the molecularity of the reaction, but will not in cases where rapid equilibria are involved. Furthermore, the rate equation yields no information on the structure of the transition state of the rate-limiting reaction, or on the number and nature of any fast steps, which precede or follow the rate-limiting step. If the rate equation of a reaction cannot be relied upon to establish either the order or the molecularity of the reaction, and tells nothing about fast steps or transition state structures, why bother to make the kinetic study in the first place? The answer to this question lies in the fact that the kinetic data exclude all mechanisms from which the observed rate equation cannot be derived. In other words, the chief utility of reaction kinetics in mechanisms studies lies not in establishing the correct mechanism, but in ruling out all of the possible mechanisms which are inconsistent with the kinetic data.

6.4.1 The Kinetic Isotope Effect

Kinetic Isotope Effects (KIEs) are used to determine reaction mechanisms by determining rate limiting steps and transition states and are commonly measured using NMR to detect isotope location or GC/MS to detect mass changes. In a KIE experiment, its isotope replaces an atom and the change in rate of the reaction is observed. A very common isotope substitution is when hydrogen is replaced by deuterium. This is known as a deuterium effect and is expressed by the ratio k_H/k_D , where k_H and k_D are the rates of reaction associated with R-H and the isotope substituted R-D (Saunders et al., 1981). Normal KIEs for the deuterium effect are around 1 to 7 or 8. Large effects are seen because the percentage mass change between hydrogen and deuterium is great (Lowry et al., 1987). Heavy atom isotope effects involve the substitution of carbon, oxygen, nitrogen, sulfur, and bromine, with effects that are much smaller and are usually between 1.02 and 1.10 (Simmons et al., 2012). The difference in KIE magnitude is directly related to the percentage change in mass. Large effects are seen when hydrogen is replaced with deuterium because the percentage mass change is very large (mass is being doubled) while smaller percent mass changes are present when an atom like carbon is replaced with its isotope (increased by one mass unit). The greater the mass the more energy is needed to break bonds. A heavier isotope forms a stronger bond. The resulting molecule has less of a tendency to dissociate. The increase in activation energy (energy needed to break the bond) results in a slower reaction rate and the observed isotope effect (Saunders et al., 1981).

Primary kinetic isotope effects are rate changes due to isotopic substitution at a site of bond breaking in the rate-determining step of a reaction. Secondary kinetic isotope effects are rate changes due to isotopic substitutions at a site other than the bond-breaking site in the rate-determining step of the reaction. These come in three forms: α , β , and γ effects. β secondary isotope effects occur when the isotope is substituted at a position next to the bond being broken. This is thought to be due to hyperconjugation in the transition state. Hyperconjugation involves a transfer of electron density from a sigma bond to an empty p orbital (Lowry et al., 1987; Saunders et al., 1981).

6.4.2 Kinetic Isotope Effect Experiments

Simmons and Hartwig (2012) refer to the following three cases as the main types of kinetic isotope effect experiments involving C-H bond functionalization.

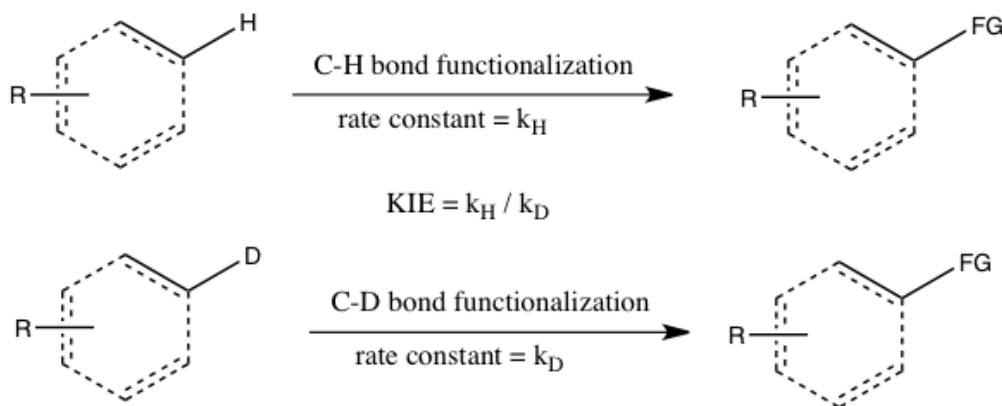


Figure 6.17: Experiment A; KIE determined from absolute rates of two parallel reactions as depicted (Simmons and Hartwig, 2012).

In this experiment (**Fig 6.17**), the rate constants for the normal substrate and its isotopically labeled analogue are determined independently, and the KIE is obtained as a ratio of the two. The accuracy of the measured KIE is severely limited by the accuracy with which each of these rate constants can be measured. Furthermore, reproducing the exact conditions in the two parallel reactions can be challenging. Nevertheless, this measurement of the kinetic isotope effect is the only one that may tell that C-H bond cleavage occurs in the rate-determining step without a doubt (Saunders et al., 1981).

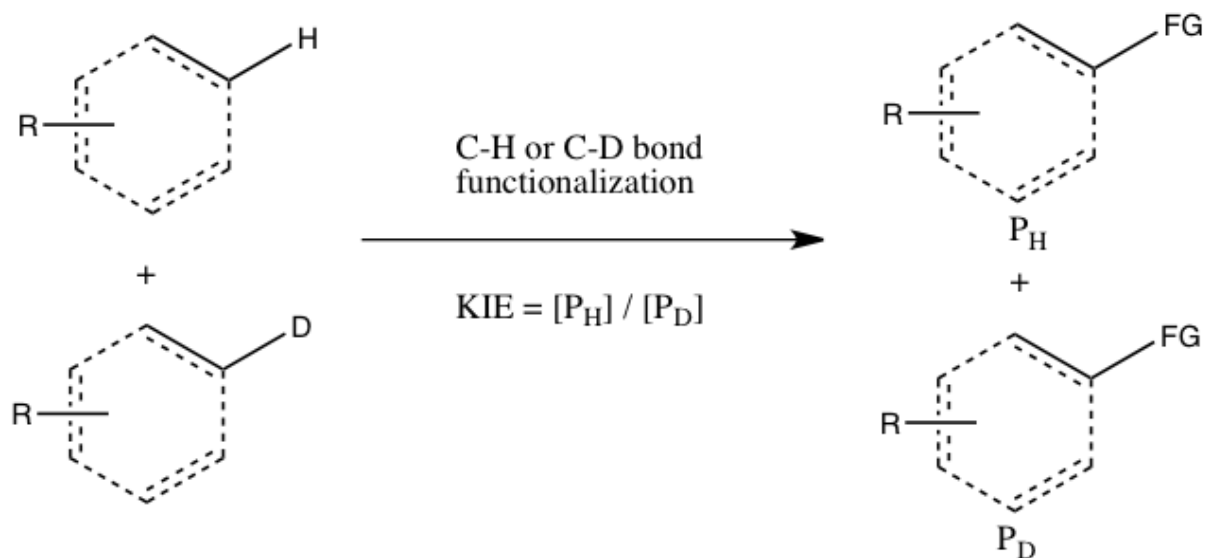


Figure 6.18: Experiment B; KIE determined from an intermolecular competition as depicted (Simmons and Hartwig, 2012).

In this type of experiment (**Fig 6.18**), the same substrates that are used in Experiment A are employed, but they are allowed to react in the same container, instead of two separate containers. The kinetic isotope effect from this experiment is determined by the relative amount of products formed from C-H versus C-D functionalization (or it can be obtained from the relative amounts of starting materials that are unreacted). It is necessary to quench the reaction before it goes to completion to observe the kinetic isotope effect. This experiment type ensures that both C-H and C-D bond functionalisations occur under exactly the same conditions, and the ratio of products from C-H and C-D bond functionalisations can be measured with much greater precision than the rate constants in Experiment A (Simmons et al., 2012). Moreover, only a single measurement of product concentrations from a single sample is required. However, an observed kinetic isotope effect from this experiment is more difficult to interpret, since it may either mean that C-H bond cleavage occurs during the rate-determining step or at a product-determining step ensuing the rate-determining step. The absence of a kinetic isotope effect, at least according to Simmons and Hartwig, is nonetheless indicative of the C-H bond cleavage not occurring during the rate-determining step (Simmons et al., 2012).

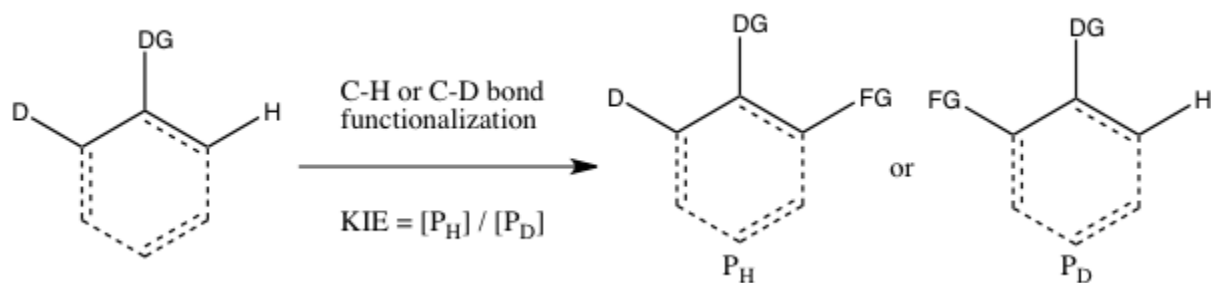


Figure 6.19: Experiment C; KIE determined from an intramolecular competition as depicted (Simmons and Hartwig, 2012).

This type of experiment (**Fig 6.19**) is analogous to Experiment B, except this time there is an intramolecular competition for the C-H or C-D bond functionalization. In most cases, the substrate possesses a directing group (DG) between the C-H and C-D bonds. Calculation of the kinetic isotope effect from this experiment and its interpretation follow the same considerations as that of Experiment B. This type of experiment is analogous to Experiment B, except this time there is an intramolecular competition for the C-H or C-D bond functionalization. In most cases, the substrate possesses a directing group (DG) between the C-H and C-D bonds. Calculation of the kinetic isotope effect from this experiment and its interpretation follow the same considerations as that of Experiment B (Simmons et al., 2012).

Carbon-13 Isotope Effects

Most organic reactions involve the breaking and making of bonds to a carbon; thus, it is reasonable to expect detectable carbon isotope effects. When ^{13}C is used as the label, the change in mass of the isotope is only ~8%, though, which limits the observable kinetic isotope effects to much smaller values than the ones observable with hydrogen isotope effects (Saunders et al., 1981).

6.4.3 A Comparison between Kinetic Studies of Phenol- ^{12}C and Phenol- ^{13}C .

Kinetic experiments were conducted to determine average rate constants as shown in **Fig 6.20**. Experiments were carried out under the same conditions for both phenol- ^{12}C and ^{13}C labeled phenol experiments for comparison. Average rate constants (k) were determined graphically and are reported, **Table 6.9**, and Table 6.10 for phenol- ^{12}C and ^{13}C labeled phenol, respectively.

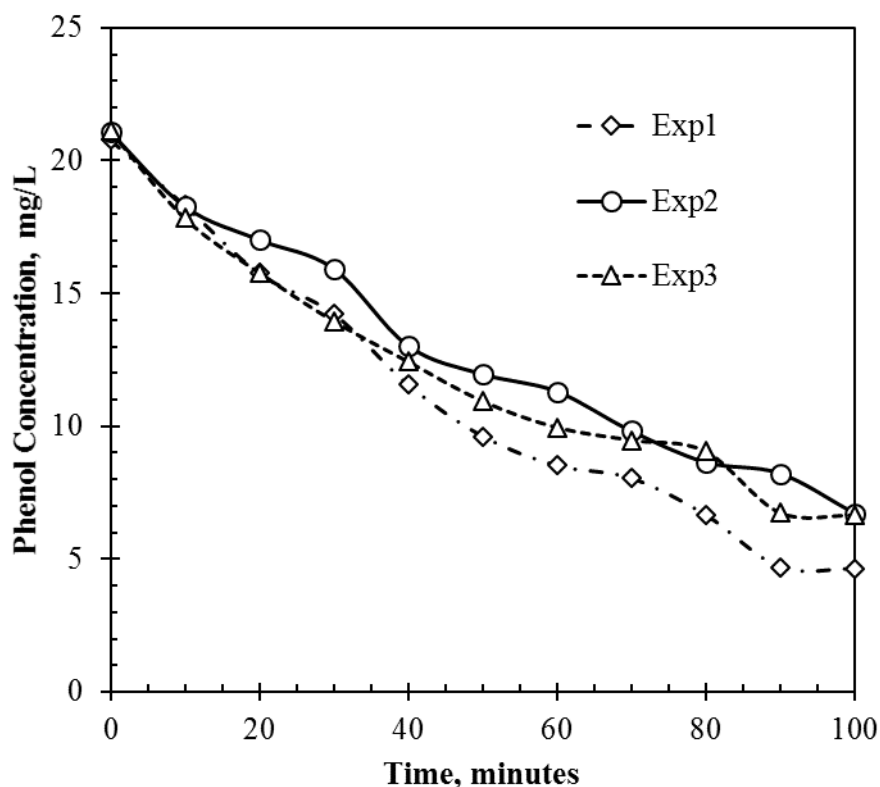


Figure 6.20: The photo degradation profile of phenol C-13 over TiO_2 .

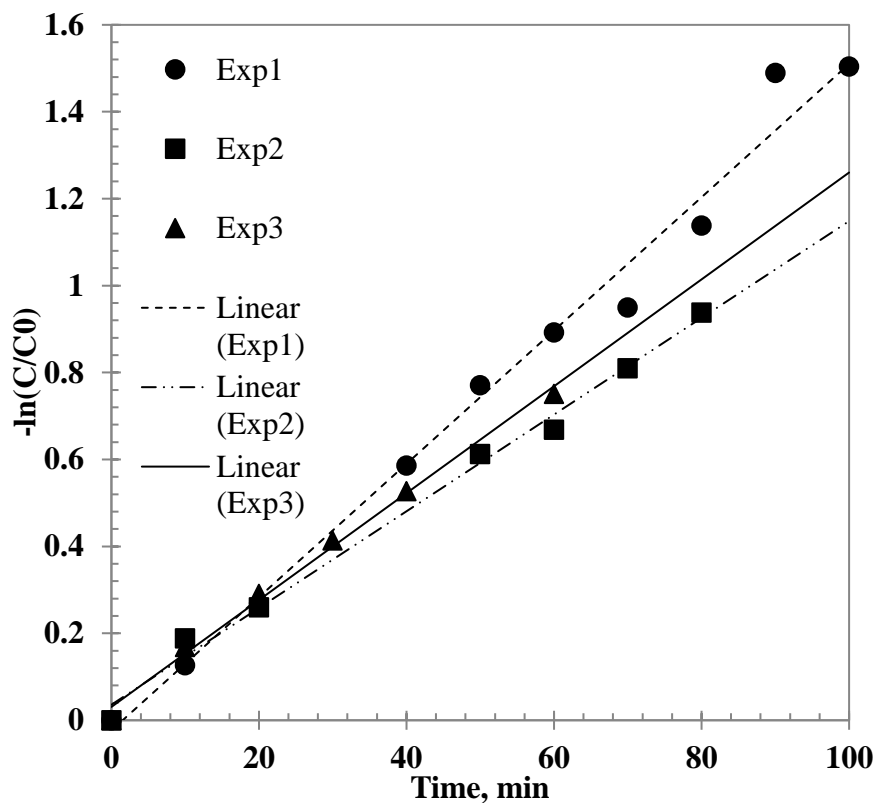


Figure 6.21: A linear plot of the Langmuir-Hinshelwood equation to determine rate constant, k , for phenol- ^{13}C experiments.

Table 6.11: Average values of rate constants (k) for phenol C-13 and their regression coefficients (R^2).

<i>Experiment #</i>	<i>Rate constant, k, min^{-1}</i>	<i>Linear equation</i>	<i>R^2</i>
1	0.0153	$y = 0.0153x - 0.023$	0.9947
2	0.0111	$y = 0.0111x + 0.0358$	0.9935
3	0.0123	$y = 0.0123x + 0.0307$	0.9853
Average rate constant, k	0.0129		

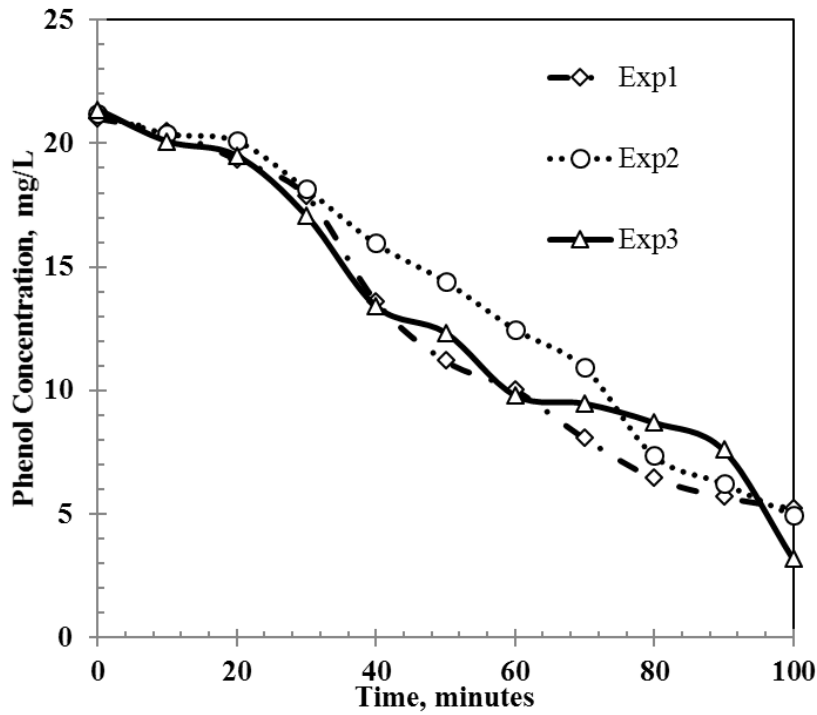


Figure 6.22: The photo degradation profile of phenol-¹²C over TiO₂.

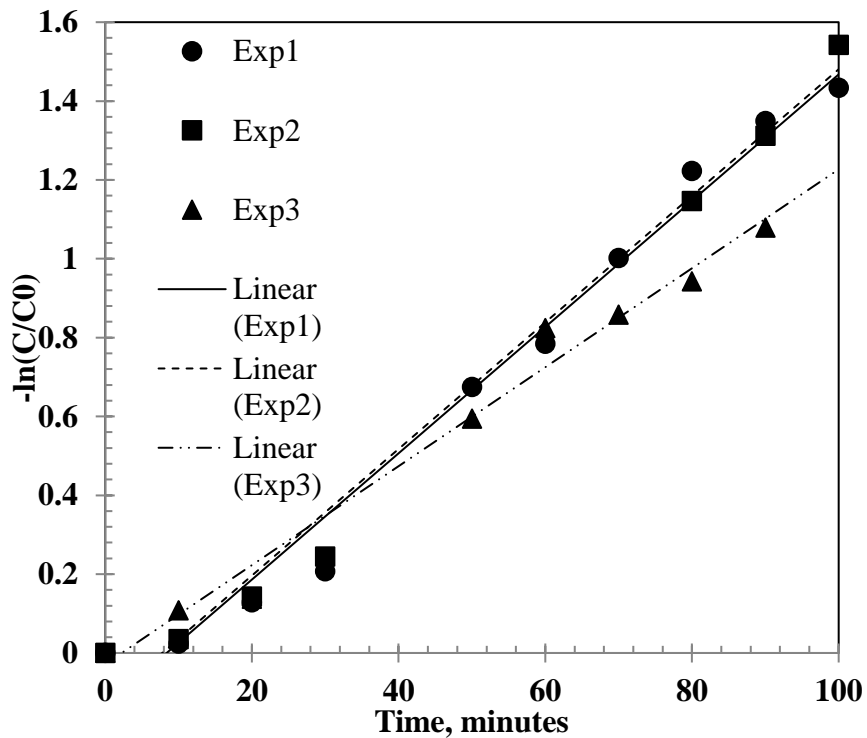


Figure 6.23: A linear plot of the Langmuir-Hinshelwood equation to determine rate constant, k , for phenol-¹²C experiments.

Table 6.12: Average values of rate constants (k) for phenol C-12 and their regression coefficients (R²).

<i>Experiment #</i>	<i>Rate constant, k, min⁻¹</i>	<i>Linear equation</i>	<i>R²</i>
1	0.0161	y = 0.0161x - 0.1247	0.987
2	0.016	y = 0.016x - 0.1342	0.9682
3	0.0125	y = 0.0125x - 0.0281	0.9845
<i>Average rate constant, k</i>	0.0149		

Kinetic Isotope Effect

$$KIE = \frac{k_{c-12}}{k_{c-13}} = \frac{0.0149}{0.0129} = 1.16$$

From the above-calculated KIE, it can be concluded that the isotopically labeled phenol atom is part of the rate-determining step. This is referred to as a primary isotope effect. It is also noted that the above-calculated KIE is slightly above the ‘normal’ KIE values (1.0-1.10) for heavy isotope atoms (Simmons et al.,2012). This can be attributed to inaccuracies during experiments.

6.4.4 Evaluation of Kinetic Isotope Effects in a Multi-Step Reaction:

A large part of the kinetic isotope effect arises from vibrational zero-point energy differences between the reactant ground state and the transition state that vary between the reactant and its isotopically substituted analogue. While it is possible to carry involved calculations of kinetic isotope effects using computational chemistry, much of the work done is of simpler order that involves the investigation of whether particular isotopic substitutions produce a detectable kinetic isotope effect or not. Vibrational changes from isotopic substitution at atoms away from the site where the reaction occurs tend to cancel between the reactant and the transition state. Therefore, the presence of a kinetic isotope effect indicates that the isotopically labeled atom is at or very near the reaction site.

The absence of an isotope effect is more difficult to interpret: It may mean that the isotopically labeled atom is away from the reaction site, but it may also mean that there are certain compensating effects that lead to the lack of an observable kinetic isotope effect. For example, the differences between the reactant and the transition state zero-point energies may be identical between the normal reactant and its isotopically labeled version. Alternatively, it may mean that

the isotopic substitution is at the reaction site, but vibrational changes associated with bonds to this atom occur after the rate-determining step.

The existence of a kinetic isotope effect is indicative of a change to the vibrational force constant of a bond associated with the isotopically labeled atom at or before the rate-controlling step. Intricate calculations may be used to learn a great amount of detail about the transition state from observed kinetic isotope effects. More commonly, though, the mere qualitative knowledge that a bond associated with the isotopically labeled atom is altered in a certain way can be very useful.

6.5 KINETICS AND MODELING

6.5.1 Langmuir-Hinshelwood (LH) Kinetic Model

Langmuir–Hinshelwood (LH) kinetics is the most commonly used kinetic expression to explain the kinetics of the heterogeneous catalytic processes. The Langmuir–Hinshelwood expression that explains the kinetics of heterogeneous catalytic systems is given by:

$$r = -\frac{dC}{dt} = \frac{k_r KC}{1+KC} \quad (6.1)$$

where r represents the rate of reaction that changes with time.

The parameters k_r and K which are a function of C can be predicted by linearizing the Eq. as follows:

$$\frac{1}{r} = \frac{1}{k_r} + \frac{1}{k_r KC} \quad (6.2)$$

In the case of Eq. (5.1), the constants k_r and K can be calculated from the corresponding integrated expression. This equation can be integrated between the limits: $C = C_0$ at $t = 0$ and $C = C$ at $t = t$. The integrated expression is given by:

$$\ln\left(\frac{C_0}{C}\right) + K(C_0 - C) = k_r Kt \quad (6.3)$$

If the term $KC \ll 1$ then Eq. (5.1) is reduced to:

$$r = k_r KC \quad (6.4)$$

Integrating Eq. (5.4) with respect to limits: $C = C_0$ at $t = 0$ and $C = C$ at $t = t$, LH expression reduces to a first order kinetics and is given by:

$$-\ln\left(\frac{C}{C_0}\right) = k_1 t \quad (6.5)$$

where $k_1 = k_r K$

6.5.2 Adsorption Isotherms

Adsorption equilibrium is a fundamental property in adsorption studies; considering that fact, numerous studies have been conducted in order to determine the amount of species adsorbed under a given set of conditions. In order to optimise the design of an adsorption system, it is important to find the most appropriate correlation for the equilibrium curve. Adsorption isotherm models are described in many mathematical forms, some of which are based on a simplified physical description of adsorption and desorption, while others are purely empirical and intended to correlate experimental data. In this work, the Langmuir-Hinshelwood adsorption isotherm model was used.

The Langmuir theory has, as its basic assumption, that adsorption occurs at specific homogeneous sites inside of the adsorbent and, once a substrate molecule occupies a site, no additional adsorption can occur there. The Langmuir isotherm model can be described as in equation 6.1.

$$\frac{C_e}{Q_e} = \frac{C_e}{q_m} + \frac{1}{K_L q_m} \quad 6.1$$

where q_m is the maximum monolayer adsorption capacity (mol g^{-1}), K_L is the Langmuir constant (L mol^{-1}), and q_e and C_e are the adsorption capacity (mol g^{-1}) and equilibrium concentration (mol L^{-1}), respectively. This equation can be linearized by plotting Q_e^{-1} versus C_e^{-1} . This results in a straight line of slope $1/q_m$ and intercept $1/K_L q_m$. The Langmuir adsorption constants (K_L) were calculated as recorded in **Table 6.**

Phenol adsorption experiments were conducted in five experiments in order to determine the Langmuir adsorption constants. Photocatalytic experiments were conducted with different initial phenol concentrations (10mg/L, 20 mg/L, 30 mg/L, 50 mg/L and 100mg/L) to determine how well phenol adsorbs on the TiO₂ surface. The TiO₂ concentration was kept at 8mg/L throughout all experiments. Data collected in 5 experiments is graphically represented in **Fig 6.24**.

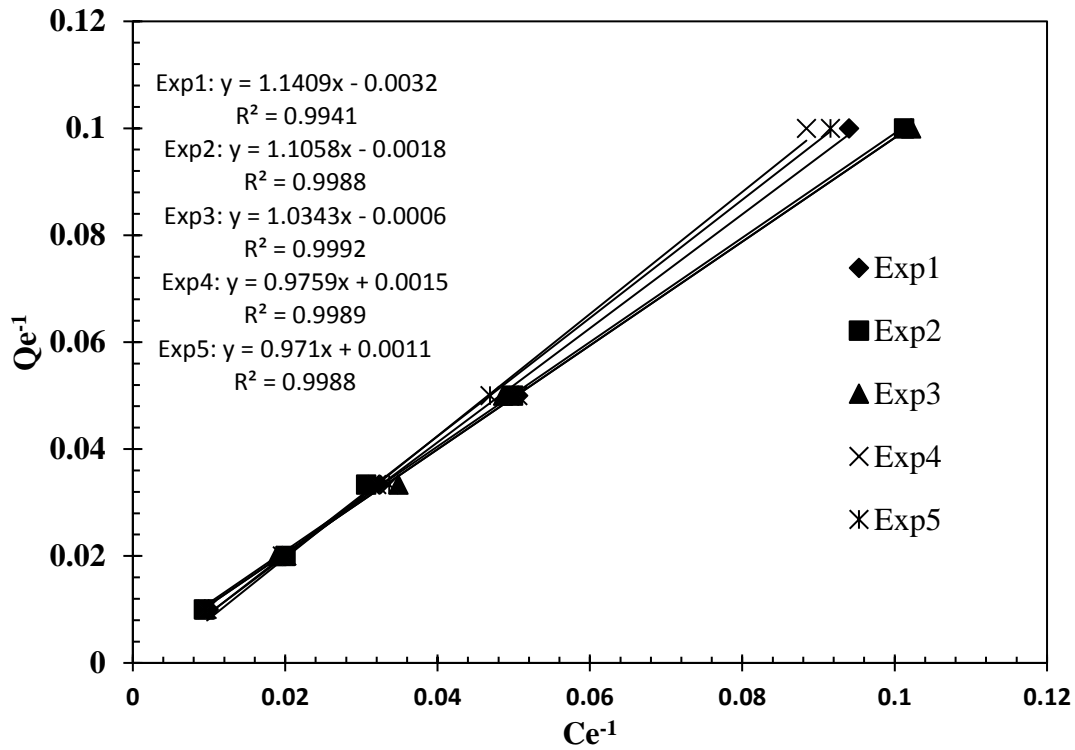


Figure 6.24: Langmuir adsorption isotherm plots of phenol.

Table 6.13: The average and standard deviation of the data collected in 5 experiments as shown in Figure 6.24.

<i>Q_e</i>	<i>C_e (average)</i>	<i>Standard Deviation</i>	
10	0.096685	0.006255	0.006255
20	0.049181	0.001477	0.001477
30	0.032903	0.001622	0.001622
50	0.019744	0.000528	0.000528
100	0.009611	0.000268	0.000268

Table 6.14: The parameters of Langmuir isotherms for the adsorption of phenol onto TiO₂.

<i>K_L (L.mol⁻¹)</i>	<i>q_m (mol.g⁻¹) (10⁴)</i>	<i>R²</i>	<i>Std. dev.</i>
0.0846	96.04	0.9980	0.0525

6.6 MODELING AND SIMULATION

Excel was used for processing and statistical analysis. Aquasim 2.0 computer program was used to model and simulate the photocatalytic degradation profile, and parameter estimations. The simulated data and the model fit is shown in **Figure 6.25**.

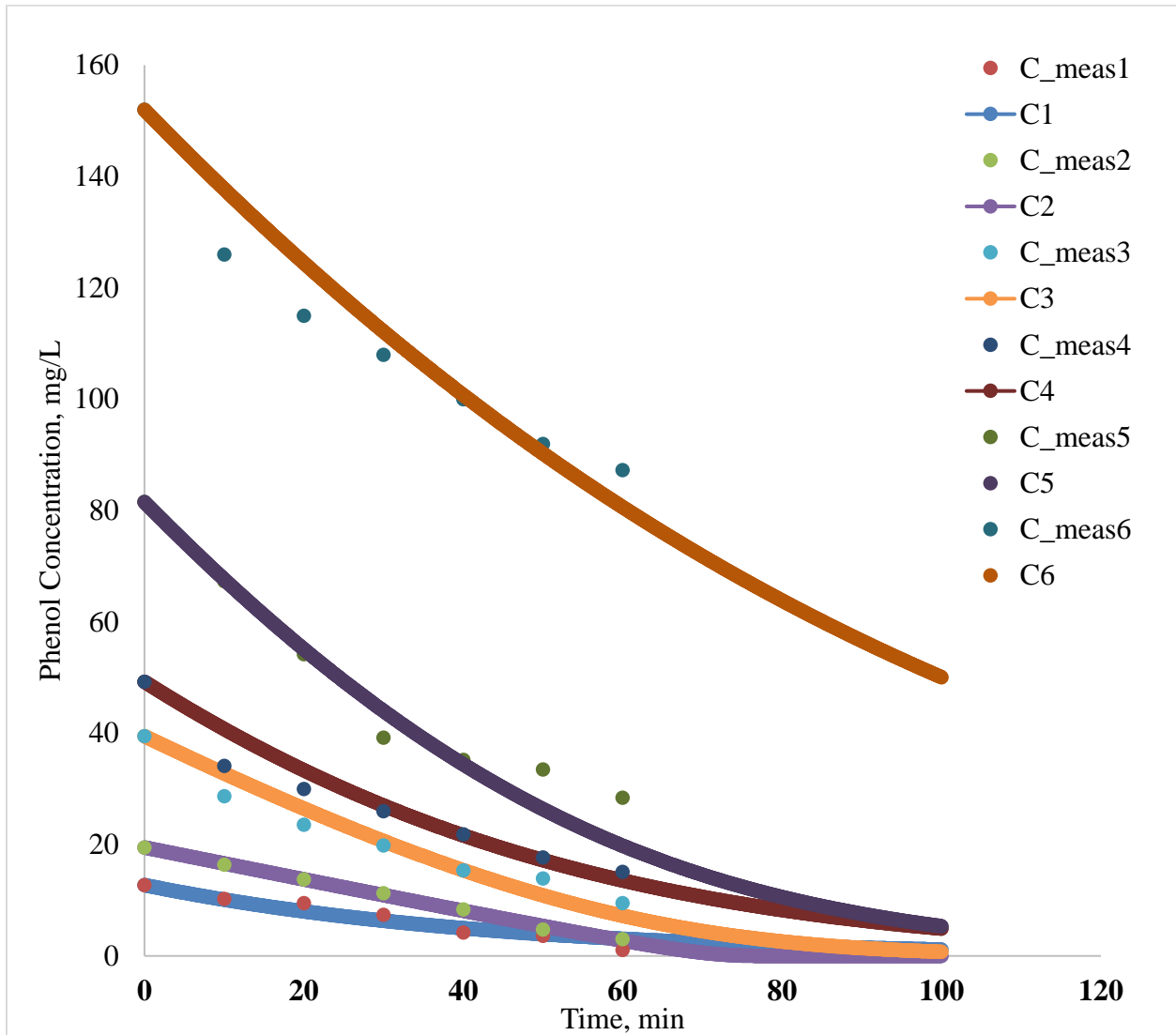


Figure 6.25: A depiction of the fit of the Langmuir model against measured data for different initial phenol concentrations (mg/L).

The Langmuir- Hinshelwood (L-H) kinetic model described the kinetics;

$$r = -\frac{dC}{dt} = \frac{k_r K_a C}{1 + K_a C}$$

where k_r is the rate constant (min^{-1}), K_a is the adsorption constant (L/mol) and C is the phenol concentration (mg/L).

Table 6.15: The simulated values for Langmuir adsorption constant (K_a), rate constant (k_r) and their Chi^2 values for different initial phenol concentrations.

<i>Initial Phenol Concentration(mg/L)</i>	<i>Ka (L/mol)</i>	<i>kr (min⁻¹)</i>	<i>Chi²</i>
10	0.005896	4.16149	8.08539
20	1.968875	0.29525	0.69161
40	0.074214	0.91829	40.2209
50	0.010092	2.72416	59.0798
80	0.013608	2.76201	150.100
150	0.003142	4.55234	294.253

6.7 CONCLUSION

A mechanism has been proposed, that explains the photo degradation of phenol over UV/TiO₂. Carbon-13 tracking results revealed that Hydroquinone, Resorcinol and Maleic Acid were the main intermediates containing the C-13 isotope. Various studies (Chen et al, 2002; Turchi, et al, 1989; Okamoto et al, 1985) had similar findings, suggesting that phenol degradation mainly proceeds through its hydroxylated products. Results obtained in this study are in agreement with this. Further hydroxylation of these hydroxylated products leads to the cleavage of the aromatic compound(s) into various sub-intermediates including carboxylic acids such as maleic acid, which eventually undergo decarboxylation until they're converted to carbon dioxide and water.

Reaction conditions were manipulated and a different set of results was obtained. This suggests that the photocatalytic degradation of phenol can proceed via different reaction pathways depending on reaction conditions. Under anaerobic conditions (absence of O₂ electron scavenger), ¹³C tracking results revealed Benzoquinone, Maleic acid and Hydroquinone as the main intermediates containing the ¹³C isotope. The benzoquinone-to-hydroquinone conversion occurs in the absence of electron scavenger, however, it ineffectively consumes the photogenerated radicals, thus

reducing the photo-oxidation efficiency of phenol as was observed with the slower phenol degradation rate.

Isotope effects are a very powerful tool for determining all aspects of mechanisms, starting with the kinetic mechanism and ending up with the chemical mechanism and the structure of the transition state. Studies (Cook, 1998; Weistheimer, 1961; Simmons et al, 2012) have proven this. However, in this particular study, the isotope marking did not unravel the phenol degradation mechanism as expected. The knowledge acquired in this study could have been obtained without the use of the carbon-13 labelled phenol. The study was limited because phenol degradation intermediates could not be quantified and therefore the photocatalytic degradation mechanism could not be studied in detail. The degradation mechanism was not clear from the experimental results obtained in this study; however, results were supported by various similar studies from literature.

7 CHAPTER 7: CONCLUSIONS AND RECOMMENDATIONS

- ❖ TiO_2 exists as three powder forms; Anatase, Rutile and P-25 Degussa. Each of these powders exhibit different physical properties. Each of these powders were characterized by means of XRD, XRF, SEM and BET analyses. Anatase was revealed to have 98.4% purity by X-ray fluorescence analysis, Degussa at 96.7% and Rutile at 75.7% was reported to have the most impurities (~25%). Experiments compared the effect of each powder on the photocatalytic performance. Experiments showed that Degussa degraded phenol more efficiently than rutile and anatase in several reaction systems. It has been demonstrated, in literature, that metal doping of nanocrystal TiO_2 improves its photocatalytic performance. It is therefore recommend that one explores photocatalysis in this regard.
- ❖ UV/ TiO_2 Photocatalysis has proven to be a successful treatment method for recalcitrant organics including phenol. However, there are a number of factors affecting the performance of UV/ TiO_2 photocatalytic degradation; this study explored some of these factors. Experiments revealed that the performance of photocatalysis depends strongly on reaction conditions such as pollutant loading, catalyst loading, UV irradiation, reaction pH etc.,.
- ❖ The artificial generation of photons required for the detoxification of polluted water is the most important source of costs during the operating of photocatalytic wastewater treatment plants. This constitutes one of the major drawbacks particularly for the rapid commercialisation of photocatalytic water treatment units. Therefore to lower operational costs, explore the use of solar irradiation instead of UV light.
- ❖ Photocatalysis versus photolysis experiments revealed that there was phenol degradation in the absence of the catalyst. This suggests that the catalyst is not the main cause of degradation and that the UV light is. It was also observed that there was minimum phenol removal at high catalyst concentrations. High catalyst concentrations resulted in a high turbidity reaction solution. The photoactivity was then limited due to the suspended catalyst blocking the UV light and thereby inhibiting the photocatalytic reaction. It can therefore be concluded that the catalyst is effective in small concentrations. Going forward, it is

recommended that a different reactor configuration is employed to optimize photocatalysis, i.e. an immobilized catalyst reactor system.

- ❖ A carbon-13 isotope labeled phenol was employed to study the degradation mechanism of phenol. The evolution of intermediates was studied and the movement of C-13 isotope during phenol degradation was followed. The phenol degradation mechanism was postulated under UV/TiO₂ photocatalytic conditions. However, it was observed that the reaction mechanism changed with different reaction conditions. It is therefore recommended that one explores how the different reaction conditions affect the reaction mechanism.
- ❖ One of the limitations of this study was that there was only one labeled compound to experiment with. Going forward, it is recommended that one explores a differently labeled compound, preferably a di-labeled compound (labeled in 2 positions) or more.

8 REFERENCES

- Akpan, U. G. and Hameed, B. H. (2009) 'Parameters affecting the photocatalytic degradation of dyes using TiO₂-based photocatalysts: A review', *Journal of Hazardous Materials*, 170(2–3), pp. 520–529. doi: 10.1016/j.jhazmat.2009.05.039
- Antoniou, M. G. et al. (2016) *of Organic Contaminants in Water: Process Optimization and Degradation Pathways* †. The Royal Society of Chemistry. doi: 10.1039/9781782627098-00001.
- Bamuza-Pemu, E. E. and Chirwa, E. M. (2012) 'Photocatalytic degradation of geosmin: Reaction pathway analysis', *Print* = *Water SA*, 38(5). doi: 10.4314/wsa.v38i5.6.
- Bamuza-Pemu, E. E. and Chirwa, E. M. N. (2013) 'Profile of aromatic intermediates of titanium dioxide mediated degradation of phenol', *Chemical Engineering Transactions*, 35, pp. 1333–1338. doi: 10.3303/CET1335222.
- Behnajady, M. A. et al. (2007) 'Photocatalytic degradation of an azo dye in a tubular continuous-flow photoreactor with immobilized TiO₂ on glass plates', *Chemical Engineering Journal*. doi: 10.1016/j.cej.2006.09.013.
- Bui, T. D. et al. (2010) 'Determination of Oxygen Sources for Oxidation of Benzene on TiO₂ Photocatalysts in Aqueous Solutions Containing', (11), pp. 8453–8458.
- Bui, T. D. et al. (2011) 'Two routes for mineralizing benzene by TiO₂-photocatalyzed reaction', *Applied Catalysis B: Environmental*. Elsevier B.V., 107(1–2), pp. 119–127. doi: 10.1016/j.apcatb.2011.07.004.
- Chen D, Ray AK. Photo-degradation kinetics of 4-nitrophenol in TiO₂ suspension. *Water Res.* 1998;32: 3223–3234.
- Chen D, Ray AK. Photocatalytic kinetics of phenol and its derivatives over UVirradiated TiO₂. *Appl. Catal., B* 1999;23: 143–157
- Chen, J.; Eberlein, L.; Langford, C. H. Pathways of Phenol and Benzene Photooxidation Using TiO₂ Supported on a Zeolite. *J. Photochem. Photobiol., A* 2002, 148, 183–189.
- Chen, W. et al. (2007) 'Photocatalytic oxidation of phenol in aqueous solutions with oxygen catalyzed by supported metallophthalocyanine catalyst', *Science in China, Series B: Chemistry*, 50(3), pp. 379–384. doi: 10.1007/s11426-007-0055-3.
- Chowdhury P, Moreira J, Goma H, Ray AK. Visible-solar-light-driven photocatalytic degradation of phenol with dye-sensitized TiO₂: Parametric and kinetic study. *Ind. Eng. Chem. Res.* 2012;51: 4523–4532.
- Chun, H., Yizhong, W. and Hongxiao, T. (2000) 'Destruction of phenol aqueous solution by photocatalysis or direct photolysis', *Chemosphere*, 41(8), pp. 1205–1209. doi: 10.1016/S0045-6535(99)00539-1.
- Corona, D. et al. (2005) 'Synthesis, proton and ¹³C NMR and reaction mechanism studies of novel isoindolones derivatives, obtained through TAWERS procedure', *Spectrochimica Acta - Part A*:

Molecular and Biomolecular Spectroscopy, 61(11–12), pp. 2788–2795. doi: 10.1016/j.saa.2004.10.025.

Devi LG, Rajashekhar KE. A kinetic model based on non-linear regression analysis is proposed for the degradation of phenol under UV/solar light using nitrogen-doped TiO₂. *J. Mol. Catal. A: Chem.* 2011;334: 65–76.

Fujishima, A., Rao, T. N. and Tryk, D. A. (2000) ‘Titanium dioxide photocatalysis’, *Journal of Photochemistry and Photobiology C: Photochemistry Reviews*, 1(1), pp. 1–21. doi: 10.1016/S1389-5567(00)00002-2.

Fujishima, A. and Zhang, X. (2006) ‘Titanium dioxide photocatalysis: present situation and future approaches’, *Comptes Rendus Chimie*, pp. 750–760. doi: 10.1016/j.crci.2005.02.055.

Fujishima, A., Zhang, X. and Tryk, D. A. (2008) ‘TiO₂ photocatalysis and related surface phenomena’, *Surface Science Reports*, pp. 515–582. doi: 10.1016/j.surfrep.2008.10.001.

Gaya, U. I. and Abdullah, A. H. (2008) ‘Heterogeneous photocatalytic degradation of organic contaminants over titanium dioxide: A review of fundamentals, progress and problems’, *Journal of Photochemistry and Photobiology C: Photochemistry Reviews*, 9(1), pp. 1–12. doi: 10.1016/j.jphotochemrev.2007.12.003.

Gökhan Eğılmez, Gürsel A. Süer, Özgüner, O. (2012) ‘World’s largest Science, Technology & Medicine Open Access book publisher’, *Design, Control and Applications of Mechatronic Systems in Engineering*, pp. 135–152. doi: 10.5772/67458.

Guo, Z., Ma, R. and Li, G. (2006) ‘Degradation of phenol by nanomaterial TiO₂ in wastewater’, *Chemical Engineering Journal*, 119(1), pp. 55–59. doi: 10.1016/j.cej.2006.01.017.

Hänel, A. *et al.* (2010) ‘Photocatalytic activity of TiO₂ immobilized on glass beads’, *Physicochemical Problems of Mineral Processing*, 45, pp. 49–56.

Hoffmann, M. R. *et al.* (1995) ‘Environmental Applications of Semiconductor Photocatalysis’, *Chemical Reviews*, 95(1), pp. 69–96. doi: 10.1021/cr00033a004.

Ibhadon, A. O. and Fitzpatrick, P. (2013) ‘Heterogeneous Photocatalysis: Recent Advances and Applications’, *Catalysts*, 3, pp. 189–218. doi: 10.3390/catal3010189.

Kisch, H. (2013) ‘Semiconductor Photocatalysis—Mechanistic and Synthetic Aspects’, *Angewandte Chemie International Edition*, 52(3), pp. 812–847. doi: 10.1002/anie.201201200.

Kobayakawa, K. *et al.* (1998) ‘Continuous-flow photoreactor packed with titanium dioxide immobilized on large silica gel beads to decompose oxalic acid in excess water’, *Journal of Photochemistry and Photobiology A: Chemistry*, 118(1), pp. 65–69. doi: 10.1016/S1010-6030(98)00348-7.

Kumar, K. V., Porkodi, K. and Rocha, F. (2008) ‘Langmuir-Hinshelwood kinetics - A theoretical study’, *Catalysis Communications*, 9(1), pp. 82–84. doi: 10.1016/j.catcom.2007.05.019.

Kabra, K., Chaudhary, R. and Sawhney, R. L. (2004) ‘Treatment of Hazardous Organic and Inorganic Compounds through Aqueous-Phase Photocatalysis: A Review’, *Industrial & Engineering Chemistry Research*, 43(24), pp. 7683–7696. doi: 10.1021/ie0498551.

Li, D. *et al.* (2014) 'A novel double-cylindrical-shell photoreactor immobilized with monolayer TiO₂-coated silica gel beads for photocatalytic degradation of Rhodamine B and Methyl Orange in aqueous solution', *Separation and Purification Technology*. Elsevier B.V., 123, pp. 130–138. doi: 10.1016/j.seppur.2013.12.029.

Li, Y. *et al.* (2012) 'Pathway of Oxygen Incorporation from O₂ in TiO₂ Photocatalytic Hydroxylation of Aromatics: Oxygen Isotope Labeling Studies', pp. 2030–2039. doi: 10.1002/chem.201103446.

Liu, W. *et al.* (2016) 'Simultaneous removal of Cr(VI) and 4-chlorophenol through photocatalysis by a novel anatase/titanate nanosheet composite: Synergetic promotion effect and autosynchronous doping', *Journal of Hazardous Materials*. Elsevier B.V., 317, pp. 385–393. doi:10.1016/j.jhazmat.2016.06.002.

Maitra, U. and Chandrasekhar, J. (1997) 'Use of isotopes for studying reaction mechanisms', *Resonance*, 2(10), pp. 29–37. doi: 10.1007/BF02835976.

Mandal, T. *et al.* (2010) 'Advanced oxidation process and biotreatment: Their roles in combined industrial wastewater treatment', *Desalination*. doi: 10.1016/j.desal.2009.04.012.

Michałowicz, J. and Duda, W. (2007) 'Phenols - Sources and toxicity', *Polish Journal of Environmental Studies*.

Miyamoto, S. *et al.* (2014) 'Singlet molecular oxygen generated by biological hydroperoxides', *Journal of Photochemistry and Photobiology B: Biology*. Elsevier B.V., 139, pp. 24–33. doi: 10.1016/j.jphotobiol.2014.03.028.

Morita K. *et al.*, (2016), 'Characterisation of titanium dioxide nanoparticles modified with polyacrylic acid and H₂O₂ for use as a novel radiosensitiser' *Free Radic Res.* 2016 Dec;50(12):1319-1328.

Nan, M. *et al.* (2010) 'Recent developments in photocatalytic water treatment technology: A review', *Water Research*. Elsevier Ltd, 44(10), pp. 2997–3027. doi: 10.1016/j.watres.2010.02.039.

Ng, Y. H. *et al.* (2012) 'A perspective on fabricating carbon-based nanomaterials by photocatalysis and their applications', *Energy & Environmental Science*, 5(11), p. 9307. doi: 10.1039/c2ee22128d.

Ola, O. and Maroto-Valer, M. M. (2015) 'Review of material design and reactor engineering on TiO₂ photocatalysis for CO₂ reduction', *Journal of Photochemistry and Photobiology C: Photochemistry Reviews*. Elsevier B.V., 24, pp. 16–42. doi: 10.1016/j.jphotochemrev.2015.06.001.

Ohno, T. *et al.* (2001) 'Morphology of a TiO₂ Photocatalyst (Degussa, P-25) Consisting of Anatase and Rutile Crystalline Phases', *Journal of Catalysis*, 203(1), pp. 82–86. doi: 10.1006/jcat.2001.3316.

Olujimi, O. O. *et al.* (2010) 'Endocrine disrupting chemicals (phenol and phthalates) in the South African environment: A need for more monitoring', *Water SA*, 36(5), pp. 671–682. doi: 10.4314/wsa.v36i5.62001.

- Porter, J. F., Li, Y. G. and Chan, C. K. (1999) 'Effect of calcination on the microstructural characteristics and photoreactivity of Degussa P-25 TiO₂', *Journal of Materials Science*, 34(7), pp. 1523–1531. doi: 10.1023/A:1004560129347.
- Palmisano, G. *et al.* (2006) 'Influence of the substituent on selective photocatalytic oxidation of aromatic compounds in aqueous TiO₂ suspensions.', *Chemical communications (Cambridge, England)*, (9), pp. 1012–1014. doi: 10.1039/b515853b.
- Palmisano, L.; Schiavello, M.; Sclafani, A.; Martra, G.; Borello, E.; Coluccia, S. Photocatalytic Oxidation of Phenol on TiO₂ Powders; a Fourier-Transform Infrared Study. *Appl. Catal., B* 1994, 3, 117–132.
- Pang, X. *et al.* (2014a) 'Unraveling the photocatalytic mechanisms on TiO₂ surfaces using the oxygen-18 isotopic label technique', *Molecules*, 19(10), pp. 16291–16311. doi: 10.3390/molecules191016291.
- Pang, X. *et al.* (2014b) 'Unraveling the Photocatalytic Mechanisms on TiO₂ Surfaces Using the Oxygen-18 Isotopic Label Technique', pp. 16291–16311. doi: 10.3390/molecules191016291.
- Rand, E. and Company, W. (2006) 'Handbook for the Operation of Wastewater Treatment Works Water Institute of Southern Africa', (March).
- Simmons, E.M.; Hartwig, J.F. *Angew. Chem. Int. Ed.* 2012, 51, 3066-307
- Saunders, W.H., Melander, L. *Reaction Rates of Isotopic Molecules*, Wiley, New York, 1981
- Lowry, T.H., Richardson, K.S. *Mechanism and Theory in Organic Chemistry*, Harper and Row, New York, 1987
- Su, R. *et al.* (2012) 'Promotion of phenol photodecomposition over TiO₂ Using Au, Pd, and Au-Pd nanoparticles', *ACS Nano*, 6(7), pp. 6284–6292. doi: 10.1021/nn301718v.
- Sun, Q. and Xu, Y. (2010) 'Evaluating intrinsic photocatalytic activities of anatase and rutile TiO₂ for organic degradation in water', *Journal of Physical Chemistry C*, 114(44), pp. 18911–18918. doi: 10.1021/jp104762h.
- Vaiano, V. *et al.* (2015) 'From the design to the development of a continuous fixed bed photoreactor for photocatalytic degradation of organic pollutants in wastewater', *Chemical Engineering Science*, 137, pp. 152–160. doi: 10.1016/j.ces.2015.06.023.
- Vezzoli, M. (2012) 'Intrinsic kinetics of titania photocatalysis: Simplified Models for their investigation by', (February).
- Wang, L. *et al.* (2008) 'Photocatalytic reduction of Cr(VI) over different TiO₂ photocatalysts and the effects of dissolved organic species', *Journal of Hazardous Materials*. doi: 10.1016/j.jhazmat.2007.06.063.
- Xia, J. *et al.* (2011) 'Water Quality Management in China: The Case of the Huai River Basin', *International Journal of Water Resources Development*, 27(1), pp. 167–180. doi: 10.1080/07900627.2010.531453.
- Yang, P. *et al.* (2002) 'Titanium dioxide nanoparticles co-doped with Fe³⁺ and Eu³⁺ ions for photocatalysis', *Materials Letters*, 57(4), pp. 794–801. doi: 10.1016/S0167-577X(02)00875-3.

9 APPENDICES

9.1 APPENDICE A: AQUASIM FILE PROGRAMME LISTING

SYSTEM DEFINITION

AQUASIM Version 2.0 (win/mfc) - Listing of System Definition

Date and time of listing: 11/06/2017 12:53:43

Variables

C: Description: Phenol Concentration
 Type: Dyn. Volume State Var.
 Unit: mg/L
 Relative Accuracy: 1e-006
 Absolute Accuracy: 1e-006

C_meas1: Description: Measured Data
 Type: Real List Variable
 Unit: mg/L
 Argument: Time
 Standard Deviations: global
 Rel. Stand. Deviat.: 0
 Abs. Stand. Deviat.: 1
 Minimum: 0
 Maximum: 1e+009
 Interpolation Method: linear interpolation
 Sensitivity Analysis: inactive
 Real Data Pairs (7 pairs):
 0 12.75
 10 10.25
 20 9.53
 30 7.39
 40 4.23
 50 3.64
 60 1.09

C_meas2: Description: Real List Variable
 Type: Real List Variable
 Unit: Time
 Argument: Time
 Standard Deviations: global
 Rel. Stand. Deviat.: 0
 Abs. Stand. Deviat.: 1

Minimum: 0
 Maximum: 1e+009
 Interpolation Method: linear interpolation
 Sensitivity Analysis: inactive
 Real Data Pairs (7 pairs):
 0 19.5
 10 16.39
 20 13.79
 30 11.31
 40 8.35
 50 4.76
 60 3.01

C_meas3: Description: Real List Variable
 Type: Real List Variable
 Unit:
 Argument: Time
 Standard Deviations: global
 Rel. Stand. Deviat.: 0
 Abs. Stand. Deviat.: 1
 Minimum: 0
 Maximum: 1e+009
 Interpolation Method: linear interpolation
 Sensitivity Analysis: inactive
 Real Data Pairs (7 pairs):
 0 39.49
 10 28.7
 20 23.58
 30 19.86
 40 15.4
 50 13.92
 60 9.5

C_meas4: Description: Real List Variable
 Type: Real List Variable
 Unit:
 Argument: Time
 Standard Deviations: global
 Rel. Stand. Deviat.: 0
 Abs. Stand. Deviat.: 1
 Minimum: 0
 Maximum: 1e+009
 Interpolation Method: linear interpolation
 Sensitivity Analysis: inactive
 Real Data Pairs (7 pairs):
 0 49.27
 10 34.15
 20 30
 30 26.02
 40 21.85
 50 17.73
 60 15.14

C_meas5: Description: Measured Data

Type: Real List Variable
 Unit: mg/L
 Argument: Time
 Standard Deviations: global
 Rel. Stand. Deviat.: 0
 Abs. Stand. Deviat.: 1
 Minimum: 0
 Maximum: 1e+009
 Interpolation Method: linear interpolation
 Sensitivity Analysis: inactive
 Real Data Pairs (7 pairs):

0	81.56
10	67.32
20	54.24
30	39.21
40	35.24
50	33.52
60	28.45

C_meas6: Description: Measured Data
 Type: Real List Variable
 Unit:
 Argument: Time
 Standard Deviations: global
 Rel. Stand. Deviat.: 0
 Abs. Stand. Deviat.: 1
 Minimum: 0
 Maximum: 1e+009
 Interpolation Method: linear interpolation
 Sensitivity Analysis: inactive
 Real Data Pairs (7 pairs):

0	152.01
10	126
20	115
30	108
40	100.03
50	92
60	87.3

Ka1: Description: Adsorption constant
 Type: Constant Variable
 Unit: L/mol
 Value: 0.0058957093
 Standard Deviation: 0.025558473
 Minimum: 0
 Maximum: 2000
 Sensitivity Analysis: inactive
 Parameter Estimation: inactive

Ka2: Description: Adsorption constant
 Type: Constant Variable
 Unit: L/mol
 Value: 1.9688753
 Standard Deviation: 3.1634878

	Minimum:	0
	Maximum:	100
	Sensitivity Analysis:	inactive
	Parameter Estimation:	inactive

Ka3:	Description:	Adsorption constant
	Type:	Constant Variable
	Unit:	L/mol
	Value:	0.074214022
	Standard Deviation:	1
	Minimum:	0
	Maximum:	100
	Sensitivity Analysis:	inactive
	Parameter Estimation:	inactive

Ka4:	Description:	Adsorption constant
	Type:	Constant Variable
	Unit:	L/mol
	Value:	0.010092485
	Standard Deviation:	1
	Minimum:	0
	Maximum:	100
	Sensitivity Analysis:	inactive
	Parameter Estimation:	inactive

Ka5:	Description:	Adsorption Constant
	Type:	Constant Variable
	Unit:	L/mol
	Value:	0.013607836
	Standard Deviation:	1
	Minimum:	0
	Maximum:	100
	Sensitivity Analysis:	inactive
	Parameter Estimation:	inactive

Ka6:	Description:	Adsorption Constant
	Type:	Constant Variable
	Unit:	
	Value:	0.0031420427
	Standard Deviation:	1
	Minimum:	0
	Maximum:	100
	Sensitivity Analysis:	inactive
	Parameter Estimation:	active

kr1:	Description:	Rate constant
	Type:	Constant Variable
	Unit:	min ⁻¹
	Value:	4.1614948
	Standard Deviation:	6.571687
	Minimum:	0
	Maximum:	100
	Sensitivity Analysis:	inactive
	Parameter Estimation:	inactive

kr2: Description: Rate constant
 Type: Constant Variable
 Unit: min⁻¹
 Value: 0.29525015
 Standard Deviation: 0.021823028
 Minimum: 0
 Maximum: 100
 Sensitivity Analysis: inactive
 Parameter Estimation: inactive

kr3: Description: Rate constant
 Type: Constant Variable
 Unit: min⁻¹
 Value: 0.91882898
 Standard Deviation: 1
 Minimum: 0
 Maximum: 100
 Sensitivity Analysis: inactive
 Parameter Estimation: inactive

kr4: Description: Rate constant
 Type: Constant Variable
 Unit: min⁻¹
 Value: 2.7241606
 Standard Deviation: 1
 Minimum: 0
 Maximum: 100
 Sensitivity Analysis: inactive
 Parameter Estimation: inactive

kr5: Description: Rate constant
 Type: Constant Variable
 Unit: min⁻¹
 Value: 2.762008
 Standard Deviation: 1
 Minimum: 0
 Maximum: 100
 Sensitivity Analysis: inactive
 Parameter Estimation: inactive

kr6: Description: Rate constant
 Type: Constant Variable
 Unit: min⁻¹
 Value: 4.5523437
 Standard Deviation: 1
 Minimum: 0
 Maximum: 100
 Sensitivity Analysis: inactive
 Parameter Estimation: active

Time: Description: Time
 Type: Program Variable
 Unit: min

```

Reference to:      Time
*****

*****
Processes
*****
Degradation1:  Description:      Degradation
                Type:           Dynamic Process
                Rate:           (kr1*Ka1*C)/(1+Ka1*C)
                Stoichiometry:
                Variable : Stoichiometric Coefficient
                C : -1
-----
Degradation2:  Description:      Degradation
                Type:           Dynamic Process
                Rate:           (kr2*Ka2*C)/(1+Ka2*C)
                Stoichiometry:
                Variable : Stoichiometric Coefficient
                C : -1
-----
Degradation3:  Description:      Degradation
                Type:           Dynamic Process
                Rate:           (kr3*Ka3*C)/(1+Ka3*C)
                Stoichiometry:
                Variable : Stoichiometric Coefficient
                C : -1
-----
Degradation4:  Description:      Degradation
                Type:           Dynamic Process
                Rate:           (kr4*Ka4*C)/(1+Ka4*C)
                Stoichiometry:
                Variable : Stoichiometric Coefficient
                C : -1
-----
Degradation5:  Description:      Degradation
                Type:           Dynamic Process
                Rate:           (kr5*Ka5*C)/(1+Ka5*C)
                Stoichiometry:
                Variable : Stoichiometric Coefficient
                C : -1
-----
Degradation6:  Description:      Degradation
                Type:           Dynamic Process
                Rate:           (kr6*Ka6*C)/(1+Ka6*C)
                Stoichiometry:
                Variable : Stoichiometric Coefficient
                C : -1
*****

*****

```

Compartments

Batch1: Description:
 Type: Mixed Reactor Compartment
 Compartment Index: 0
 Active Variables: C
 Active Processes: Degradation1
 Initial Conditions:
 Variable(Zone) : Initial Condition
 C(Bulk Volume) : 12.75
 Inflow: 0
 Loadings:
 Volume: 1
 Accuracies:
 Rel. Acc. Q: 0.001
 Abs. Acc. Q: 0.001
 Rel. Acc. V: 0.001
 Abs. Acc. V: 0.001

Batch2: Description:
 Type: Mixed Reactor Compartment
 Compartment Index: 0
 Active Variables: C
 Active Processes: Degradation2
 Initial Conditions:
 Variable(Zone) : Initial Condition
 C(Bulk Volume) : 19.5
 Inflow: 0
 Loadings:
 Volume: 1
 Accuracies:
 Rel. Acc. Q: 0.001
 Abs. Acc. Q: 0.001
 Rel. Acc. V: 0.001
 Abs. Acc. V: 0.001

Batch3: Description:
 Type: Mixed Reactor Compartment
 Compartment Index: 0
 Active Variables: C
 Active Processes: Degradation3
 Initial Conditions:
 Variable(Zone) : Initial Condition
 C(Bulk Volume) : 39.49
 Inflow: 0
 Loadings:
 Volume: 1
 Accuracies:
 Rel. Acc. Q: 0.001
 Abs. Acc. Q: 0.001
 Rel. Acc. V: 0.001
 Abs. Acc. V: 0.001

Batch4: Description:


```

Type:                Mixed Reactor Compartment
Compartment Index:  0
Active Variables:   C
Active Processes:   Degradation4
Initial Conditions:
  Variable(Zone) : Initial Condition
  C(Bulk Volume) : 49.27
Inflow:            0
Loadings:
Volume:           1
Accuracies:
  Rel. Acc. Q:     0.001
  Abs. Acc. Q:     0.001
  Rel. Acc. V:     0.001
  Abs. Acc. V:     0.001

```

```

-----
Batch5:             Description:
                   Type:                Mixed Reactor Compartment
                   Compartment Index:  0
                   Active Variables:   C
                   Active Processes:   Degradation5
                   Initial Conditions:
                     Variable(Zone) : Initial Condition
                     C(Bulk Volume) : 81.56
                   Inflow:            0
                   Loadings:
                   Volume:           1
                   Accuracies:
                     Rel. Acc. Q:     0.001
                     Abs. Acc. Q:     0.001
                     Rel. Acc. V:     0.001
                     Abs. Acc. V:     0.001

```

```

-----
Batch6:             Description:
                   Type:                Mixed Reactor Compartment
                   Compartment Index:  0
                   Active Variables:   C
                   Active Processes:   Degradation6
                   Initial Conditions:
                     Variable(Zone) : Initial Condition
                     C(Bulk Volume) : 152.01
                   Inflow:            0
                   Loadings:
                   Volume:           1
                   Accuracies:
                     Rel. Acc. Q:     0.001
                     Abs. Acc. Q:     0.001
                     Rel. Acc. V:     0.001
                     Abs. Acc. V:     0.001

```

CALCULATIONS

```
*****
Definitions of Calculations
*****
calc1:      Description:
            Calculation Number:  0
            Initial Time:        0
            Initial State:       given, made consistent
            Step Size:           0.1
            Num. Steps:          1500
            Status:              active for simulation
                                inactive for sensitivity analysis
*****
```

PARAMETER ESTIMATION

```
*****
Definitions of Parameter Estimation Calculations
*****
fit1:      Description:
            Calculation Number:  0
            Initial Time:        0
            Initial State:       given, made consistent
            Status:              inactive
            Fit Targets:
            Data : Variable (Compartment,Zone,Time/Space)
            C_meas1 : C (Batch1,Bulk Volume,0)
-----
fit2:      Description:
            Calculation Number:  0
            Initial Time:        0
            Initial State:       given, made consistent
            Status:              inactive
            Fit Targets:
            Data : Variable (Compartment,Zone,Time/Space)
            C_meas2 : C (Batch2,Bulk Volume,0)
-----
fit3:      Description:
            Calculation Number:  0
            Initial Time:        0
            Initial State:       given, made consistent
            Status:              inactive
            Fit Targets:
            Data : Variable (Compartment,Zone,Time/Space)
            C_meas3 : C (Batch3,Bulk Volume,0)
-----
fit4:      Description:
            Calculation Number:  0
            Initial Time:        0
            Initial State:       given, made consistent
            Status:              inactive
```

Fit Targets:
Data : Variable (Compartment,Zone,Time/Space)
C_meas4 : C (Batch4,Bulk Volume,0)

fit5: Description:
Calculation Number: 0
Initial Time: 0
Initial State: given, made consistent
Status: inactive
Fit Targets:
Data : Variable (Compartment,Zone,Time/Space)
C_meas5 : C (Batch5,Bulk Volume,0)

fit6: Description:
Calculation Number: 0
Initial Time: 0
Initial State: given, made consistent
Status: active
Fit Targets:
Data : Variable (Compartment,Zone,Time/Space)
C_meas6 : C (Batch6,Bulk Volume,0)

Plot Definitions

all: Description:
Abscissa: Time
Title: Phenol Degradation
Abscissa Label: Time, min
Ordinate Label: Concentration, mg/L
Curves:
Type : Variable [CalcNum,Comp.,Zone,Time/Space]
Value : C [0,Batch1,Bulk Volume,0]
Value : C_meas1 [0,Batch1,Bulk Volume,0]
Value : C [0,Batch2,Bulk Volume,0]
Value : C_meas2 [0,Batch2,Bulk Volume,0]
Value : C [0,Batch3,Bulk Volume,0]
Value : C_meas3 [0,Batch1,Bulk Volume,0]
Value : C [0,Batch4,Bulk Volume,0]
Value : C_meas4 [0,Batch1,Bulk Volume,0]
Value : C [0,Batch5,Bulk Volume,0]
Value : C_meas5 [0,Batch5,Bulk Volume,0]
Value : C [0,Batch6,Bulk Volume,0]
Value : C_meas6 [0,Batch1,Bulk Volume,0]

plot1: Description: Phenol Degradation
Abscissa: Time
Title: Phenol Degradation
Abscissa Label: Time, min
Ordinate Label: Concentration, mg/L
Curves:
Type : Variable [CalcNum,Comp.,Zone,Time/Space]

Value : C [0,Batch1,Bulk Volume,0]
Value : C_meas1 [0,Batch1,Bulk Volume,0]

plot2: Description: Phenol Degradation
Abscissa: Time
Title: Phenol Degradation
Abscissa Label: Time, min
Ordinate Label: Concentration, mg/L
Curves:
Type : Variable [CalcNum,Comp.,Zone,Time/Space]
Value : C [0,Batch2,Bulk Volume,0]
Value : C_meas2 [0,Batch2,Bulk Volume,0]

plot3: Description: Phenol Degradation
Abscissa: Time
Title: Phenol Degradation
Abscissa Label: Time, min
Ordinate Label: Concentration, mg/L
Curves:
Type : Variable [CalcNum,Comp.,Zone,Time/Space]
Value : C [0,Batch3,Bulk Volume,0]
Value : C_meas3 [0,Batch3,Bulk Volume,0]

plot4: Description: Phenol Degradation
Abscissa: Time
Title: Phenol Degradation
Abscissa Label: Time, min
Ordinate Label: Concentration, mg/L
Curves:
Type : Variable [CalcNum,Comp.,Zone,Time/Space]
Value : C [0,Batch4,Bulk Volume,0]
Value : C_meas4 [0,Batch4,Bulk Volume,0]

plot5: Description: Phenol Degradation
Abscissa: Time
Title: Phenol Degradation
Abscissa Label: Time, min
Ordinate Label: Concentration, mg/L
Curves:
Type : Variable [CalcNum,Comp.,Zone,Time/Space]
Value : C [0,Batch5,Bulk Volume,0]
Value : C_meas5 [0,Batch5,Bulk Volume,0]

plot6: Description: Phenol Degradation
Abscissa: Time
Title: Phenol Degradation
Abscissa Label: Time, min
Ordinate Label: Concentration, mg/L
Curves:
Type : Variable [CalcNum,Comp.,Zone,Time/Space]
Value : C [0,Batch6,Bulk Volume,0]
Value : C_meas6 [0,Batch6,Bulk Volume,0]

Calculation Parameters

Numerical Parameters: Maximum Int. Step Size: 1
 Maximum Integrat. Order: 5
 Number of Codiagonals: 1000
 Maximum Number of Steps: 1000

 Fit Method: secant
 Max. Number of Iterat.: 100

Calculated States

Calc. Num. Num. States Comments
0 1501 Range of Times: 0 - 150

9.2 APPENDIX B: HPLC CHROMATOGRAMS

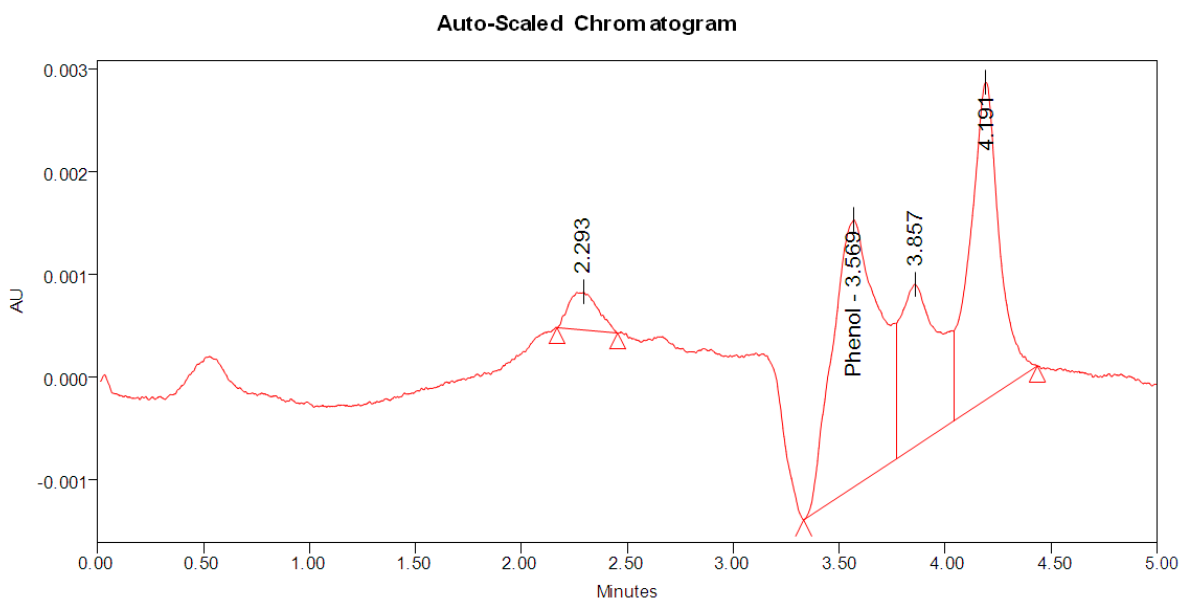


Figure 9A-1: A chromatogram from HPLC analysis for the degradation of phenol C-12 over TiO_2 .

Table 9A-1: The table reports the peak results during the photocatalytic degradation of phenol C-12.

	<i>Name</i>	<i>Retention time(min)</i>	<i>Area</i>	<i>Height</i>	<i>Amount</i>	<i>Units</i>
1		2.293	3535	369		
2	Phenol	3.569	39775	2598	9.634	mg/L
3		3.857	19786	1581		
4		4.191	30054	3089		

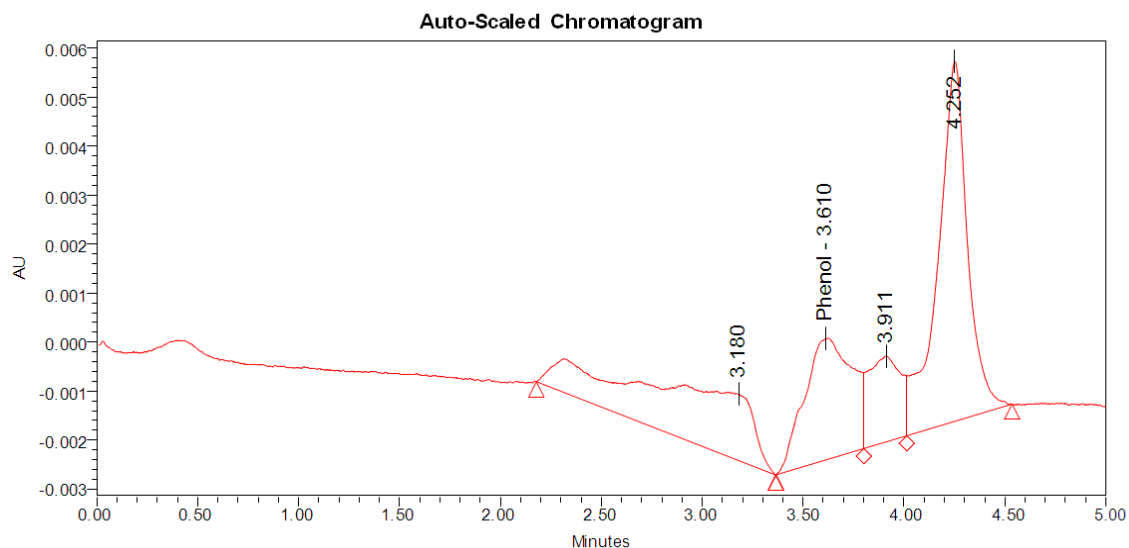


Figure 9A-2: A chromatogram from HPLC analysis for the degradation of phenol C-13 over TiO_2 .

Table 9A-2: The table reports the peak results during the photocatalytic degradation of C-13 labeled phenol.

	<i>Name</i>	<i>Retention time (min)</i>	<i>Area</i>	<i>Height</i>	<i>Amount</i>	<i>Units</i>
1		3.180	55959	1353		
2	Phenol	3.610	40712	2472	9.861	mg/L
3		3.911	19663	1751		
4		4.252	75454	7335		

9.3 APPENDIX C: GC-MS CHROMATOGRAM

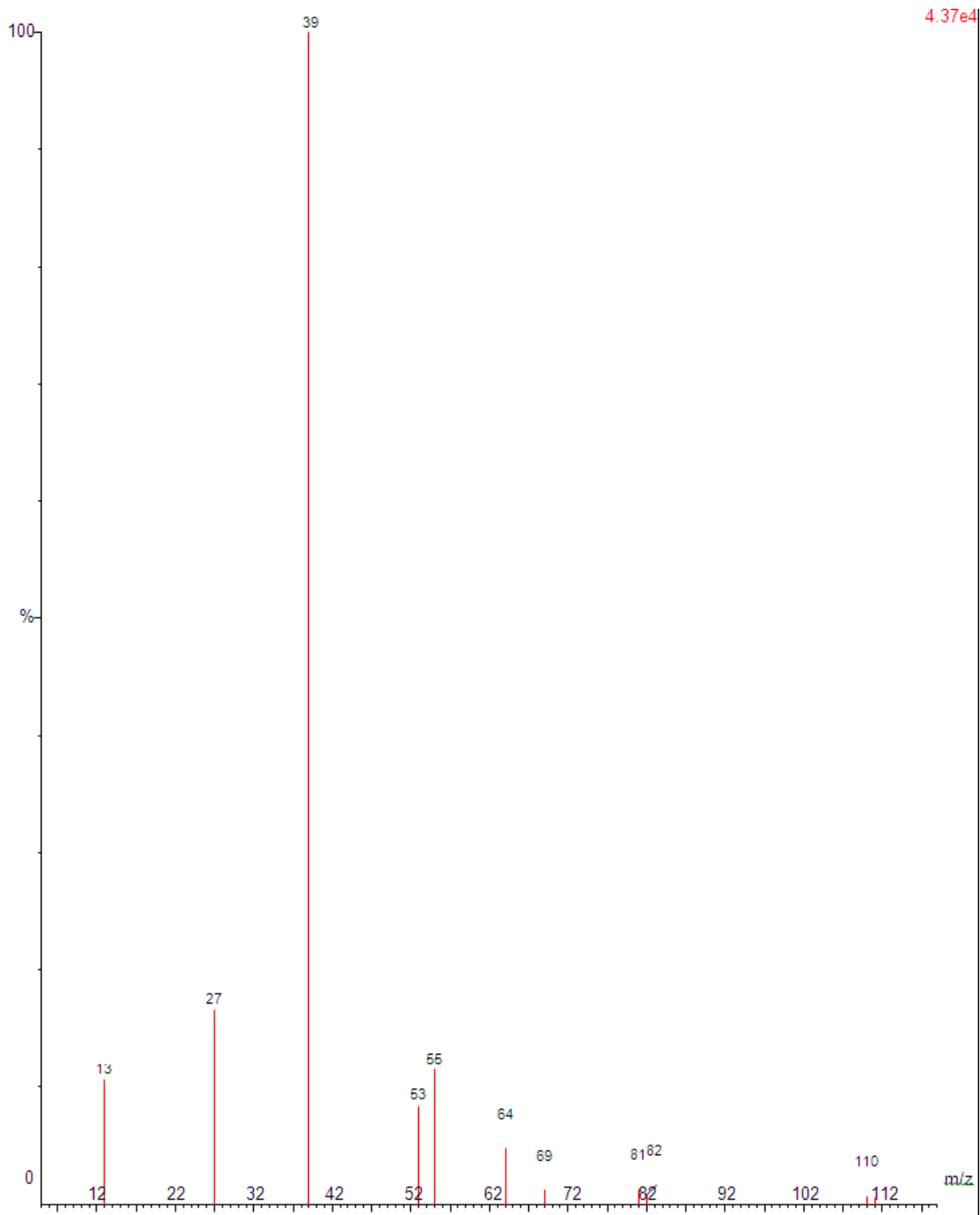


Figure 9B-1: A chromatogram of Resorcinol from the photodegradation of phenol C-12.

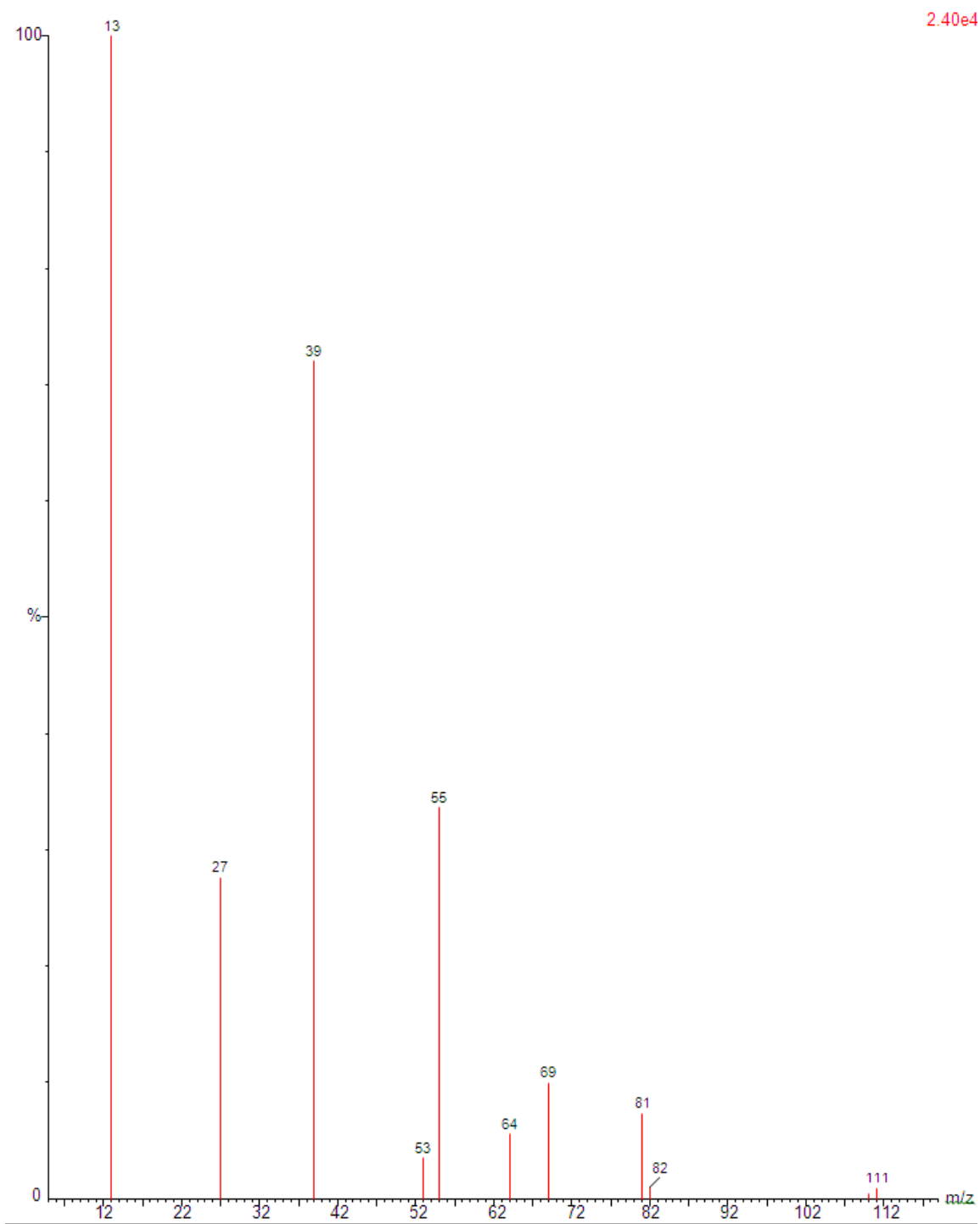


Figure 9B-2: A chromatogram of Resorcinol from the photodegradation of phenol-C-13.

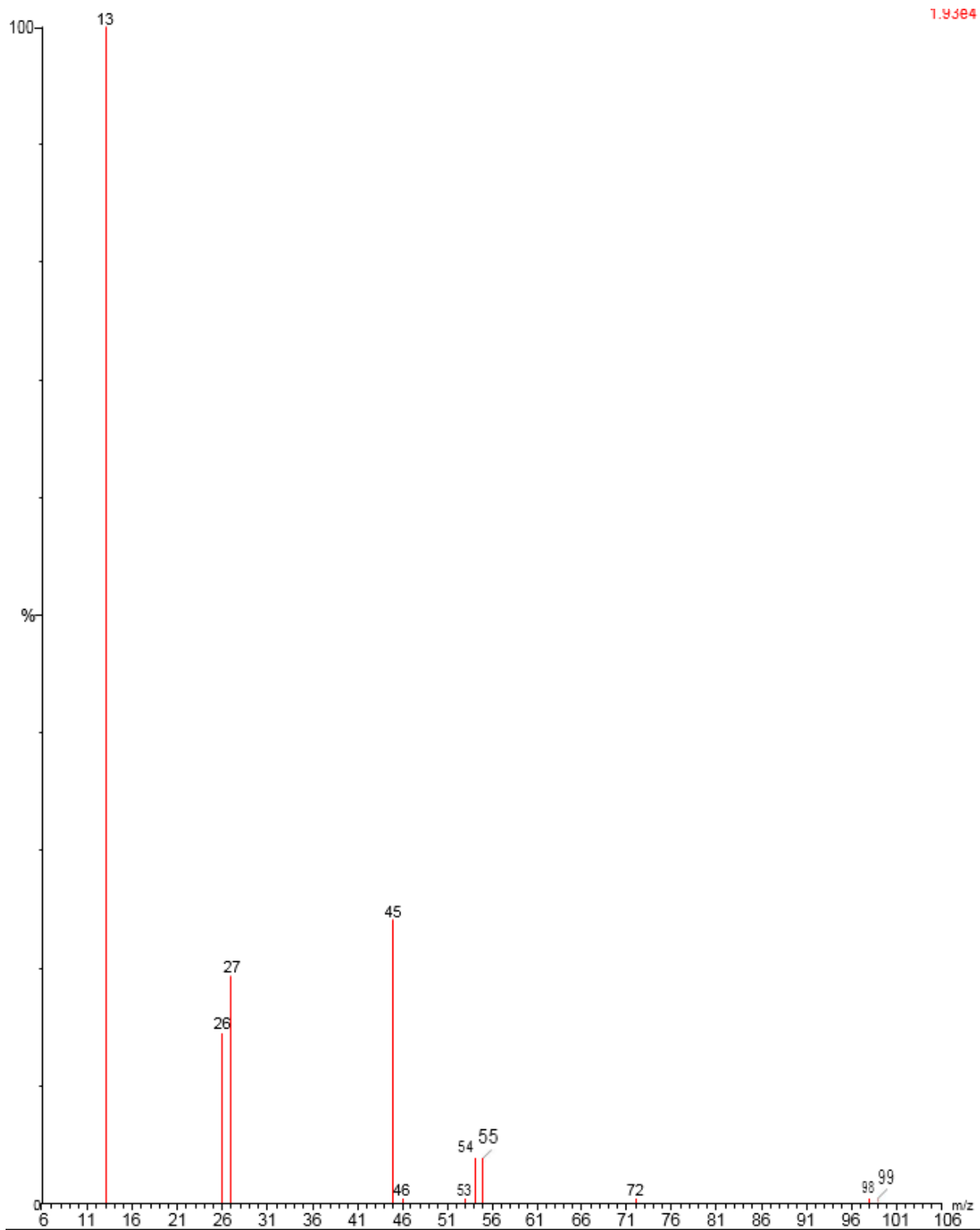


Figure 9B-3: A chromatogram of Maleic acid from the photodegradation of phenol-C-13.

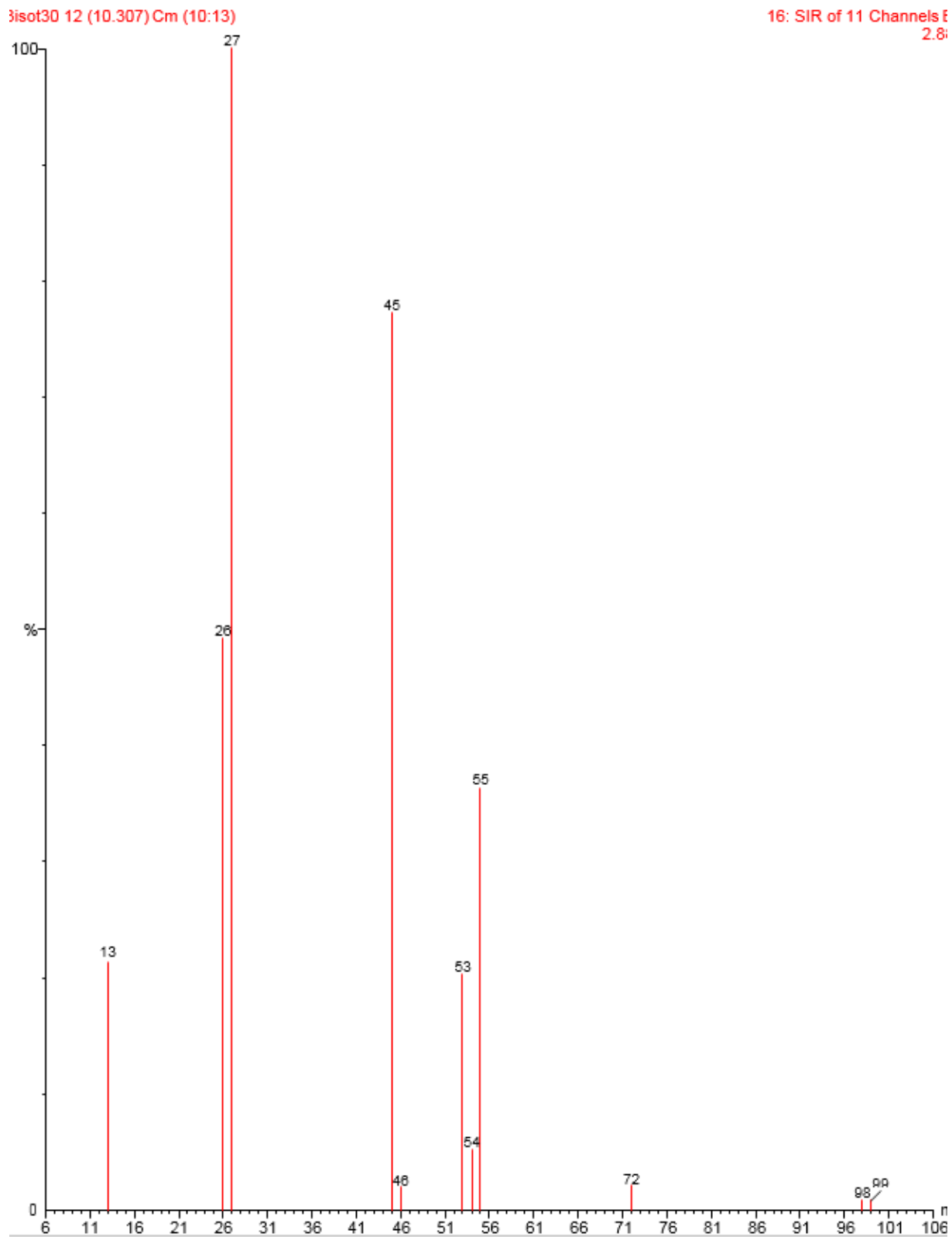


Figure 9B-4: A chromatogram of Maleic acid from the photodegradation of phenol C-12.

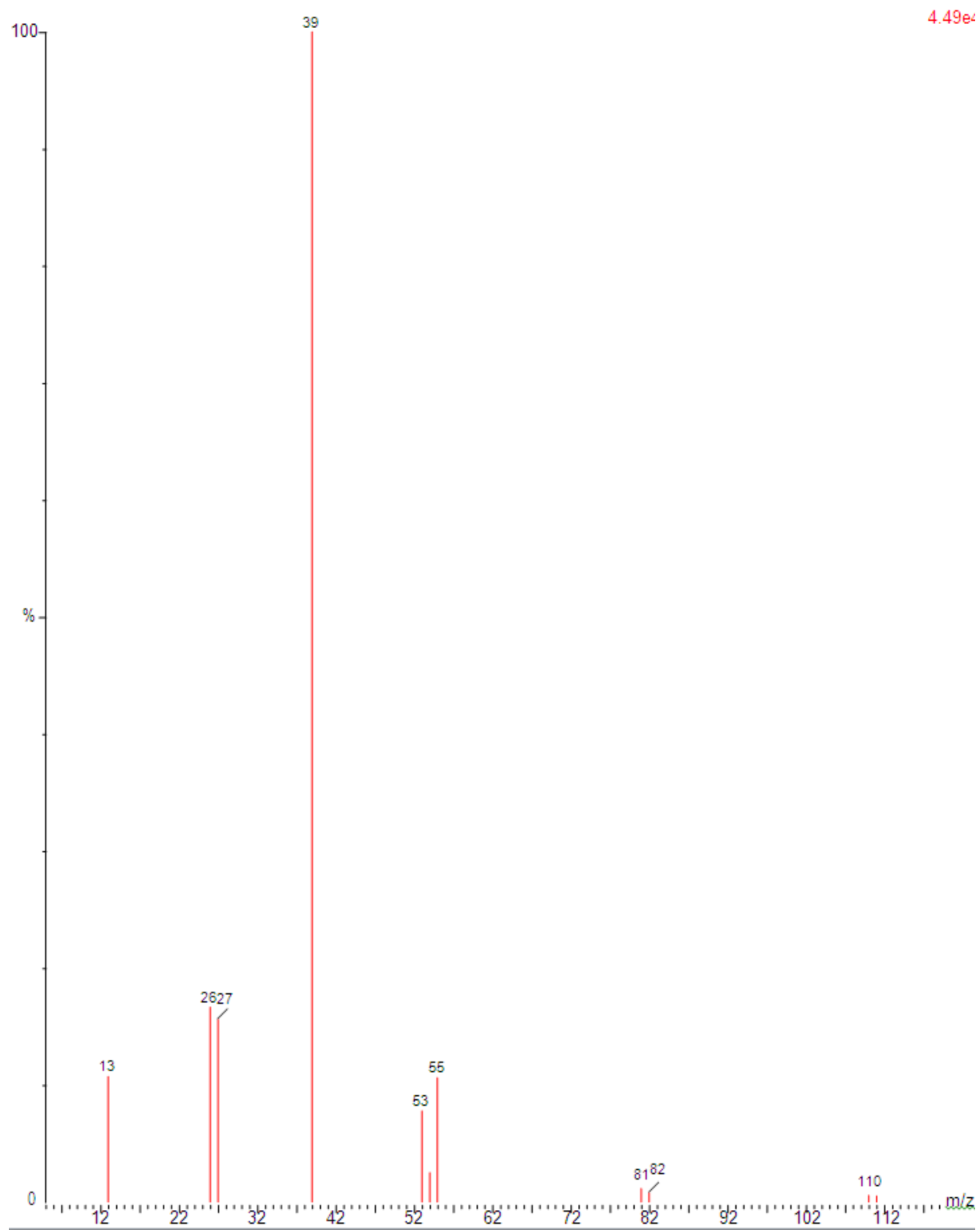


Figure 9B-5: A chromatogram of hydroquinone from the photodegradation of phenol-C-12.

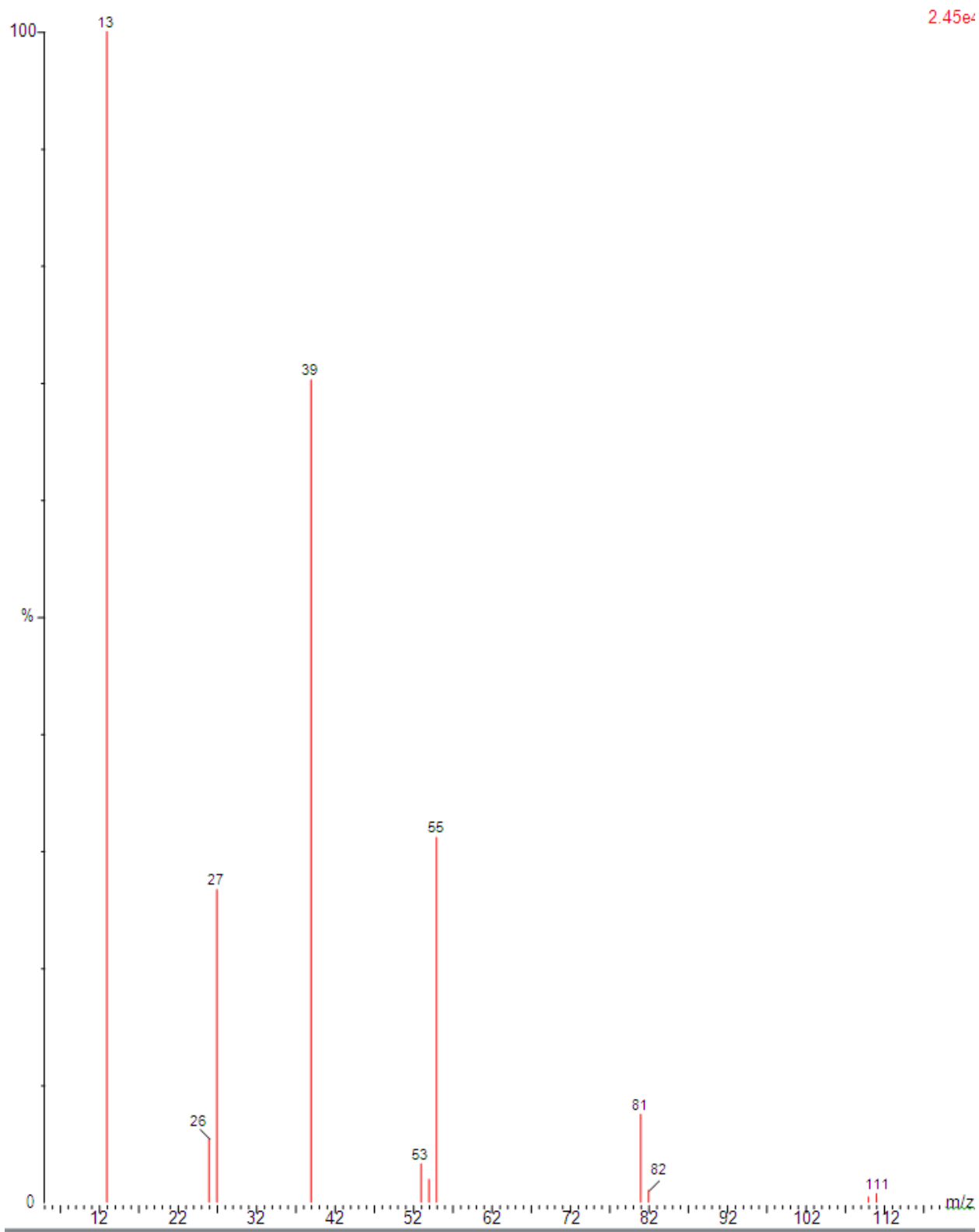


Figure 9B-6:A chromatogram of hydroquinone from the photodegradation of phenol C-13.

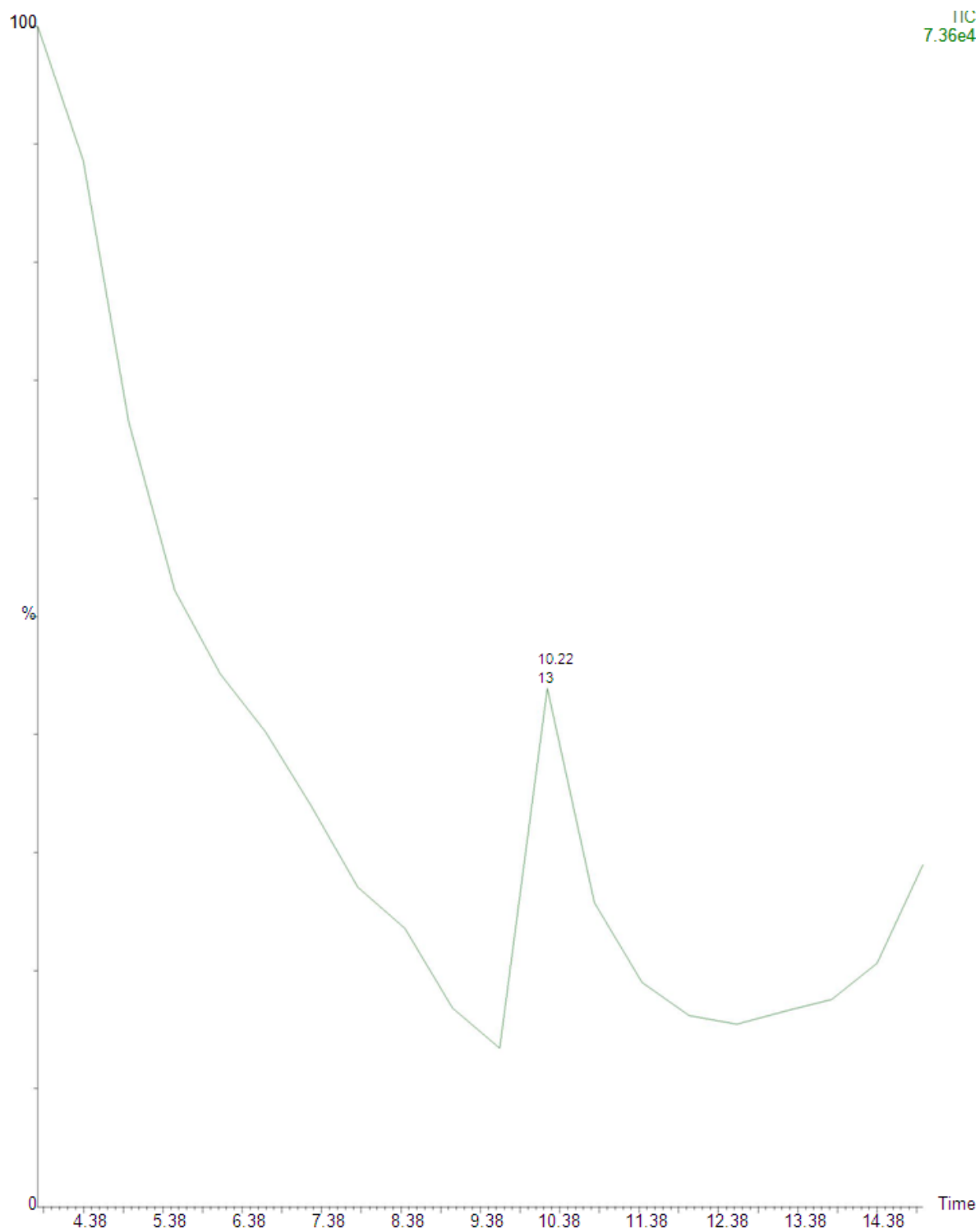


Figure 9B- 7: A chromatogram of the Hydroquinone peak.